Quantum Computation and Information Storage in Quantum Double Models

Thesis by
Anna Kómár

In Partial Fulfillment of the Requirements for the
Degree of
Doctor of Philosophy

CALIFORNIA INSTITUTE OF TECHNOLOGY
Pasadena, California

2018
Defended May 3, 2018

Anna Kómár
ORCID: 0000-0002-4701-4931

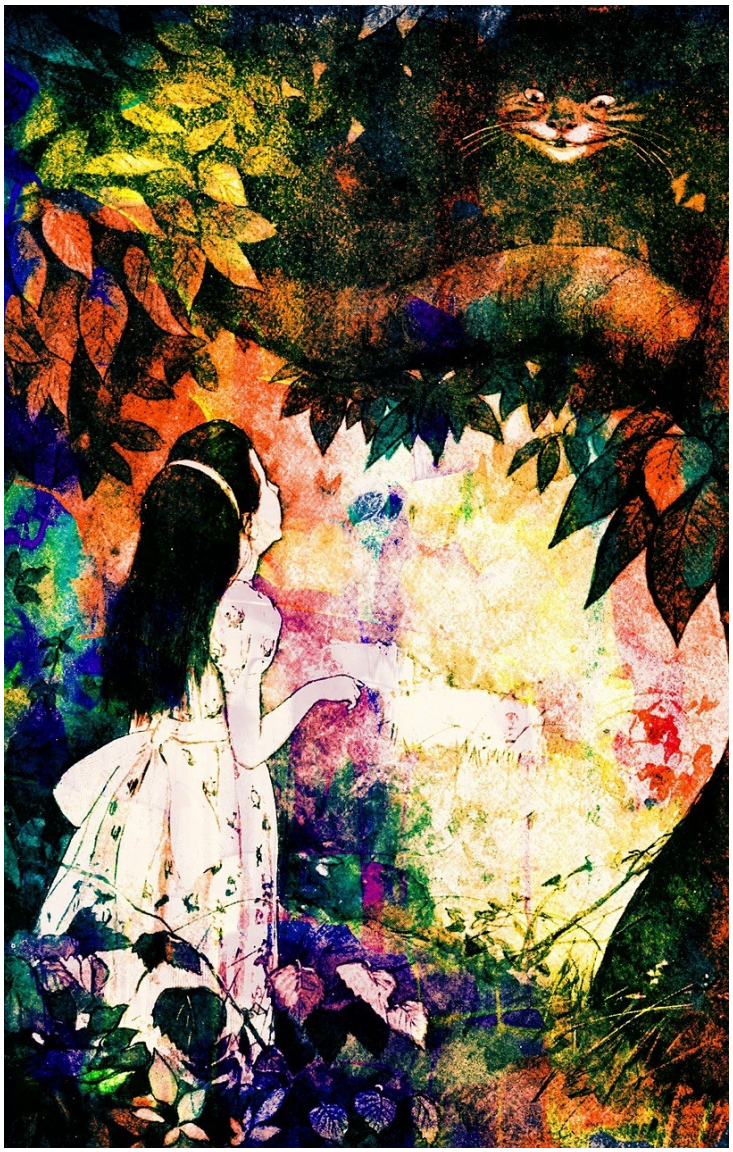

‘Would you tell me, please, which way I ought to go from here?’

‘That depends a good deal on where you want to get to,’ said the Cat.

‘I don’t much care where–’ said Alice.

‘Then it doesn’t matter which way you go,’ said the Cat.

‘–so long as I get *somewhere*,’ Alice added as an explanation.

‘Oh, you’re sure to do that,’ said the Cat, ‘if only you walk long enough.’

Alice in Wonderland [1, 2]
Lewis Carroll

ACKNOWLEDGEMENTS

I would like to thank John Preskill, for taking the risk of becoming my advisor, and for guiding my academic growth throughout the years. I could always count on his physical intuition and patience during our discussions. I thank Olivier Landon-Cardinal for being my mentor, for supporting me, both academically and personally, throughout the years; and for putting up with my trivial questions about physics. I thank my thesis committee: Xie Chen, Manuel Endres, Alexei Kitaev, and John Preskill for their valuable comments about the first version of this thesis, especially those regarding Chapter 4.

I would like to thank my collaborators and colleagues: Kristan Temme, for helping me take my first steps as a researcher in the field; Elizabeth Crosson, for helping me appreciate Markov chains more; Sujeet Shukla, Burak Sahinoglu and Dave Aasen, for their time and patience while discussing quantum doubles and ribbon operators with me; Aleksander Kubica, for always being there when I needed advice. I thank Alexei Kitaev for his time he spent discussing quantum doubles with me; and David Poulin and Anirudh Krishna for making me feel welcome in Sherbrooke during my visit.

Spending five years at Caltech made me appreciate the importance of personal relationships. I would like to thank all my Caltech friends for being there during these five years, for throwing board game nights, coming to dinners, and playing Dungeons & Dragons together. You're all awesome.

Special thanks is due to Ioana Craiciu, my mentee then friend, with whom I could discuss topics encompassing quantum physics, philosophy, travel, arts and crafts, and so much more. To my other best friend, Lena Murchikova: you're the strongest person I know, and I feel honored to be your friend.

I wouldn't be here without the two people who helped me start my career in science, my former advisors: Gergő Pokol and Tünde Fülöp. Thank you for helping me realize that doing research is fun, and for supporting me even after I left the field.

Last, but not least, I thank my family for their continuing support, in particular my parents, Antal and Erzsébet, for raising me to be a curious, skeptical, hard-working adult, for teaching me to never give up. I thank you both for encouraging and consoling me throughout all these years, and for accepting that I decided to move thousands of miles away from home. I thank my brother, Péter, for being a friend, a role model, someone who's always there to help. Thank you for being a caring big brother.

Finally, I would like to thank my husband, Dávid, for being there with me along the road. I thank you for listening to my ramblings about quantum physics, for celebrating milestones with me, and for picking up my pieces when needed. You have been my anchor throughout these years.

ABSTRACT

The results of this thesis concern the real-world realization of quantum computers, specifically how to build their "hard drives" or quantum memories. These are many-body quantum systems, and their building blocks are qubits, the same way bits are the building blocks of classical computers.

Quantum memories need to be robust against thermal noise, noise that would otherwise destroy the encoded information, similar to how strong magnetic field corrupts data classically stored in magnetic many-body systems (e.g., in hard drives). In this work I focus on a subset of many-body models, called quantum doubles, which, in addition to storing the information, could be used to perform the steps of the quantum computation, i.e., work as a "quantum processor".

In the first part of my thesis, I investigate how long a subset of quantum doubles (qudit surface codes) can retain the quantum information stored in them, referred to as their memory time. I prove an upper bound for this memory time, restricting the maximum possible performance of qudit surface codes.

Then, I analyze the structure of quantum doubles, and find two interesting properties. First, that the high-level description of doubles, utilizing only their quasi-particles to describe their states, disregards key components of their microscopic properties. In short, quasi-particles (anyons) of quantum doubles are not in a one-to-one correspondence with the energy eigenstates of their Hamiltonian. Second, by investigating phase transitions of a simple quantum double, $\mathcal{D}(S_3)$, I map its phase diagram, and interpret the physical processes the theory undergoes through terms borrowed from the Landau theory of phase transitions.

PUBLISHED CONTENT AND CONTRIBUTIONS

Anna Kómár, Olivier Landon-Cardinal, and Kristan Temme. Necessity of an energy barrier for self-correction of Abelian quantum doubles. *Physical Review A*, 93 (5):052337, 2016. DOI: 10.1103/PhysRevA.93.052337.

The project idea was conceived during discussions between AK, OLC and KT, as a non-trivial extension of the pioneering work done by KT [3]. AK derived the main result (upper bound on memory time), and proved that it is a constant. The value of the prefactor of the bound was derived and proven collaboratively by AK and OLC. The writing of the manuscript was led by AK, and collaboratively done by all authors.

Anna Kómár, and Olivier Landon-Cardinal. Anyons are not energy eigenspaces of quantum double Hamiltonians. *Physical Review B*, 96(19):195150, 2017. DOI: 10.1103/PhysRevB.96.195150.

The project idea was conceived during discussions between AK and OLC. AK derived the main results (construction of projectors, including their commutative and orthogonality properties). The proofs and interpretations of the results were finalized during discussions between AK and OLC. The writing of the manuscript was led by AK, and collaboratively done by the authors.

Anna Kómár, and Olivier Landon-Cardinal. Topological phase diagram of $\mathcal{D}(S_3)$ induced by forbidding charges and fluxes. *arXiv preprint: 1805.00032*.

The project idea was conceived during discussions between AK and OLC. AK derived the main results (what new phases emerge in each case of phase transition), and categorized the intermediate processes during these phase transitions. The writing of the manuscript was led by AK, and collaboratively done by the authors.

TABLE OF CONTENTS

NOMENCLATURE

The purpose of this nomenclature is to provide an easily accessible reference to the reader of this thesis. The terms presented here will be explained in more detail in the main text, and don't form an exhaustive list.

Abelian anyons. *Anyons* whose *braiding statistics* is described by a phase, rather than a non-trivial operation (c.f. *non-Abelian anyons*).

Abelian group. A group whose elements all commute (c.f. *non-Abelian group*).

Abstract quantum double. A field theory that has the same excitations as a *lattice quantum double*, but no underlying microscopic structure is assumed.

Anyon(s). Indistinguishable excitations of a two-dimensional field theory, exhibiting non-trivial *braiding statistics*. Bosons and fermions are special (trivial) cases of anyons, with braiding statistics $+1$ and -1.

Braiding, Braiding statistics. Taking one particle around another; also equivalent to a double exchange of two particles. Braiding statistics of two particles refers to the outcome of braiding two particles with each other, e.g., fermionic braiding statistics yields a -1 phase.

Decoherence time. The characteristic time-scale of a system after which it *decoheres*.

Decoherence. The process when a quantum state (e.g., a set of *qubits*) loses coherence, usually due to it coming into contact with its environment. As a result, entanglement and information is lost in the computation.

Flavors (of an anyon). The distinct inner states of a *non-Abelian anyon*. For example, different class representatives of a flux label are different flavors of an anyon with that flux.

Lattice quantum double. The lattice spin system introduced by Kitaev [4] that exhibits topological order, and has *anyonic* excitations which can be utilized to apply computational gates.

Logical operator. Operator in a many-body system/*code* which acts non-trivially on the ground space/code space (e.g., by taking the encoded *qubit* from the "0" state to the "1" state).

Non-Abelian anyons. *Anyons* whose *braiding statistics* is described by a non-trivial unitary operation (c.f. *Abelian anyons*).

Non-Abelian group. A group whose elements don't (all) commute (c.f. *Abelian group*).

Qubit. The unit of computation in a quantum computer, the counterpart of a classical bit. Qubits can not only be in a state of "0" or "1", but also in a state of superposition.

Qudit. A generalized *qubit*, with d number of distinct orthogonal states. A qubit is a qudit with $d = 2$.

Stabilizer codes. Quantum error-correcting codes introduced by Gottesman [5]. For a full definition, please refer to Sec. 1.1.3.

Chapter 1

OVERVIEW

The concept of quantum computers was first introduced by Richard Feynman [6], in the context of using a quantum system to simulate quantum phenomena. He believed that "there's plenty of room at the bottom" [7], and he was right. Since then, the field of quantum computation underwent an enormous development: from when David Deutsch demonstrated the power of "parallel computing with qubits" [8], when Peter Shor constructed his factoring algorithm [9], to the first concept of quantum error-correcting codes (also pioneered by Shor [5, 10, 11]), all the way to today, when several research groups, both academic and commercial, already have or are on the brink of realizing working quantum computers [12, 13].

What Deutsch and Shor utilized in their works is the power of entanglement, which can arise when a system is made of more than one elementary parts (qubits). Entanglement in many-body quantum systems wouldn't be possible without a unique property of qubits: that they can be in a state of *superposition*. While the blocks of classical computations, *bits*, are either in a state labeled as "0", or in a state labeled "1", *qubits* in a quantum computation are in states of superposition:

$$a|\,0\rangle + b|\,1\rangle, \tag{1.1}$$

where a and b are complex numbers, and normalization of the state dictates that $|a|^2 + |b|^2 = 1$.

Now, imagine having not one, but several, hundreds, or thousands of qubits, the joint state of which is then going to be a superposition of all possible states:

$$\sum_{\mathbf{x}\in\{0,1\}^n} a_{\mathbf{x}}|\,x_1, x_2, x_3, \ldots x_n\rangle. \tag{1.2}$$

Here $\mathbf{x} = (x_1, x_2, x_3, \ldots x_n)$ denotes a state of all n qubits, each x_i element of which could take the value of 0 or 1, independently of the rest.

Depending on the $a_{\mathbf{x}}$ constants, the state described by Eq. (1.2) may be written as a

product of the state of all the qubits:

$$\left(\sum_{x_1=0,1} a_{x_1}|\,x_1\rangle\right)\otimes\left(\sum_{x_2=0,1} a_{x_2}|\,x_2\rangle\right)\otimes\left(\sum_{x_3=0,1} a_{x_3}|\,x_3\rangle\right)\otimes\ldots\left(\sum_{x_n=0,1} a_{x_n}|\,x_n\rangle\right), \quad (1.3)$$

and we call such states *product states*. Any state of n qubits that can't be written as a product state is an *entangled state*, having *entanglement* between its qubits.

It is easy to see that the space that these states span is going to be exponentially larger than the space available for computation with classical bits only. The power of a quantum computer lies in the fact that the computations, when designed appropriately like Shor's [9, 14] or Grover's algorithm [15, 16], can take advantage of entanglement between qubits of the system.

However, what is an advantage of quantum states is also their greatest weakness, when considering performing computations on them: the nature of entanglement is delicate. When qubits come into contact with their environment, their states could lose entanglement and *decohere*. Decoherence of quantum states, when it happens during a quantum computation scheme, will result in the loss of the quantum advantage (transforming the computation into a classical scheme), and needs to be avoided at all costs. This requires the isolation of the qubits from the environment, as well as efforts to reduce and correct the errors that are unavoidably introduced to the system while performing the quantum operations.

In order to build a working quantum computer, we need to address the following main aspects of a computational scheme:

1. preparation of states
2. reliable storage of information
3. implementation of the computational steps
4. readout of information

In this thesis I will focus on the middle two: information storage and how to implement the computational steps. There are several computational schemes available [17–19], and the exact divide between "storage" and "steps of computation" might differ in each. In the current overview I will focus on the scheme referred to as *circuit-based quantum computation* [20]. In this scheme the computational steps are gates: distinct unitary operations applied to one or more qubits of the system.

In Sec. 1.1 I will introduce the concept of topological quantum computation: in Sec. 1.1.1 I provide an overview of systems that exhibit topological order and non-Abelian anyons, braiding processes of which can realize a universal gate-set, followed by an overview of said anyons in Sec. 1.1.2. Sec. 1.1.3 is dedicated to the question of reliable information storage. In Sec. 1.1.4 these concepts meet: I introduce the toric code, which both exhibits topological order, and serves as an error-correcting code.

Finally, in Sec. 1.2, building on the concepts introduced in Sec. 1.1, I give an overview of the main results of this thesis.

1.1 Topological Quantum Computation

One concept to store and manipulate quantum information is that of *topological quantum computation*, introduced by Kitaev [4]. In this scheme, the quantum information is encoded into topological degrees of freedom, in a way that performing local operations on the system will neither yield the encoded information, nor decohere it: the encoded information is *topologically protected*. As a result, the information can only be encoded and decoded by performing operations on a global scale (although it could be possible to realize this as a series of local operations).

This encoding can be done in various ways. One way to perform it is to encode into the degenerate vacuum space of a field theory. Then, one of the degenerate states would correspond to the state $|0\rangle$, another to the state $|1\rangle$. This type of encoding is typically done when the focus is on information storage: in the case of quantum memories. Another option would be to encode into the excitation spectrum of a theory. If the excitations (anyons) are non-Abelian, then the joint state of a pair of anyons can have multiple outcomes, and we can label these orthogonal outcomes to be the computational $|0\rangle$ and $|1\rangle$ states. This method is typically chosen for the purposes of performing topological quantum computation.

Quantum computation in these theories can be performed by utilizing the anyons of the field theory. Braiding anyons with each other will apply gates on the encoded information. For certain (non-Abelian) field theories, the braiding statistics are such that the resulting set of gates will be *universal* for quantum computation [21–23] (i.e., the gates can approximate any unitary transformation). For other theories (including Abelian ones) the resulting set of gates will have to be supplemented to achieve universality [24].

1.1.1 Topological order

Many examples of topologically ordered systems are now known in the literature. The most well-known ones are quantum Hall-states in two-dimensional electron gases in a high magnetic field [25]. Other proposals include Kitaev's honeycomb model [26], whose Hilbert space can be mapped unto that of a system of Majorana fermions [27, 28], and its ground state is in the same universality class as that of a chiral p-wave superconductor [25]. Another example of systems with topological order and non-Abelian anyons are the Levin-Wen models [29], one example of which has a topological phase that exhibits Fibonacci anyons, supporting universal quantum computation. Yet different constructions are Kitaev's quantum double models [4], which are based on spins placed on a lattice, each spin labeled by an element of a group G. The anyons quantum doubles exhibit are non-Abelian if the group G is non-Abelian, and the group can be chosen such that the resulting braiding statistics is universal for quantum computation [21, 22]. An interesting relation between these models and the more physical honeycomb model (whose interactions are two-body), is that in the right regime of parameters the honeycomb model reduces to the simplest quantum double: the toric code.

In my thesis, I focus on Kitaev's quantum double models, exactly solvable models that are promising for quantum computation. In Ref. [4] Kitaev showed that we can realize a topological field theory by placing physical qubits (or qudits) on a lattice, and engineering interactions between those qubits. The resulting theory, a quantum double, will have all the properties of the field theory: its excitations, the topological protection, the possibility to realize quantum gates through braiding. Several useful properties of topological order and quantum doubles have since been proven, including their robustness against perturbations [30], and their properties in thermal environments [31, 32]. All this makes topological field theories and quantum doubles prime candidates for the real-world realization of quantum computers.

1.1.2 Anyons

Anyons are particles, or quasi-particles of two-dimensional field theories. While in three dimensions exchanging two particles twice can only yield one of two outcomes: $+1$ (bosons), and -1 (fermions), a double exchange of particles (or quasi-particles) a and b in two dimensions can yield an arbitrary phase:

$$R_{ab}^2 |\, a, b\rangle = \exp(i\varphi_{a,b}) |\, a, b\rangle, \tag{1.4}$$

where R_{ab} is the (counterclockwise) exchange operation of particles a and b. When $\varphi_{a,b} = 0$ we have bosons, when $\varphi_{a,b} = \pi$ we have fermions, and for any other value a and b are nontrivial Abelian anyons.

In contrast, non-Abelian anyons are particles or quasi-particles whose double exchange is one step less trivial: it results in a nontrivial unitary operation, $U_{a,b}$, on their joint wave function:

$$R_{ab}^2 |\, a, b\rangle = U_{a,b} |\, a, b\rangle. \tag{1.5}$$

For a convenient labeling of anyons, and a summary of their properties, [33] is an excellent reference. I will review their most important properties in the introductory sections of Chapters 3-4. Here, I will give an illustrative example of non-Abelian anyons: spin-$1/2$ particles.

Another defining property of non-Abelian anyons is that their *fusion*, when we pull two particles together and consider their joint space as that of one particle. The fusion of non-Abelian anyons is non-deterministic. In the example of spin-$1/2$ particles, fusion is equivalent to combining the angular momentum of two particles, and it can result in multiple outcomes:

$$|\,\psi_{1/2}\rangle \times |\,\psi_{1/2}\rangle = \begin{cases} |\uparrow\uparrow\rangle \\ |\downarrow\downarrow\rangle \\ (|\uparrow\downarrow\rangle + |\downarrow\uparrow\rangle)/\sqrt{2} \\ (|\uparrow\downarrow\rangle - |\downarrow\uparrow\rangle)/\sqrt{2} \end{cases}. \tag{1.6}$$

The first three states are all symmetric, and we may consider them as being different internal states of a symmetric subspace, i.e., a symmetric anyon S (*triplet state*). The last, antisymmetric state can be regarded as another anyon, A (*singlet state*).

Then, rewriting this fusion yields:

$$|\,\psi_{1/2}\rangle \times |\,\psi_{1/2}\rangle = |\,S\rangle \oplus |\,A\rangle. \tag{1.7}$$

It is important to remember that S has different internal states, while A only has a single one. This can be formalized through the concept of *quantum dimension*. While a proper definition of it will be given in Chapters 3-4, it is essentially the dimension of the Hilbert space the anyon occupies [34], and in certain cases it can be interpreted as the number of different internal states the anyon has. In the above example, S has quantum dimension $d_S = 3$, and A has dimension $d_A = 1$. In general,

non-Abelian anyons have quantum dimensions higher than 1.

1.1.3 Error Correction

During the process of quantum computation we have to protect the information from decoherence. The topological models detailed in Sec. 1.1.1 have an intrinsic topological protection, nevertheless, given a finite error rate and long enough time, independent local errors in the theory will eventually accumulate to form a global operation, and result in a logical error.

We can have additional protection of our information, if we manage to monitor the accumulation of errors, but without directly measuring the qubits (which would decohere them). This can be achieved by utilizing quantum error-correcting codes [5, 10, 11], generalizations of classical codes (henceforth referred to as *codes*). The underlying concept in both classical and quantum coding theory is to encode information with redundancy. The simplest example of an error-correcting code is the classical *repetition code*, wherein we encode the logical states $\bar{0}$ and $\bar{1}$ into several physical bits, e.g., three:

$$\bar{0} \rightarrow 000 \tag{1.8}$$

$$\bar{1} \rightarrow 111. \tag{1.9}$$

Then, if, e.g., the third physical bit flips, we find the states

$$\bar{0} \rightarrow 001 \tag{1.10}$$

$$\bar{1} \rightarrow 110. \tag{1.11}$$

Now, we might not know which bit(s) have flipped, but as long as the probability of a physical bit flip is small enough ($p < 0.5$ for this code), we can take a simple majority vote on the physical bits. This will give us the correct state of the logical bit.

We can utilize this idea of repetition code to construct a simple quantum error-correcting code: by using physical qubits instead of classical bits. However, determining the place of a qubit-error is less straightforward: we can't simply measure the states of the qubits, as that would decohere them! Instead, we should make *parity-check* measurements, where we compare the states of pairs of qubits.

In the above example, measuring the state of the qubits would mean applying Pauli-Z

operators on each qubit individually ($\sigma_z = Z$):

$$Z_1 \quad \text{or} \quad Z_2 \quad \text{or} \quad Z_3$$

while the parity-check measurements would be

$$Z_1 Z_2 \quad \text{or} \quad Z_2 Z_3 \quad \text{or} \quad Z_1 Z_3.$$

Notice how the latter measurements don't give us information about the specific states of the individual qubits, they don't decohere them. Instead, they give a $+1$ or -1 result depending on whether the two qubits in question are in the same state or not. By applying all three parity-checks one after another we can deduce which qubit has flipped, and simply flip it back by applying an X_i operation on it (Pauli-X on the ith qubit).

The concept behind this repetition code would be sufficient to correct physical errors that manifest as a (qu)bit-flip like those above, but not those that arise as a phase error in our qubits (e.g., $|0\rangle + |1\rangle \rightarrow |0\rangle - |1\rangle$). This is a fundamentally new problem, one that classical codes don't but quantum codes would have to handle: the problem that quantum error-correcting codes will have to correct both *flip* and *phase* errors. This is exactly what stabilizer codes do.

Stabilizer codes follow the construction of classical codes [5, 20]. We define a generator set, the set of Pauli operators ($\sigma_x \equiv X$, $\sigma_z \equiv Z$ and $\sigma_y \equiv Y$) acting on n qubits: $\mathcal{P}_n$. For example, $\mathcal{P}_1$ is

$$\mathcal{P}_1 = \{\mathbb{1}, X, Y, Z\}. \tag{1.12}$$

Then, we choose the stabilizer operators (which generate the stabilizer group $\mathcal{S}$) to be a subset of the generator set, $\mathcal{P}_n$. The code space, $V_{\mathcal{S}}$, is going to be the space invariant under the operations in the group $\mathcal{S}$:

$$V_{\mathcal{S}} = \text{span}\{|v\rangle \mid s|v\rangle = |v\rangle \quad \forall s \in \mathcal{S}\}. \tag{1.13}$$

The power of stabilizer codes is that measuring elements of the stabilizer group won't decohere the physical qubits. Such a measurement doesn't give us the state of any individual qubit, rather it gives us *relative* information about the state of the qubits, when compared to each other.

For example, the (quantum) repetition code, detailed above, is a stabilizer code.

Its stabilizer generators are the parity-checks: Z_1Z_2, Z_2Z_3, Z_1Z_3. The states $|000\rangle$, $|111\rangle$ are the *code words* that span the code space V_S. Then, X_3 would be a detectable error (it is exactly the flip-error in Eqs. (1.10)-(1.11)), while $X_1X_2X_3$ is a logical error. Further, a single Z_1 is also a logical error, which shows that this code can't handle phase-errors.

Another well-known example of stabilizer codes is the toric code, which I will now describe in detail.

1.1.4 Toric code

The toric code [4] is a stabilizer code that exhibits topological order (thus it lies at the intersection of Secs. 1.1.1 and 1.1.3), and is referred to as a *topological code*. It is a quantum double (the simplest, based on the group $\mathbb{Z}_2$), and as such, it carries all the useful properties of quantum doubles: it can be utilized for topological quantum computation. At the same time, it is a stabilizer code, and therefore it carries the beneficial properties of error-correcting codes: we may monitor the propagation of errors in this theory by performing stabilizer measurements (usually referred to as "syndrome measurements").

The toric code is constructed from $n = 2L^2$ qubits, where L is a scalable parameter. The fact that the toric code can be scaled up arbitrarily is an additional useful property of this code, as it increases its tolerance to errors.

The stabilizer group of the toric code is generated by two stabilizer operators: the X-type ($A(v)$), and the Z-type ($B(p)$). Each of these act on 4 qubits of the code, and all commute with each other:

$$[A(v), A(v')] = 0 \tag{1.14}$$

$$[B(p), B(p')] = 0 \tag{1.15}$$

$$[A(v), B(p)] = 0 \tag{1.16}$$

even when $v \neq v'$ and $p \neq p'$, i.e., when they are distinct operators.

These operators are defined such that we can visualize the code as embedded into a lattice (see Fig. 1.1): qubits sit on edges of the lattice, the $A(v)$ operators act on all edges that are joined up at the vertex v, and the $B(p)$ operators act on edges that are around a plaquette p of the lattice. The (1.14)-(1.16) commutation relations are then trivially satisfied: for any pair of stabilizer generators the number of overlapping edges (qubits) is even, thus even though $XZ = -ZX$ for a single qubit, the factors will cancel for the vertex- and plaquette-operators.

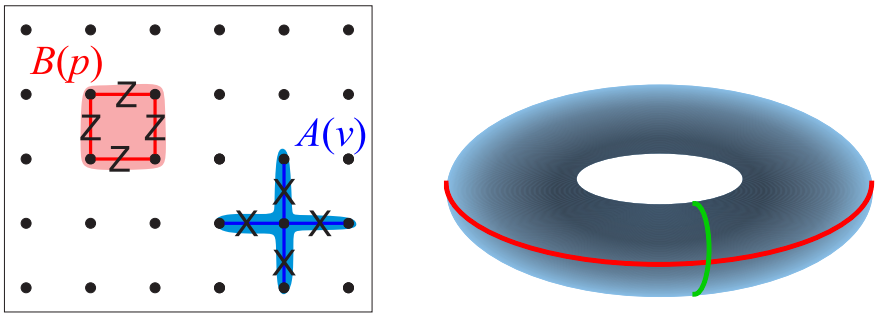

Figure 1.1: (a) A patch of the toric code on a square lattice. Vertices of the lattice are shown, qubits reside on edges between nearest-neighbor vertices. $A(v)$ and $B(p)$ are the vertex- and plaquette-operators, acting on four qubits each. (b) The toric code without its microscopic details shown. The two loops that wind around the torus are two of the four logical operators this theory has (two X-type and two Z-type logical operators).

We can assign a Hamiltonian to this many-body qubit system [4]:

$$H = -\sum_v A(v) - \sum_p B(p), \tag{1.17}$$

and the ground space of this Hamiltonian will coincide with the space stabilized by operators of the stabilizer group (the code space), i.e., it is left invariant by them.

Now, how to store information in this system? We can introduce a non-trivial topology, i.e., embed this system on the surface of a torus, hence the name "toric code". Then, the ground space becomes 4-fold degenerate, allowing us to store 2 logical qubits in the ground space. In this new topology, we will have Pauli operators which leave the ground space invariant (they commute with the stabilizer group), but are not in the stabilizer group themselves: we call these *logical operators*. Logical operators, in fact, transform one ground state of the degenerate ground space to another (orthogonal) state. For the toric code, these operators are loop-like X (and Z) operators that wind around the torus (see Fig. 1.1).

Excitations of the toric code are (Abelian) anyons, and they can be charges (**e**), fluxes (**m**), or dyons (**em**). Creating a pair of **e** charges from the vacuum, and then moving one around a nontrivial loop of the torus and annihilating it with its pair, corresponds to applying a logical Z operator to the code space. Similarly, creating a pair of **m** fluxes, and moving one of them in a nontrivial loop and then annihilating it back again applies a logical X operator unto (one of the) qubit(s) encoded into the ground space. Performing the same operation with a dyon (**em**) applies the combination of a logical X and Z operator.

The toric code is a promising construction to serve as a *quantum memory*, a system to store quantum information in. The requirements for a D-dimensional quantum memory have been summarized in Ref. [35] as the "Caltech rules":

1. (Finite spins) The model consists of finite-dimensional spins, embedded into $\mathbb{R}^D$, with a finite density.
2. (Bounded local interactions) Its Hamiltonian is composed of finite density interactions, with bounded strength and range.
3. (Nontrivial code space) Its code space is at least 2-fold degenerate, thus we can encode at least 1 qubit in it.
4. (Perturbative stability) The logical space corresponding to (at least one of the) qubits is stable under perturbations.
5. (Efficient decoding) There exists a polynomial-time decoding algorithm for the encoded qubit.

For *self-correcting* quantum memories, the topic of Chapter 2 of this thesis, there is one additional rule: that the lifetime of the encoded qubit scales (exponentially) with the number of spins (when the system is coupled to a thermal bath).

It is clear that the toric code satisfies the first, second and third rules, by construction. About its stability: its robustness against local errors was shown in Ref. [4], and its stability under perturbations was proven in Ref. [30]. The question of decoding was first explored in Ref. [36], where an error threshold was proven, below which increasing the size of the toric code improves its performance, proving the toric code is a good *active* error-correcting code.

Passive error correction would additionally require the property of self-correction, mentioned above as an additional "Caltech rule". An intuitive argument for why the toric code doesn't have such a long lifetime for its encoded qubits (*memory time* of the code) can be constructed based on the *energy barrier* of the code.

The energy barrier of a code is the minimum amount of energy required in order to take the system from a code state to a (nearly) orthogonal code state through a sequence of local errors. If the energy barrier is large, e.g., it scales with the number of spins, losing the encoded information due to noise from the environment would take an exponentially long time. Meanwhile, if the energy barrier is a constant, then intuitively, the thermal environment only needs to supply a small amount of energy for the information to be lost.

The toric code has a constant energy barrier [3, 31]. The environment could simply create a pair of anyons (this requires constant energy only), move one of them around the torus (this doesn't require additional energy), and then annihilate the anyon with its pair (this gives energy to the environment). This process applies a logical operator unto the encoded qubit, while only requiring a small (constant amount of) energy. In contrast, the four-dimensional toric code has an energy barrier that scales with the number of qubits, and is a self-correcting memory [32, 36]. This intuitive concept of energy barrier will be formalized in Chapter 2.

Surface codes

While the toric code has all the aforementioned useful properties, its toroidal geometry is experimentally unfeasible. However, we can use the intuition gained here, and instead build a surface code [36, 37]. Surface codes have the same microscopic details (identical stabilizer group, same lattice geometry) to those of the toric code, except for the fact that they are built on a trivial 2D sheet with two types of boundaries. These boundaries (smooth- and rough-edges) serve as sources and sinks of excitations in the model, e.g., an excitation created at one rough edge can be annihilated at any other rough edge. The logical operators in these models are X- (Z-) type strings that start at a smooth (rough) edge and end at another smooth (rough) edge.

It is also possible to cut out parts of the code and thus introduce holes: each new hole adds a new pair of logical operators: one of them winds around the hole, while the other extends from the perimeter of the hole to another edge (of the same type). The number of independent errors this code can tolerate (the *code distance*) is half of the shortest distance between pairs of smooth (or rough) edges. (For the toric code there is only one such linear distance: L, and the code distance there is $L/2$.)

Surface codes are so promising for quantum computation that there has been extensive research done on them in the last decade [38–41], and they are the focus of several research groups working on the experimental realizations of quantum computers [40, 42].

1.2 Summary of results

In this thesis I focus on qudit surface codes (Abelian quantum doubles) and non-Abelian quantum doubles, to determine key properties of them related to quantum information.

The toric code introduced in Sec. 1.1.4 is the simplest quantum double, it is the

quantum double of $\mathbb{Z}_2$. The Abelian quantum doubles investigated in Chapter 2 are based on cyclic groups, $\mathbb{Z}_d$. In Chapters 3-4, the focus is on non-Abelian doubles, and their definitions and descriptions can be found in the introductory sections of those chapters.

The results of this thesis can be divided into two main parts: those concerning the thermal properties (memory time of information storage) of Abelian quantum doubles (Chapter 2), and those that concern the structure of non-Abelian quantum doubles (and have consequences on quantum computation, see Chapters 3-4).

1.2.1 Memory time of Abelian quantum doubles

In Chapter 2 I will present my result (an upper bound) on the memory time of Abelian quantum doubles, obtained in collaboration with IQIM postdocs Olivier Landon-Cardinal (moved to McGill U) and Kristan Temme (moved to IBM).

The first rigorous upper bound on the memory time of a stabilizer Hamiltonian was derived for the two-dimensional toric code model in Ref. [31]. Other no-go results for stabilizer quantum memories [43, 44] in lower dimensions rely on the absence of an energy barrier E_B, c.f. [43, 45]. The argument proceeds to connect the energy barrier to the memory's lifetime through the phenomenological Arrhenius law $t_{mem} \sim e^{\beta E_B}$. It has been an open question, whether there is in fact a rigorous connection between the energy barrier E_B and thermalization time of a quantum system. Recent results, c.f. Ref. [46], indicate that the Arrhenius law can only serve as an upper bound to the lifetime of the quantum memory.

Since a rigorous connection between the energy barrier and the thermal lifetime of a quantum memory has not been established, a different kind of protection, coined *entropy protection*, has been suggested recently in Ref. [44]. Entropy protection would protect the quantum memory, in spite of the absence of a scaling energy barrier. The idea is that even if there exists a sequence of local errors corrupting the quantum information which only requires a constant amount of energy – thus the model only has a constant energy barrier – this sequence might be very atypical. Typical sequences, however, might require the system to go through an energy barrier which does scale with system size. In this sense, entropy-protected codes would be the quantum equivalent of classical spin glasses [47]. Up to this point, the only known proposal by Brown *et al* for an entropy-protected code, without an energy barrier, has been analyzed numerically in Ref. [48]. The authors found that in a specific temperature regime the memory time scaled super-exponentially with the inverse temperature $t_{mem} \propto \exp(c\beta^2)$. So far, this form of *partial self-correction*

has only been shown to exist in Haah's 3D cubic code [46], which does have a logarithmically diverging energy barrier.

In Chapter 2 of this thesis, I will show the following. When considering quantum memories based on Abelian quantum doubles and subjecting these to the full Davies dynamics as noise model, we can conclude the following: the presence of an energy barrier for the logical operators is in fact, although not sufficient, a necessary condition for a thermally stable quantum memory. This result is a generalization of Ref. [3], where a similar bound was proven for quantum memories based on Pauli stabilizers.

That is, I prove an upper bound to the memory time that is of the form of the Arrhenius law. In particular I observe that the super-exponential scaling in temperature observed in Ref. [48] for a particular temperature range is bounded by a linear scaling that holds for all temperatures, since the generalized energy barrier is independent of system size for these models.

This means that entropic protection is not possible for Abelian models, i.e., the scaling of the memory time can't increase above this barrier. Nevertheless, a form of *entropic enhancement* is still possible: entropy can help prolong the memory time (e.g., by a constant factor), like in the construction of Ref. [48].

1.2.2 Computation with non-Abelian quantum doubles

As mentioned in Sec. 1.1, systems exhibiting excitations with non-Abelian exchange statistics can be used to implement a universal gate-set for quantum computation. Therefore, it is worthwhile to investigate such models in detail, in order to find any properties that might improve or hinder their use for quantum computation.

In the second half of my thesis I consider the structural properties of non-Abelian quantum doubles, a work done in collaboration with Olivier Landon Cardinal, initiated at the end of OLC's postdoc at Caltech and continued after he took his new postdoc position at McGill U. In Chapter 3 I investigate the microscopic details of quantum doubles, and find that their anyonic excitations are not in one-to-one correspondence with the energy eigenspaces of Kitaev's original Hamiltonian. This could lead to the spontaneous decoherence of anyons during the computational process. In Chapter 4 I analyze phase transitions in the simplest non-Abelian quantum double, $\mathcal{D}(S_3)$, and find processes that parallel those of the Landau-theory of phase transitions [49].

Structural properties of $\mathcal{D}(G)$

In Chapter 3 of my thesis I investigate the structural properties of quantum doubles. Anyons of a quantum double can be grouped into *charges*, *fluxes*, and *dyons*. The way Kitaev's construction is introduced is through a Hamiltonian that projects out the vacuum state of the model as the ground state. This results in an energy landscape where charges and fluxes have mass 1, while dyons have mass 2. My first goal was to make this energy landscape even richer, by introducing a Hamiltonian that assigns different mass to each different anyon, similar to the way masses of Abelian anyons were shown to be possible to tune [48, 50].

As quantum doubles are candidates for topological quantum memories, a richer energy landscape could be the foundation of self-correction, as the system will react differently when put in contact with a thermal environment. This has been proposed in Ref. [48], and even though a substantial increase of memory time has been outruled in Ref. [50] for Abelian models (Chapter 2 of the current thesis), it is not clear whether a richer landscape can or cannot yield a self-correcting quantum memory for non-Abelian theories.

Introducing a tunable mass Hamiltonian is a nontrivial goal for non-Abelian quantum doubles, as Ref. [4] only defines the flux and vacuum projectors, and other works [51, 52] only extend this mathematical description to charge projectors. Introducing projectors unto dyons of a non-Abelian theory is nontrivial[1] since the fluxes and charges don't immediately decouple in a non-Abelian model.

In Chapter 3 I introduce a tunable mass Hamiltonian for quantum doubles based on any finite group G, by defining projectors unto all charge-type anyons. I prove that the charge projectors defined and the flux projectors (based on those of Ref. [4]) commute for all vertices and plaquettes. This, in the case of charge projectors, is a nontrivial consequence of the great orthogonality theorem in group theory. Furthermore, I argue that the combination of flux- and a charge projectors is sufficient to label dyons.

The Hamiltonian thus introduced is made of 4-body, commuting terms. Introducing this tunable Hamiltonian helped me realize the second (and main) result of this work: that eigenspaces of both this and the original Hamiltonian defined in Ref. [4] are not in one-to-one correspondence with anyons of the theory.

Non-Abelian anyons have a quantum dimension higher than 1, which we refer to as

[1] It is nontrivial in the sense that it is unclear which of the several different options would be the appropriate physical way to do it. This point ties to the main result of Chapter 3.

having different *flavors*. A main result of this chapter is that the 4-body Hamiltonian constructions widely used in the literature will distinguish between different flavors of the same anyon: they will assign a different energy to it based on its underlying charge flavor. Meanwhile, flavors of an anyon should be indistinguishable in a field theory!

I find that this disagreement is due to the underlying lattice structure of quantum doubles. Anyons live on a combination of a vertex and a plaquette of the lattice (a *site*), and a vertex and a plaquette have a finite separation from each other, due to the finite lattice spacing (even if they are on the same site). This separation makes it possible for an adversary (e.g., the environment) to braid an anyon *only around the vertex*, i.e., only with the charge of a dyon, thus making it possible to separate out charge flavors of the dyon. Such a process is not possible in a continuous field theory, as there is no lattice separation there.

Therefore, I conclude that the excitation spectrum of quantum doubles realized on a lattice don't completely correspond to their ideal field-theory counterparts. (Even though the ground spaces are the same.) It is unclear whether this introduces a fundamental issue when one would try to utilize the excitations of quantum doubles for quantum computation. One problem could be if the decoherence of anyon flavors, induced by this property of the Hamiltonian, would lead to the loss of information encoded in the fusion channels. This question is explored more in the discussion section of Chapter 3.

Emergent phases of $\mathcal{D}(S_3)$

In Chapter 4 I will present an analysis of phase transitions in the simplest non-Abelian quantum double, $\mathcal{D}(S_3)$. Phase transitions are well-described phenomena for systems without topological order, and are described by Landau's theory [49]. Understanding phase transitions in systems that exhibit topological order, however, is an active area of research. In this part of my thesis, I consider the quantum double $\mathcal{D}(S_3)$, and describe its phase transitions into new theories, in a framework that is parallel to the Landau theory.

The double $\mathcal{D}(S_3)$, is based on the group S_3, isomorphic to the symmetry transformations of an equilateral triangle. It is a non-Abelian group, a property that is inherited by the excitations of the quantum double. I chose this double as the focus of my analysis, as we may expect non-trivial phases emerging, as well as interesting processes being induced from non-Abelian doubles, and $\mathcal{D}(S_3)$ is the simplest of them.

Focusing on $\mathcal{D}(S_3)$ as a topological field theory, without considering microscopic details, I provide a description of phase transitions in this model. The phase transitions are induced by forbidding certain anyon labels (*charge* and *flux* labels) in the quantum double. Forbiddance in this context means anyons and anyon flavors related to the forbidden label won't be created, neither through fusion of other anyons, nor from the vacuum through thermal processes.

I also provide proposals for realizing such phase transitions. Quantum doubles can be realized on a lattice, as per Kitaev's construction [4]. To induce a phase transition in this construction, we will have to project out part of the Hilbert space, which can be done through a non-deterministic procedure (it involves measurements). However, this operation can be approximated by adding 4-local terms to the topological (6-local) Hamiltonian of the theory, strongly increasing their couplings to make the corresponding excitations have large energy. As a result, the creation of anyons related to the labels of the tuned terms will be thermally suppressed: it would require too much energy to create one of those anyons (E_{anyon}), and their creation probability will be $\propto \exp(-E_{\text{anyon}}/k_B T)$ in a thermal environment with temperature T. Tuning these couplings to the extreme ($E_{\text{anyon}} \to \infty$) will realize the forbiddance of that anyon as a limit of this operation.

Analyzing the phase transitions of $\mathcal{D}(S_3)$ I summarize the processes a double undergoes while transitioning into new theories: *condensation* and the *split-up* of higher-dimensional anyons. At the end of a series of these processes, a new topological theory emerges. I investigate the possible theories that $\mathcal{D}(S_3)$ could transition into, and find that doubles of subgroups ($\mathcal{D}(\mathbb{Z}_3)$) as well as their chargeon and fluxon sectors ($\mathbb{Z}_3$ and $\mathbb{Z}_2$) emerge. For the latter examples I conclude that they can't live on their own, without nontrivial fluxes or charges to differentiate between the excitations, and all anyons condense to form a trivial theory.

Chapter 2

SELF CORRECTION REQUIRES AN ENERGY BARRIER FOR ABELIAN QUANTUM DOUBLES

Anna Kómár, Olivier Landon-Cardinal, and Kristan Temme. Necessity of an energy barrier for self-correction of Abelian quantum doubles. *Physical Review A*, 93 (5):052337, 2016.

Abstract

We rigorously establish an Arrhenius law for the mixing time of quantum doubles based on any Abelian group $\mathbb{Z}_d$. We have made the concept of the energy barrier therein mathematically well-defined; it is related to the minimum energy cost the environment has to provide to the system in order to produce a generalized Pauli error, maximized for any generalized Pauli errors, not only logical operators. We evaluate this generalized energy barrier in Abelian quantum double models and find it to be a constant independent of system size. Thus, we rule out the possibility of entropic protection for this broad group of models.

2.1 Introduction

Whether it is possible to preserve arbitrary quantum information over a long period of time is a question of both fundamental and practical interest. *Active* quantum error correction provides a way to protect quantum information but requires keeping track of and correcting the errors over a short time scale. Alternatively, quantum self-correcting systems would *passively* preserve quantum information in the presence of a thermal environment without the need for external intervention on the system. The dynamics of these quantum "memories" would be such that the probability of an error occurring on the encoded information is exponentially suppressed with system size, resulting in an exponentially long memory time. Candidates for self-correction are typically systems governed by a local Hamiltonian whose degenerate ground space stores quantum information.

Assessing whether a system is self-correcting requires estimating the scaling of its memory time with system size. This difficult problem is often reduced to evaluating the *energy barrier*, loosely defined as the maximal energy of intermediate states in a sequence of local transformations taking a ground state to an orthogonal ground state, minimized over all such possible sequences. This sequence of excited states

mimics the evolution of the system under thermalization and decoding. The intuition (and implicit conjecture) is that the system obeys the phenomenological Arrhenius law which relates the memory time t_{mem} to the energy barrier ΔE^* and the inverse temperature $\beta \equiv 1/k_B T$

$$t_{\text{mem}} \propto e^{\beta \Delta E^*}. \tag{2.1}$$

The Arrhenius law is a useful guiding principle. For classical models, one can intuitively understand the exponentially long (classical) memory time of the ferromagnetic 2D Ising model by realizing that its energy barrier is proportional to the linear system size. Indeed, to go from the all up state to the all down state, one needs to flip a macroscopic droplet of spins whose energy scale with its perimeter. For quantum models, the most widely known example of a self-correcting quantum memory is the 4D Kitaev's toric code [4, 32, 36] whose energy barrier is also proportional to the linear system size.

The scaling energy barrier of a quantum model is intimately related to the geometrical support of operators mapping a ground state to a different orthogonal ground state, called *logical operators*. For the 4D toric code, logical operators are the tensor product of single qubit operators acting on a two-dimensional sheet-like subset of qubits, similar to the logical operator of the 2D Ising model which flips all spins.

While the 4D Kitaev's toric code is self-correcting, it requires addressable long-range interactions if embedded in a lattice of lower dimensionality. Various attempts have been made to decrease the dimensionality of such a self-correcting code, while retaining a large energy barrier of the system [35, 53, 54]. A typical shortcoming of these codes includes sensitivity to perturbations [55], while genuine topological systems are known to be robust [30]. Finding a self-correcting system in three dimensions (or lower) is still an ongoing research direction.

Following the intuition based on the Arrhenius law, it is believed that quantum self-correction requires a *scaling* energy barrier, i.e., an energy barrier that is an increasing function of system size. However, a formal relation between self-correction and a scaling energy barrier has not been established and the Arrhenius law has only be proven for a few models while there are known counterexamples. Moreover, it was recently suggested that there might exist a different kind of protection [44], one that does not require a scaling energy barrier, coined *entropy protection*. The intuition is that while there exist paths in phase space mapping a ground state to an orthogonal ground state while only introducing a constant amount of energy, these paths might not be the typical. Typical paths, however, might require the system

to go through a scaling energy barrier. We could think of such a model as having an effective free energy barrier, i.e., there are free energy valleys in the landscape between the two ground states, and in order to get out of such a valley the system would have to overcome an effective barrier.

In 2014, Brown et al. proposed a local 2D Hamiltonian which seemed to realize entropy protection [48] since its memory time exhibits a super exponential scaling, albeit only in a limited range of temperature. This model consists of a toric code-like structure, where instead of qubits d-level spins (qudits) are placed on the edges of a square lattice. This model also corresponds to the quantum double of $\mathbb{Z}_d$. Its elementary excitations are d different electric and d different magnetic anyons. Specifically, in Ref. [48] $d = 5$, and due to charge-flux duality, it is convenient to think only in terms of e.g., electric charges. Then there are 5 different charges, grouped as vacuum, light particle, heavy particle, heavy antiparticle, and light antiparticle. Particle-antiparticle pairs have the same mass, and furthermore the masses are set such that $m_{\text{heavy}} > 2m_{\text{light}}$ to ensure that thermal evolution of the system favors the decay of a heavy particle into two light particles. The authors of Ref. [48] further introduce defect lines to the system by modifying local terms of the Hamiltonian. When a light particle crosses such a line, it becomes a heavy one and vice versa. This construction results in fractal-like splitting of typical anyon-paths, resembling the fractal geometrical support of logical operators in Haah's cubic code [46, 56]. The authors of Ref. [48] numerically observed a memory time for this entropic code similar to the cubic code, that is, it grows super-exponentially with the inverse temperature ($t_{\text{mem}} \propto \exp(c\beta^2)$). A striking difference between the cubic code and Brown's entropic code is, however, that while the former has an energy barrier that grows logarithmically with system size, the energy barrier of the entropic code is a constant, independent of system size. Thus, Brown's entropic code seems to have a better scaling of memory time than the one predicted by the Arrhenius law. However, it was also remarked that the super-exponential scaling did not remain valid at arbitrarily low temperature, i.e., in the limit of very large β. Thus, Brown's entropic code argues for the possibility of entropy protection but failed to settle the question of whether entropy can protect quantum information and lead to a better scaling of than memory time than the one predicted by Arrhenius law.

Here, we settle this question in the negative by proving that a scaling energy barrier is necessary for self-correction for any quantum double model of an Abelian group, a general framework which contains Brown's entropic code. Thus, entropy cannot protect quantum information in the absence of a scaling energy barrier for those models. Technically, we establish a rigorous version of the Arrhenius law as an

upper bound for the mixing time of quantum doubles of Abelian groups. We prove that the mixing time – defined as the longest time an initial state takes to thermalize to the Gibbs state – and thus the memory time are upper bounded by $\mathrm{poly}(N)\exp(2\beta\overline{\epsilon})$, where N is the size of the system and $\overline{\epsilon}$ is the *generalized energy barrier*. We rigorously define $\overline{\epsilon}$ by a natural quantity arising from our analysis which straightforwardly extends the intuitive notion of energy barrier. Finally, we evaluate the generalized energy barrier and show that it is independent of system size or temperature for two-dimensional Abelian quantum double models. As our bound holds for any temperature, this means that Abelian quantum doubles don't allow for entropy protection, i.e., their memory time can at most scale exponentially with inverse temperature. Our results are based on the method presented in Ref. [3] and are a generalization of the results therein, where the author has derived a similar Arrhenius law bound and energy barrier for any commuting Pauli stabilizer codes in any dimensions.

The paper is organized as follows. In Sec. 2.2.1 and 2.2.2 we introduce the framework of our analysis: the construction of Abelian quantum doubles and the noise model used to simulate the thermal environment. In Sec. 2.3 we present our main result: the upper bound on the mixing time and the formula for the generalized energy barrier, followed by a discussion on the physical interpretation of this result in Sec. 2.4. We present the details of the derivation of the bound in Sec. 2.5. Finally, we conclude with possible future directions in Sec. 2.6.

2.2 Framework

We now introduce the framework in which our result is valid. First, we introduce the systems of interests, i.e., the quantum double of Abelian groups. Second, we model the thermalization of such a system by the Davies map.

2.2.1 Abelian quantum doubles

Abelian quantum doubles are a special case of the quantum double construction introduced by Kitaev [4], where the quantum double is based on the cyclic group $\mathbb{Z}_d$. This was the model investigated in Ref. [48] with $d = 5$, and it is a generalized toric code construction (the toric code is the quantum double of $\mathbb{Z}_2$) acting on d-level spins or *qudits*.

Generalized Pauli operators

We will choose a basis for the Hilbert space of a qudit to be labeled by orthonormal states $\{|\,\ell\rangle\}$ where $\ell \in \mathbb{Z}_d \cong \{0,\ldots,d-1\}$. We introduce the generalized Pauli

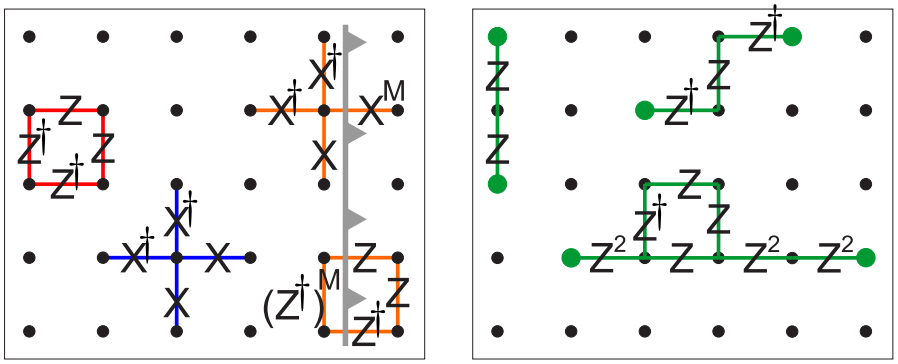

Figure 2.1: (a) Star operator $A(v)$ in blue and plaquette operator $B(p)$ in red. A defect line is shown as a thick gray line traversing the lattice, with the modified star and plaquette operators near such a line in orange. (b) Examples of anyon paths for an Abelian quantum double ($d > 2$).

operators, X^k and Z^k, $k \in \mathbb{Z}_d$. They act on a qudit according to:

$$X^k |\ell\rangle = |\ell \oplus k\rangle, \tag{2.2}$$
$$Z^k |\ell\rangle = \omega^{k\ell} |\ell\rangle, \tag{2.3}$$

where $\oplus$ is the addition modulo d and $\omega^\ell = \exp(i2\pi\ell/d)$, $\ell \in \mathbb{Z}_d$ are the dth roots of unity. The eigenvalues of the Z generalized Pauli operator but also the X generalized Pauli operator are precisely the dth roots of unity. In our convention, the identity is a generalized Pauli operators with $k = 0$. One can straightforwardly derive the following useful identities:

$$X^\dagger = X^{d-1} \quad Z^\dagger = Z^{d-1} \quad Z^{k'} X^k = \omega^{kk'} X^k Z^{k'}. \tag{2.4}$$

Hamiltonian

We now define the Hamiltonian of the quantum double of $\mathbb{Z}_d$ on $2N$ d-level spins or qudits located on the edge of a two dimensional square lattice with N vertices. We define a (generalized) Pauli operator to be a $2N$-tensor product of single-qudit (generalized) Pauli operator X^k or Z^k, $k \in \mathbb{Z}_d$. For convenience, we will henceforth omit the (generalized) modifier. We note $\mathcal{P}_M$ the set of Pauli operators acting non-trivially on at most $M \leq 2N$ qudits. The qudits on which a Pauli operator acts non-trivially are its (geometrical) support.

The local interactions of the Hamiltonian will be Pauli operators supported on four qudits neighboring either a vertex v of the lattice for star operators $A(v)$ or a plaquette p for plaquette operators $B(p)$, see Fig. 2.1(a). A star (and a plaquette) is the union

of four edges or, equivalently, qudits located on those edges. It is convenient to label the qudits around a star + or plaquette □ using the cardinal points: East, South, West, and North. The star operator $A(v)$ for vertex v is

$$A(v_i) = X_E \otimes X_S \otimes X_W^\dagger \otimes X_N^\dagger \quad (E, S, W, N) = +_v \tag{2.5}$$

and the plaquette operator $B(p)$ for plaquette p is

$$B(p) = Z_E \otimes Z_S^\dagger \otimes Z_W^\dagger \otimes Z_N \quad (E, S, W, N) = \square_p. \tag{2.6}$$

The eigenvalues of star and plaquette operators are the dth roots of unity, inherited from the single-qudit Pauli operators. The projector unto the eigenvalue ω^a of the star operator at vertex v is

$$P_v^{a(v)} = \frac{1}{d} \sum_{k=0}^{d-1} (\omega^a A(v))^k. \tag{2.7}$$

Similarly, the projector unto the eigenvalue ω^a of the plaquette operator at plaquette p is

$$Q_p^{b(p)} = \frac{1}{d} \sum_{k=0}^{d-1} (\omega^b B(p))^k. \tag{2.8}$$

Note that those projectors commute since every star operator commute with every plaquette operator.

The Hamiltonian of the $\mathbb{Z}_d$ quantum double is [4, 48]

$$H = \sum_v \sum_{a=0}^{d-1} J_v^{a(v)} P_v^{a(v)} + \sum_p \sum_{b=0}^{d-1} J_p^{b(p)} Q_p^{b(p)}, \tag{2.9}$$

where $J_v^{a(v)}$ and $J_p^{b(p)}$ are non-negative numbers. We set $\forall v, p\ J_v^0 = J_p^0 = 0$ such that a ground state $|\,\Omega\rangle$ is a common +1 eigenvector of all P_v^0 and Q_p^0

$$\forall v, p \quad P_v^0 |\,\Omega\rangle = Q_p^0 |\,\Omega\rangle = +|\,\Omega\rangle. \tag{2.10}$$

The ground space is degenerate whenever this Hamiltonian is defined on a manifold with non-zero genus. For instance, on a square lattice with periodic boundary condition, i.e., a torus, the ground space is d^2-degenerate and can be used to encode quantum information. The positive numbers $J_v^{a(v)}$ and $J_p^{b(p)}$ for non-zero a and b can physically be interpreted as masses of the different excitations of the model, which

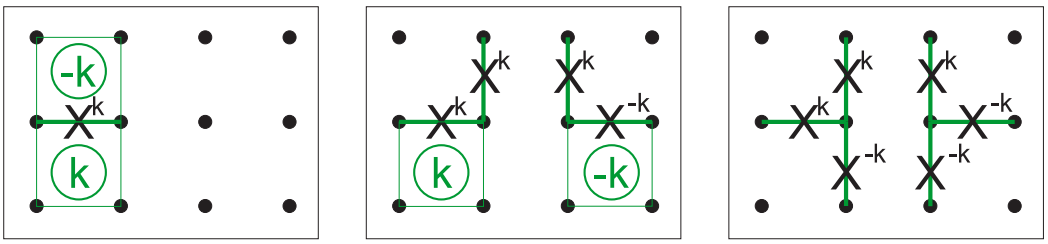

Figure 2.2: (a) Anyon pair created from vacuum, (b) one of the anyons moved and (c) the pair fused back to vacuum, all the while applying local operators.

we now discuss.

Excitations and syndromes

Every spectral projector $P_v^{a(v)}$ and $Q_p^{b(p)}$ are pairwise commuting. Moreover, they commute with the Hamiltonian. Thus, it is convenient to label an energy eigenvector $|\psi\rangle$ using the quantum numbers $\mathbf{a} = \{a_v\}$ and $\mathbf{b} = \{b_p\}$ defined by

$$a_v = \langle\psi|A(v)|\psi\rangle \tag{2.11}$$

$$b_p = \langle\psi|B(p)|\psi\rangle. \tag{2.12}$$

Using the terminology of quantum error correction, we define the *syndrome* of $|\psi\rangle$ by

$$e(|\psi\rangle) = (\mathbf{a}, \mathbf{b}) \in \mathbb{Z}_d^{N+N}. \tag{2.13}$$

Therefore, the Hamiltonian can be diagonalized using the different syndrome values, i.e.,

$$H = \sum_{(\mathrm{a,b})} \epsilon(\mathbf{a}, \mathbf{b})\Pi(\mathbf{a}, \mathbf{b}), \tag{2.14}$$

where the explicit formula for the energies $\epsilon(\mathbf{a}, \mathbf{b})$ and projectors $\Pi(\mathbf{a}, \mathbf{b})$ can be found in Sec. 2.5.1. Let us try to draw a physical picture which will help intuition.

The syndrome of an energy eigenvector is a bookkeeping of the different excitations at every vertex and plaquette. The +1 eigenvectors of $P_v^{a(v)}$ for $a(v) \neq 0$ have a point-like excitation located on the vertex v which we call an electric charge (or chargeon) of type a. Similarly, the +1 eigenvectors of $Q_p^{b(p)}$ for $b(p) \neq 0$ have a point-like excitation located on the plaquette p which we call a magnetic flux (or fluxon) of type b. The ground states of the Hamiltonian have syndrome $(\mathbf{0}, \mathbf{0})$.

Physically, the point-like excitations can (i) be created out of the vacuum by applying a local operator on a ground state, (ii) propagating on the lattice and (iii) annihilating

back to the vacuum by applying a local operator. This can be understood at the level of the syndrome. Consider on a ground state and then apply a generalized Pauli operator X^k on a qudit located on a horizontal edge (see Fig. 2.2). This will modify the eigenvalues of the plaquette operators North and South of that horizontal edge, denoted $B(p_N)$ and $B(p_S)$. Indeed, the resulting state will be a +1 eigenvector of the spectral projectors $Q_{p_N}^{-k}$ and $Q_{p_S}^{k}$. Physically, X^k created a magnetic flux of type k (resp. $-k$) on the South (resp. North) plaquettes. In other words, X^k created a pair of conjugate magnetic fluxes out of the vacuum. Similarly, Z^k would create a pair of conjugate electric charges out of the vacuum. We assign to any generalized Pauli operator $\sigma_{\boldsymbol{\eta}}$ the syndrome $\mathbf{e}(\boldsymbol{\eta})$ of the state $\sigma_{\boldsymbol{\eta}}|\,\Omega\rangle$

$$\mathbf{e}(\boldsymbol{\eta}) = \mathbf{e}(\sigma_{\boldsymbol{\eta}}|\,\Omega\rangle). \tag{2.15}$$

In our examples,

$$e(X^k) = (\mathbf{a} = \mathbf{0}, \mathbf{b} = [0, \ldots, 0, k, -k, 0, \ldots, 0]) \tag{2.16}$$

$$e(Z^k) = (\mathbf{a} = [0, \ldots, 0, k, -k, 0, \ldots, 0], \mathbf{b} = \mathbf{0}). \tag{2.17}$$

Given any energy eigenvector $|\,\psi\rangle$ and any generalized Pauli operator $\boldsymbol{\eta}$, the syndrome of the state $\sigma_{\boldsymbol{\eta}}|\,\psi\rangle$ is obtained by

$$\mathbf{e}(\sigma_{\boldsymbol{\eta}}|\,\psi\rangle) = \mathbf{e}(\boldsymbol{\eta}) \oplus \mathbf{e}(|\,\psi\rangle). \tag{2.18}$$

This very simple addition rule stems for the Abelian structure of the group $\mathbb{Z}_d$ and is related to the fusion rules of the excitations of this Abelian topological model.

Fluxons and chargeons turn out to be (Abelian) anyons, i.e., quasi-particles which are not bosonic nor fermionic. Yet their anyonic nature will not be essential in our work. However, we will from now on use the term anyon to designate a generic point-like excitation (either a fluxon or a chargeon). Moreover, chargeons and fluxons are related by an exact duality which maps the lattice to the dual lattice. Thus, it will often be convenient to focus on a single anyon type, e.g., chargeons in order to simplify our discussion and notations. Also, we would like to introduce a single index s which labels either the vertices or the plaquettes, i.e., $s = v/p$. Thus, any anyon (chargeon or fluxon) is located on a site (vertex or plaquette).

2.2.2 Thermal noise model

The model used in our work to simulate the thermalization process of the quantum double is the Davies map [57, 58], the gold standard for simulating the thermalization

of many body systems [32, 45, 46, 48]. The system is coupled to a bosonic bath and the Hamiltonian of {system+bath} reads

$$H_{\text{full}} = H_{\text{system}} + \chi \sum_{\alpha} S_\alpha \otimes B_\alpha + H_{\text{bath}}, \tag{2.19}$$

where B_α is the operator acting on the bath and $S_\alpha \equiv S^j_{\alpha'}$ is an operator acting on spin j of the system. We consider the weak coupling limit, with $\chi \ll 1$.

The density operator of the system, noted ρ, evolves according to the master equation

$$\frac{d\rho}{dt} = -i[H_{\text{eff}}, \rho] + \mathcal{L}(\rho), \tag{2.20}$$

where H_{eff} is the (Lamb-shifted) system Hamiltonian $H_{\text{eff}} = H_{\text{system}} + \sum_{\alpha,\omega} S^\dagger_\alpha(\omega) S_\alpha(\omega)$ and the Liouvillian is

$$\mathcal{L}(\rho) = \sum_{\alpha,\omega} \gamma_\alpha(\omega) \left(S_\alpha(\omega) \rho S^\dagger_\alpha(\omega) - \frac{1}{2} \{ S^\dagger_\alpha(\omega) S_\alpha(\omega), \rho \}_+ \right). \tag{2.21}$$

The operators governing the evolution of the system in energy space are the spectral jump operators, $S_\alpha(\omega)$. They take the system from energy eigenstate ϵ' to another eigenstate with energy $\epsilon = \epsilon' + \omega$, and have the form

$$S_\alpha(\omega) = \sum_{\epsilon(\mathbf{a},\mathbf{b}) - \epsilon(\mathbf{a}',\mathbf{b}') = \omega} \Pi(\mathbf{a},\mathbf{b}) S_\alpha \Pi(\mathbf{a}',\mathbf{b}'). \tag{2.22}$$

They are the Fourier transforms of $S_\alpha(t)$ (the time-dependent operator acting on the system due to its contact with the thermal bath):

$$S_\alpha(t) = \sum_{(\mathbf{a},\mathbf{b}),(\mathbf{a}',\mathbf{b}')} e^{i\epsilon(\mathbf{a},\mathbf{b})t} \Pi(\mathbf{a},\mathbf{b}) S_\alpha \Pi(\mathbf{a}',\mathbf{b}') e^{-i\epsilon(\mathbf{a}',\mathbf{b}')t}. \tag{2.23}$$

The rate with which a state of the system is taken to another state ω far in energy, by applying the jump operator $S_\alpha(\omega)$ due to its coupling to the thermal bath is the transition rate $\gamma_\alpha(\omega)$. These transition rates obey detailed balance

$$\gamma_\alpha(\omega) = e^{\beta\omega} \gamma_\alpha(-\omega). \tag{2.24}$$

This Liouvillian drives any state towards the Gibbs state

$$\rho_G \propto e^{-\beta H_{\text{system}}}, \tag{2.25}$$

which is its unique fixed point: $\mathcal{L}(\rho_G) = 0$.

Applying the Davies map to a $\mathbb{Z}_d$ quantum double we need to choose an operator basis for the jump operators S_α. For $d = 2$, a possible choice is the Pauli group, while for $d > 2$ it is the generalized Pauli group. We should be careful, since although the elements of the Pauli group are Hermitian, the elements of the generalized group are not: $X^\dagger = X^{d-1}$. We can circumvent this problem by either writing the interaction terms in the full Hamiltonian as $\sigma_{j,\alpha'} \otimes B_\alpha^\dagger + \sigma_{j,\alpha'}^\dagger \otimes B_\alpha$ with $\sigma_{j,\alpha'=(l,m)} = Z_j^l X_j^m$, and thus $S_{j,\alpha'} = Z_j^l X_j^m$ as in the $\mathbb{Z}_2$ case, or by constructing Hermitian jump operators: $S_{j,\alpha'} = 1/\sqrt{2}(\sigma_{j,\alpha'} + \sigma_{j,\alpha'}^\dagger)$. Independent of which choice we make, our results in the following sections are the same.

2.3 Generalized energy barrier

We establish a formerly ill-defined link between the energy barrier of a system and its mixing time for Abelian quantum doubles. We prove a rigorous Arrhenius law upper bound for the mixing time (Sec. 2.3.2, details of the proof in section 2.5), and give a proper definition for the energy barrier appearing in that bound (Sec. 2.3.1). In section 2.3.3 we evaluate this energy barrier for Abelian quantum doubles in two dimensions and find it is a constant independent of system size or temperature.

2.3.1 Definition of the generalized energy barrier

Recall from the introduction that the energy barrier is intuitively related to the decomposition of operators acting non-trivially within the ground space (logical operators) into a sequence of local operators. Surprisingly, the *generalized* energy barrier arising from our analysis is related to the energy cost of building an *arbitrary* Pauli operator. This seems to go against intuition since an arbitrary Pauli operator $\sigma_{\boldsymbol{\eta}} \in \mathcal{P}_{2N}$ can create an extensive amount of energy. However, excitations which appear in the final error configuration $\mathbf{e}(\boldsymbol{\eta})$ created by the Pauli operator will not contribute towards the generalized energy barrier: only intermediate excitations created in the sequential construction of this final error configuration do. Note that if $\sigma_{\boldsymbol{\eta}}$ is a logical operator, the generalized energy barrier coincides with the intuitive energy barrier.

The idea is thus to consider sequences of Pauli operators $\left\{\sigma_{\overline{\boldsymbol{\eta}}^t}\right\}$ which sequentially build the operator $\sigma_{\boldsymbol{\eta}}$ by applying Pauli operators acting on a single qudit. We call such a sequence a *local errors path*. Indeed, we think of $\boldsymbol{\eta}$ as the index of the final error which we sequentially build through single qudit errors such that the error at step t is indexed by $\overline{\boldsymbol{\eta}}^t$.

Definition 2.1 (Local errors path)**.** *A local errors path* $\{\sigma_{\overline{\boldsymbol{\eta}}^t}\}_{t\geq 0}$ *is a sequence of Pauli operators such that*

$$\sigma_{\overline{\boldsymbol{\eta}}^{t=0}} = \mathbb{I} \tag{2.26}$$

$$\textit{locality} \qquad \forall t\ \exists P \in \mathcal{P}_1 \quad \sigma_{\overline{\boldsymbol{\eta}}^{t+1}} = P \cdot \sigma_{\overline{\boldsymbol{\eta}}^t} \tag{2.27}$$

$$\textit{convergence} \qquad \exists\, \sigma_{\boldsymbol{\eta}}, T \quad t > T \Rightarrow \sigma_{\overline{\boldsymbol{\eta}}^t} = \sigma_{\boldsymbol{\eta}}. \tag{2.28}$$

At any intermediate step $t \leq T$, the Pauli operator $\sigma_{\overline{\boldsymbol{\eta}}^t}$ will create a syndrome $\mathbf{e}(\overline{\boldsymbol{\eta}}^t)$ corresponding to a pattern of anyons. At every site, only the energy of an anyon whose charge is different from the one in the syndrome $\mathbf{e}(\boldsymbol{\eta})$ contribute towards the energy barrier. Formally, we define the additional energy of the error indexed by $\overline{\boldsymbol{\eta}}^t$ with respect to the error indexed by $\boldsymbol{\eta}$ as

Definition 2.2 (Additional energy)**.** *Let* $\overline{\boldsymbol{\eta}}^t$ *and* $\boldsymbol{\eta}$ *be indices of two Pauli operators. The additional energy of the error* $\sigma_{\overline{\boldsymbol{\eta}}^t}$ *with respect to the reference operator* $\sigma_{\boldsymbol{\eta}}$ *is*

$$\overline{\epsilon}(\overline{\boldsymbol{\eta}}^t|\boldsymbol{\eta}) = \sum_s J_s^{e_s(\overline{\boldsymbol{\eta}}^t)} \left(1 - \delta_{\mathbf{e}_s(\overline{\boldsymbol{\eta}}^t),0}\right)\left(1 - \delta_{e_s(\overline{\boldsymbol{\eta}}^t),e_s(\boldsymbol{\eta})}\right). \tag{2.29}$$

Note that in Eq. (2.29), summands do not contribute if $e_s(\overline{\boldsymbol{\eta}}^t) = 0$, i.e., if the intermediate error does not create excitations on site s but also if $e_s(\overline{\boldsymbol{\eta}}^t) = e_s(\boldsymbol{\eta})$, i.e., if the intermediate error creates the same excitation on site s as the reference error $\sigma_{\boldsymbol{\eta}}$.

We are now in position to define the generalized energy barrier of an error $\sigma_{\boldsymbol{\eta}}$ and then of the Hamiltonian.

Definition 2.3 (Generalized energy barrier)**.** *Let* $\{\sigma_{\overline{\boldsymbol{\eta}}^t}\}$ *be an arbitrary local errors path converging to the Pauli operator* $\sigma_{\boldsymbol{\eta}} \in \mathcal{P}_{2N}$*. The generalized energy barrier of* $\sigma_{\boldsymbol{\eta}}$ *is*

$$\overline{\epsilon}(\boldsymbol{\eta}) = \min_{\{\sigma_{\overline{\boldsymbol{\eta}}^t}\}\to\sigma_{\boldsymbol{\eta}}} \max_t \overline{\epsilon}(\overline{\boldsymbol{\eta}}^t|\boldsymbol{\eta}). \tag{2.30}$$

The generalized energy barrier of the Hamiltonian H *is*

$$\overline{\epsilon}(H) = \max_{\eta} \overline{\epsilon}(\boldsymbol{\eta}). \tag{2.31}$$

In the next section, we will now introduce the mixing time, an upper bound on the quantum memory time, and then introduce our bound which relates it to the

generalized energy barrier through a formula similar to the Arrhenius law given in Eq. (2.1).

2.3.2 Arrhenius upper bound on the mixing time

We define the mixing time as the time scale after which the evolution of any initial state of the system becomes $\varepsilon = e^{-1/2}$-indistinguishable from the Gibbs state defined by Eq. (2.25). The $\varepsilon = e^{-1/2}$ value is chosen so the relationship between the mixing time and the gap of the Liouvillian will have a convenient form, and the exact value won't modify either the qualitative aspect of our calculations or the scaling of the bound obtained on the mixing time.

Definition 2.4 (Mixing time)**.** *The mixing time of a Liouvillian (whose fixed point is the Gibbs state ρ_G) is*

$$t_{mix}(\varepsilon) = \min\{t \mid t' > t \Rightarrow ||e^{\mathcal{L}t'}\rho_0 - \rho_G||_1 < \varepsilon \ \forall \rho_0\}, \tag{2.32}$$

with $\varepsilon = e^{-1/2}$,

where we used the trace norm, $||A||_1 = \mathrm{Tr}\left[\sqrt{A^\dagger A}\right]$, to measure the (in)distinguishability of two quantum states.

Loosely defining the quantum memory time as the maximal time after which one can recover information about the initial ground state, we immediately see it is upper bounded by the mixing time. Indeed, the Gibbs state treats all ground state on the same footing and thus information about the initial ground state has disappeared. We do not provide a formal definition of the quantum memory time in this work.

Our main result relates the generalized energy barrier to the mixing time through a relation similar to the Arrhenius law.

Theorem 2.5 (Arrhenius bound on mixing time)**.** *For any Abelian group $\mathbb{Z}_d$, for any inverse temperature β, the mixing time of the Davies map Liouvillian of the quantum double of $\mathbb{Z}_d$ is upper bounded by*

$$t_{mix} \leq O\left(\beta N \mu(N) e^{\beta(2\bar{\epsilon}+\Delta)}\right), \tag{2.33}$$

where $2N$ is the number of qudits in the system, Δ is the gap of the system Hamiltonian, $\bar{\epsilon}$ is the generalized energy barrier, and $\mu(N)$ defined by Eq. (2.36) is the length of the longest optimal local errors path.

The derivation of this result can be found in section 2.5. We will now show that for Abelian quantum double, $\bar{\epsilon}$ is bounded by a constant independent of system size in Sec. 2.3.3 and that $\mu(N)$ is bounded by $8N(d-1)$ in Sec. 2.3.4. The right hand side of Eq. (2.33) has a dependence on a low power of N, that does not qualitatively modify the scaling of the mixing time nor the behavior of the system when considered as a candidate for a quantum memory. The important physical quality of this bound is the Arrhenius law scaling. This scaling is not set by the gap of the system Hamiltonian but, more interestingly, by the generalized energy barrier, which we now evaluate.

2.3.3 Generalized energy barrier is constant for Abelian doubles

We will now evaluate the generalized energy barrier of any 2D quantum double of an Abelian group and show that it is a constant, independent of system size, more precisely $2J_{\max}$. While this was known for the $\mathbb{Z}_2$ case [3], we extend it to any $\mathbb{Z}_d$ quantum double. From now on, we consider a $\mathbb{Z}_d$ quantum double, with arbitrary d. Furthermore, we henceforth omit the 'generalized' modifier in (generalized) energy barrier for simplicity.

To evaluate the energy barrier of the Hamiltonian, given by Eq. (2.31), we want to bound the barrier of an arbitrary Pauli operator, given by Eq. (2.30). Thus, we aim to exhibit a local errors path where the additional energy of any intermediate error is a constant. To do so, we will use the following strategy. We will first turn the final error syndrome into a weighted directed graph intuitively corresponding to the worldlines of anyons. Then, we will decompose that graph into cycles and trees. Cycles correspond to pair of conjugate anyons appearing out of the vacuum, propagating and then fusing back to the vacuum. Trees represent propagation of anyons, whose position (resp. word lines) correspond to terminal vertex (resp. edges) of the tree. Finally, using different techniques for cycles and trees, we show how to build the error of each type by moving at most one anyon at a time in a way that the additional energy of any intermediate error involve at most two local terms of the Hamiltonian, resulting in an energy barrier of at most $2J_{\max}$.

Graph corresponding to an error configuration

- *Any error is the product of elementary errors whose supports are disjoint. The energy barrier of the error is the largest energy barrier of its elementary errors.*

  Let's consider an arbitrary error, i.e., a Pauli operator. Its geometrical support, i.e., qudits on which it acts non-trivially, splits into connected components.

We can decompose the global operator into a product of elementary operators, each of which is supported on one connected component. No terms of the Hamiltonian have support which intersects two connected components. Thus, we can choose the local errors path so that elementary errors are built sequentially. In any intermediate error, there is a unique elementary error under construction. The other elementary errors are either not constructed yet, or are already constructed. In either case, they do not contribute towards the energy barrier.

- *Any elementary error can be interpreted as anyons decaying and fusing together, thus forming a fully connected, directed graph with weighted edges. Due to charge conservation, this graph is a flow.*

  The error is a tensor product of single-qudit Pauli operators which create pair of conjugate anyons out of the vacuum, fuse, and move anyons. Thus, to every elementary error, we can associate a graph with weighted edges, often referred to as string-nets in the literature. Such a graph is depicted in Fig. 2.3.

  A terminal vertex, i.e., a vertex of valency 1, is an anyon. It is convenient to label terminal vertices by their anyonic charge, i.e., the value of the syndrome of the elementary error on that site. Other vertices correspond to world lines of anyons. Vertices are linked by an edge of weight k if the errors between them correspond to moving an anyon of charge k along the orientation of the edge. An edge of weight k connecting site i to site j is equivalent to an edge of weight $d - k$ connecting j to i.

  At this point, we have built a directed graph satisfying weight conservation at every vertex. Indeed, weight conservation in the graph is equivalent to charge conservation of the anyons in this Abelian topological model. Such a graph is called a graph flow.

Decomposing the graph into cycles and trees

We now use a well-known result from flow theory: any flow can be partitioned into three sets: a rotational and an irrotational flow and a harmonic component (Helmholtz-Hodge decomposition) [59].

On this discrete geometry of a graph, the rotational flow consist of loops (a.k.a cycles), the irrotational flow consists of trees which can be thought as union of strings, and the harmonic part consist of irrotational flows on the non-contractible cycles.

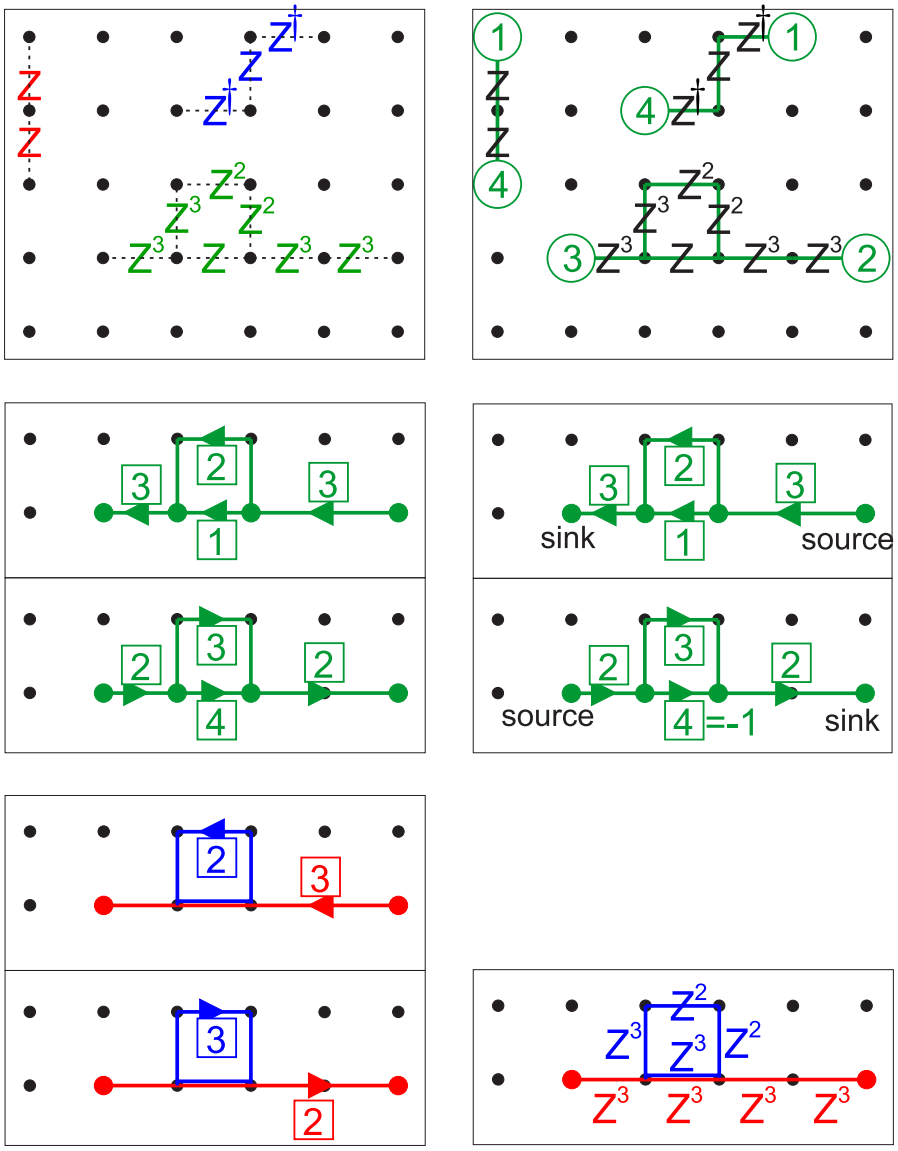

Figure 2.3: Illustration of the steps towards constructing the optimal canonical path for quantum double $\mathbb{Z}_5$: (a) the support of the error can be partitioned into three connected components, colored in red, blue and green; (b) each elementary error can be interpreted as fusions, decays and moving of anyons; (c) an elementary error can be mapped onto a fully connected directed graph with weighted edges (reversing the orientation of an edge changes the weight from k to $d - k$); (d) this can be interpreted as a flow of charges; (e) the flow can be partitioned into a rotational (blue) and irrotational (red) part; and (f) these different partitionings of the flow are all equivalent to applying the same combination of operators in either loops or strings.

This decomposition can be physically interpreted in terms of anyons which we now do in order to evaluate the energy barrier. Remember the rules of the additional energy, defined in Definition. 2.2 : an intermediate error has additional energy if an anyon at a given site is not the anyon created by the reference error. The goal is now to build the reference error by introducing as little additional energy as possible.

Evaluating the energy barrier

Loops correspond to a particle-antiparticle pair appearing out of the vacuum, then propagating and eventually fusing back to the vacuum. Such a configuration can be created by moving two anyons. Thus, loops have an energy barrier corresponding to the energy of two anyons.

We now explain how to construct an error whose support is a tree.

We can consider the tree to be a superposition of strings, each string corresponding to a pair of conjugate anyons which has been created out of the vacuum and then propagated. The terminal vertex of the tree correspond to anyons, conveniently labeled by their anyonic charge. For convenience, choose one of these terminal vertices to be the root of the tree. Other terminal vertices will now be called "leaves". The root is connected to each leaf by a path whose weight is the anyonic charge of the leaf. Each such path is a string operator connecting an anyon (at the leaf) to its conjugate anyon (at the root). See Fig. 2.4 for a graphical example.

We construct the error corresponding to the tree by iteratively choosing a random leaf and then applying the sequence of generalized Pauli operators which create the correct anyon at the site of the leaf and then move its conjugate anyon to the site of the root. We sequentially connect each leaf to the root. During any step, there will be at most two violations, one for the site of the conjugate anyon being moved to the site of the root and one for the anyon at the root which might not have the anyonic charge it should have in the error configuration. At the end of the procedure, the charge of the anyon at the root will be the one it should have in the reference error since the total anyonic charge of the tree is zero. Thus, trees have an energy barrier corresponding to the energy of two anyons, similar to the energy barrier of loops.

We have thus proven the following result:

Theorem 2.6 (Energy barrier of Abelian Quantum Doubles)**.** *For any d, the generalized energy barrier $\overline{\epsilon}$ of the quantum double of $\mathbb{Z}_d$ is at most the energy of two anyons, i.e.,*

$$\overline{\epsilon}(H_{\mathbb{Z}_d}) \leq 2J_{max}. \tag{2.34}$$

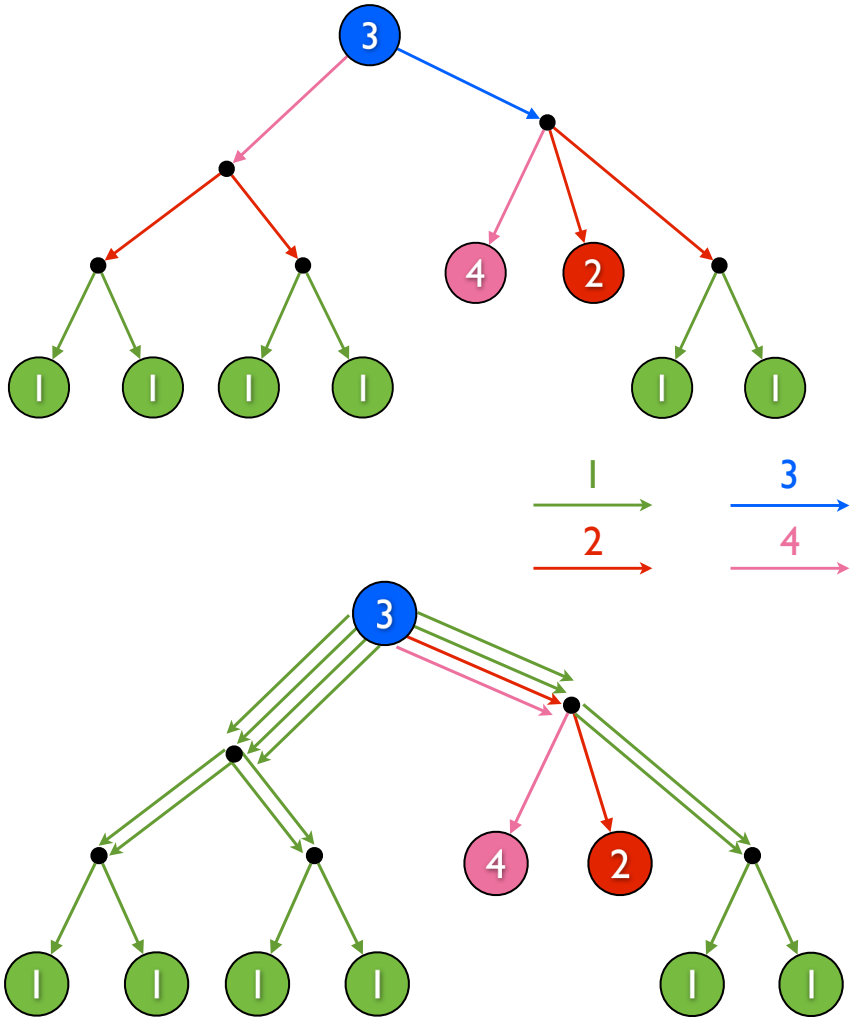

Figure 2.4: Decomposition of a tree into strings for the quantum double of $\mathbb{Z}_5$. The weight of each edge of the graph is represented by a color coding.

2.3.4 Length of the local errors path

We have established in the previous subsections that the optimal local errors path consists of partitioning the error into a product of errors, each of which is supported either on a loop or a union of strings. The question remains what is the length $\mu(N)$, i.e., the number of steps before the local errors path $\left\{\sigma_{\overline{\eta}^t}\right\}$ converges to the reference error σ_{η}. Formally, define $\left|\left\{\sigma_{\overline{\eta}^t}\right\}\right|$ to be the number of operators needed to converge to a reference error σ_{η}. We only consider *optimal* local errors path, i.e., those which realize σ_{η} with the minimal energy barrier. We then define the optimal local length

of an error to be

$$\mu(\boldsymbol{\eta}) = \min_{\substack{\{\sigma_{\overline{\boldsymbol{\eta}}^t}\}\to\sigma_{\boldsymbol{\eta}} \\ \max_t \overline{\epsilon}(\overline{\boldsymbol{\eta}}^t|\boldsymbol{\eta})=\overline{\epsilon}(\boldsymbol{\eta})}} \left|\left\{\sigma_{\overline{\boldsymbol{\eta}}^t}\right\}\right|. \tag{2.35}$$

Then, the quantity which enters in the bound of mixing time, Eq. (2.33) is the maximal optimal local length of errors

$$\mu(N) = \max_{\sigma_{\boldsymbol{\eta}}} \mu(\boldsymbol{\eta}). \tag{2.36}$$

Note that this is constrained optimization: we choose to first minimize the energy barrier and then look at the length of the local errors path realizing that minimum. This choice is dictated by the fact that the energy barrier enters the exponential in Eq. (2.33) whereas the maximal optimal local length of errors μ is only a multiplicative constant. Nonetheless, μ is an extensive quantity since for any error, $\mu(\boldsymbol{\eta})$ is lower-bounded by twice the size of the support of the error (the factor two comes from applying the X and Z part of the error independently). Thus, $4N \leq \mu$.

However, in order to minimize the energy barrier, a given qudit could be affected multiple times by single-qudit operators applied between two intermediate errors. In the language of graph, a given edge of the graph could belong to a large number of loops and trees. Indeed, one has to be careful to avoid such a phenomenon. Here we will show that the loop part of the error can be constructed with a path of length at most $4(d-1)N$ while the string part with a path of length at most $4(d-1)N$; thus the maximal optimal length is $\mu(N) \leq 8(d-1)N$.

Loops

Given a qubit, we want to bound the number of loops which act non-trivially on that qudit. A priori, the number of loops could be very large. However, we can use a simple procedure to reduce it. The idea is to look at the weight of all edges overlapping that qudit and to identify subsets of those weights which sum to 0 modulo d. In that case, we can fuse the corresponding anyons to the vacuum and get new loops which do not affect the qudit. We call this procedure *merging*. An example of merging is presented on Fig. 2.5.

This procedure can be repeated on every qudit independently. The question is then to bound the number of loops at the end of merging. In Appendix 2.A, we investigate this question using multiset theory and find that the maximal number of loops that can remain after merging is $d-1$ (see Thm. 2.9). Thus, after merging, any qudit belongs to at most (d-1) loops of type X and (d-1) loops of type Z. Since there are

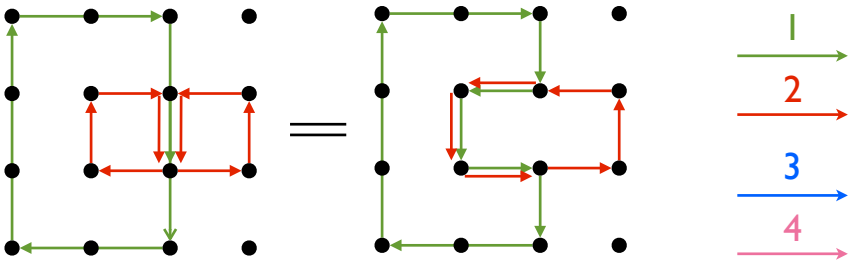

Figure 2.5: Merging of loops at a qudit initially affected by three loops for the quantum double of $\mathbb{Z}_5$. The weight of each edge of the graph is represented by a color coding.

$2N$ qudits,

$$\mu_{\text{loops}} \leq 4(d-1)N. \tag{2.37}$$

Strings

A union of strings – after removing the loops from the structure – form a tree with several "leaves", the leaves corresponding to the end position of anyons.

It will be necessary to introduce a procedure to "prune the tree", i.e., decompose a tree into a superposition of subtrees without introducing new anyons. This pruning procedure was not necessary to prove that the generalized energy barrier is at most $2J_{\max}$, but will prove useful to bound the length of the canonical path.

The pruning procedure identifies subtrees that can be removed from the original tree. Those subtrees should have leaves whose anyonic charge sum to zero modulo d so that they can be removed without affecting the root. Before identifying those subtrees, it is convenient to first "fatten the tree" by connecting every leaf of weight k to the root through a string of weight k. The pruning procedure then proceeds by visiting every vertex of the tree (for instance using a post-order depth first search [1]). At every vertex of the tree, it checks whether there exists a subset of edges with zero-sum. If so, the pruning procedure removes the subtree generated by the corresponding leaves. After visiting every vertex, the pruning stops. The tree is now decomposed into *simple* trees.

Simple trees have at most $d-1$ leaves since any set of d anyons contains a subset whose sum is zero modulo d (see Thm. 2.9). Their depth is thus bounded by $d-1$ Also, every vertex of a simple tree belongs to at most $d-1$ strings.

[1] This specific ordering of the vertices allows to find subtrees with small depth but is not crucial to our argument.

Thus, after pruning, every qudit belongs to at most $(d-1)$ loops of type X and $(d-1)$ loops of type Z. Since there are $2N$ qudits,

$$\mu_{\text{strings}} \leq 4(d-1)N. \tag{2.38}$$

2.3.5 The effect of defect lines

For Abelian quantum double, it is possible to locally modify the Hamiltonian in order to introduce defect lines, such as in the work of Brown et al. [48]. Defect lines are characterized by an invertible element $M \in \mathbb{Z}_d$ and an orientation. An anyon of type $k \in \mathbb{Z}_d$ crossing a defect line of type M along the orientation (resp. against the orientation) will be transformed into an anyon of type $M \cdot k$ (resp. $M^{-1} \cdot k$). What do we mean by "transformed"? Consider two vertices (v_-, v_+) on the lattice, one on each side of the defect line such that the orientation points from v_- to v_+. There exists a local Pauli operator which maps a +1 eigenstate of $P^k_{v_i}$ to a +1 eigenstate of $P^{M\cdot k}_{v_i}$. In other words, an excitation will locally at energy J_k become an excitation carrying energy $J_{M\cdot k}$.

In [48], Brown et al. proposed a local 2D Hamiltonian which seemed to realize entropy protection [48]. This model is the quantum double of $\mathbb{Z}_5$; and due to charge-flux duality, we're allowed to think only in terms of e.g., electric charges. Then there are 5 different charges, grouped as: vacuum, light particle, heavy particle, heavy antiparticle, light antiparticle. Particle-antiparticle pairs have the same mass, furthermore $m_{\text{heavy}} > 2m_{\text{light}}$ to ensure that during the thermal evolution of the system it is favorable for the heavy particles to decay into two light particles. In order to favor the occurrence of heavy particles, the authors of Ref. [48] introduced defect lines of type $M = 2$ to the system. The star and plaquette terms of the Hamiltonian near a defect line are slightly modified in this case, and the modified operators are shown in Fig. 2.1. This changes the dynamics so when a light particle crosses such a line, it becomes a heavy one and vice versa. Thus, the excitations in the model are typically light particles which propagate freely until they eventually cross a defect line, acquire mass, and then decay into two light particles. It was observed numerically in [48] that the memory time seems to behave like $t_{\text{mem}} \propto \exp(c\beta^2)$ over some range of parameters but seems to fail for large β. Can our bound shed new light on this model? To that end, we now analyze the effect of those defect lines on our bounds.

Syndromes for the Hamiltonian with defect lines

One could wonder whether the definition of the energy barrier given by Eq. (2.31) should be changed due to the introduction of defect lines. It does not. However, the Hamiltonian changed and thus the syndromes of Pauli errors will change too. Given a Pauli error $\boldsymbol{\xi} \in \mathcal{P}_{2N}$, its syndrome with respect to the new Hamiltonian $e^{\text{new}}(\boldsymbol{\xi})$ is related to the syndrome $e^{\text{no defect lines}}(\boldsymbol{\xi})$ it had in the absence of defect lines by simply multiplying the syndrome by the *defect line string* $T_1 \in \mathbb{Z}_d^{2N}$,

$$e^{\text{new}}(\boldsymbol{\xi}) = (T_1) \cdot e^{\text{no defect lines}}(\boldsymbol{\xi}), \tag{2.39}$$

where multiplication is understood ditwise and modulo d. The *defect line string* $T_1 \in \mathbb{Z}_d^{2N}$ is defined for every site s by

$$(T_1)_s = \begin{cases} M & \text{if } s \text{ near (and on the "}-\text{" side of) a defect line} \\ 1 & \text{otherwise} \end{cases} . \tag{2.40}$$

Therefore, there is a consistent way to get the syndromes of the quantum double $\mathbb{Z}_d$ with defect lines, and we can use this new set of syndromes to work through the same steps in the derivation as we did for the quantum doubles without defect lines. These two derivations will essentially be identical – except for the different definitions of the syndromes – and we will arrive at the same formula for the energy barrier.

Globally consistent labeling of anyon types in the presence of defect lines

The only remaining question is this: knowing that the definition of the energy barrier is the same with defect lines, does the evaluation of the energy barrier detailed in the previous sections go through the same way? The main issue is how to label the excitations. Indeed, due to the presence of defect lines, the *local* labeling of the anyon type is not consistent *globally*.

Here we explain how to recover a global labeling of anyon types, under one technical condition we call *consistency* of defect lines. We define the consistency of the defect lines of a model by requiring that when we create a pair of anyons from vacuum, then take one of them around any loop anywhere on the lattice, they fuse back to vacuum with each other. Should that transparency condition be violated, the intersection of defect lines would become a sink and a source for single anyons, which we forbid.

Furthermore, we do not know how the Hamiltonian of such a pathological model would be written down in a form similar to Eq. (2.9).

Thus, we consider *consistent* defect lines. Our goal is to take the globally inconsistent, *local* anyon syndromes which is a record of the eigenvalues of the $A(v)/B(p)$ star/plaquette operators at each site, and translate them to a consistent, *global* labeling of anyons. This translation is obtained through a global dictionary $T_2 \in \mathbb{Z}_d$ using the formula

$$e^{\text{global}}(\boldsymbol{\xi}) = (T_2) \cdot e^{\text{local}}(\boldsymbol{\xi}), \tag{2.41}$$

where $\cdot$ is multiplication ditwise and modulo d. To define the global dictionary, the idea is to label each region enclosed by defect lines. The anyon types will be defined in one (arbitrary) reference region and all other regions will carry a label to translate the local anyon type within its region to what it would be in the reference region (global syndrome).

For instance, for $\mathbb{Z}_5$, with $M = 2$ an anyon type a in the reference region might become: a or $2a$ or $4a$ or $8a(= 3a \mod 5)$, depending in which region we observe it. We can name these regions, e.g., $L = 1$, 2, 4 and 3 in the above example. Whenever we observe an anyon whose local type is b in a region with a label L, we know that anyon would have a local type $b' = L^{-1}b$ in the reference region (or any trivial $L = 1$ region). Thus, the T_2 dictionary is defined for every site by

$$(T_2)_s = L^{-1} \quad \text{for } s \in \text{region with label } L. \tag{2.42}$$

Evaluation of the generalized energy barrier and maximum length of the optimal local errors path

Finally, introducing defect lines doesn't change the allowed anyon fusion/decay processes either, since the fusion rules are the same as before in every region. Whenever a particle crosses a defect line it is essentially just renamed, i.e., it doesn't leave behind a charge at the defect line. Using the fact that the syndromes can be made consistent with the procedure of tracing all anyons back to the $L = 1$ regions, any error can still be mapped onto a graph flow of anyons, and the plan for constructing any generalized Pauli error described in Sec. 2.3.3 still works. Thus, the value of the energy barrier and the maximum length of the optimal canonical path is unchanged as well: $\bar{\epsilon} = 2J_{\max}$ and $\mu(N) \leq 8(d-1)N$.

Therefore, as neither the definition of the energy barrier, nor the structure of errors, nor the optimal canonical path for a certain error, nor the length of this path is

changed by defect lines, the Arrhenius law bound itself is unchanged by the defect lines.

2.4 Discussion

2.4.1 Possible improvements

We briefly review some possible improvements on our bounds, indicate possible avenues to achieve those improvements, and conjecture what the optimal bounds would be.

The polynomial dependence of the Arrhenius bound on mixing time can probably be improved. Indeed, we expect that better techniques would allow to get rid of the N prefactor in Eq. (2.33). However, the polynomial dependence of the length of the longest optimal local errors path $\mu \sim N$ is tight since one can find errors whose length are of the order of the number of qudits. Thus, we expect the mixing time to scale with system size. The extensiveness of mixing time is coherent with the intuition that some system relax locally.

However, the quantum memory time might be much shorter than the mixing time. A dramatic example is the three-dimensional toric code whose quantum memory time is constant whereas its mixing time is exponentially long. Indeed, one of the logical operator is string-like whereas the other logical operator is supported on a 2D sheet of qudits. The expectation value of the sheet-like logical operator thermalizes in exponential time whereas the expectation value of the string-like logical operator is short-lived. We expect the quantum memory time of 2D Abelian quantum double to be a constant, independent of system size.

2.4.2 Implication for entropy protection

In [48], authors investigate the quantum memory time of an Abelian quantum double with $d = 5$ with defect lines. By tuning the masses of anyons, they obtain a thermal dynamic in which the typical world lines of anyons have a fractal structure. Indeed, heavy particles, rather than propagate, will (with high probability) decay into two light particles propagating independently; while light particles will eventually cross a defect line, become a heavy particle (at an energy cost), which then decays into two light particles. Brown et al. numerically observe a super-exponential scaling of the memory time which they explain to be the result of this fractal structure of the world lines of excitations. It is called “entropic protection” as the world lines only have a fractal structure and thus there’s a scaling energy barrier for a *typical* worldline of anyons. There are, in fact, world lines taking the system to an orthogonal ground state with only a constant energy cost, however, the probability of such a world line

is entropically suppressed.

Applying the result of the present paper to this model, we can see that its memory time is upper bounded by a strict Arrhenius law, with an energy barrier that has no dependence on temperature or system size, even when including the effect of permuting type defect lines. Since our bound is valid for any value of the inverse temperature β, we can see that the $\exp(c\beta^2)$ scaling observed in Brown's entropic code needs to break down for sufficiently low temperatures, as the memory time can't exceed our bound. This breakdown at low temperature was forecasted in [48]. Indeed, for low temperature the thermal process resulting in fractal-like world lines of anyons is not typical anymore, since the environment can't provide the energy required for a light particle to become heavy. Rather, a light particle near a defect line won't cross, but linger there until it meets with another particle and fuse with it either to vacuum or to a heavy particle. If fused to a heavy particle, that heavy particle can then cross the defect line and lower the energy by becoming a light particle.

The low temperature behavior of Brown's entropic code agrees with the fact that our bound doesn't allow it to have a better than exponential memory time. The scaling observed in Ref. [48] is most likely limited to the region discussed there, and needs to break down for temperatures out of that region.

One question that remains open is whether the super-exponential behavior they observe is an artifact of their construction, e.g., of the decoder or a physical property of the model. Indeed, one could imagine that the introduction of defect lines does change the thermal behavior of the model over some temperature region. The super-exponential scaling could then be understood as an *entropic enhancement*. While this enhancement does not translate into a qualitatively different scaling at low temperature, it could introduce a multiplicative gain inside the exponential scaling. This conjectured scenario is represented on Fig. 2.6.

Our bound, however, is more general than to only exclude the possibility of entropic protection for the specific construction of Brown et al. The result presented in the present paper means that entropic protection doesn't exist for any Abelian quantum doubles (with or without permuting type defect lines); in order to have a self-correcting memory based on such models, one needs a scaling energy barrier. However, we should remark that a scaling energy barrier does not always ensure self-correction, as seen in the example of the welded code [60] which is expected to have a memory time which is independent of system size [45].

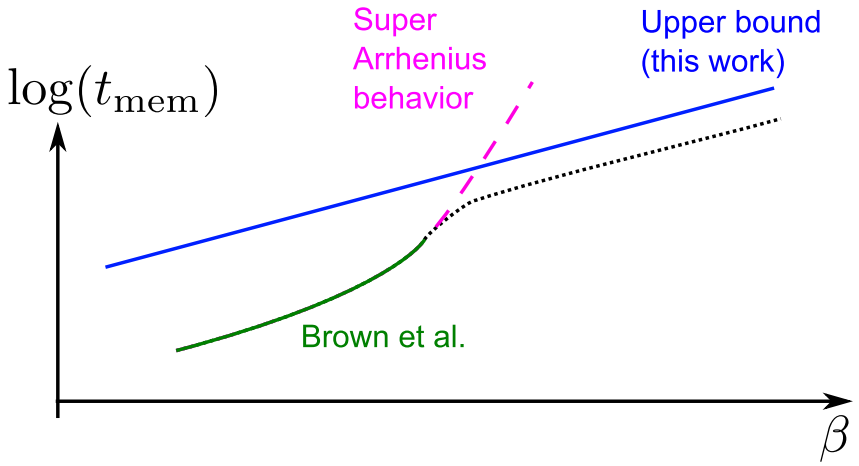

Figure 2.6: Scaling of the logarithm of the quantum memory time t_{mem} as a function of the inverse temperature β. The quadratic scaling ($t_{\text{mem}} \sim e^{c\beta^2}$) numerically observed in [48] (represented schematically by the green curve) cannot extend to arbitrary low temperature due to our upper bound (in blue). Thus, the super-Arrhenius behavior (pink dashed line) will transition to an Arrhenius behavior (black dotted line) for sufficiently low temperature.

2.5 Details of the derivation

The derivation of the upper bound and the generalized energy barrier for the $\mathbb{Z}_d$ generalized case follow the steps outlined in Ref. [3] for the $\mathbb{Z}_2$ model. Although the approach for the $\mathbb{Z}_d$ - Stabilizer models is very similar to the one presented in Ref. [3], the derivation differs in several key steps from $\mathbb{Z}_2$ due to the increased complexity of the model. In this section we present the general approach of the derivation with an emphasis on the differences from the $\mathbb{Z}_2$ case.

To obtain the bound on the thermalization time presented in Eqn. (2.33), we need to take two steps. First, we bound the mixing time t_{mix} in terms of the spectral gap λ of the Davies generator, and then we proceed to prove a lower bound on the spectral gap λ. To obtain the bound on the mixing time in terms of the gap, we employ an upper bound to the convergence in trace norm distance derived in Ref. [61]. For any initial state ρ_0 that evolves according to some semi-group $\rho_t = \exp(t\mathcal{L})\rho_0$, we can bound the distance to its fixed point ρ_G as $||\rho_t - \rho_G||_{tr} \leq \sqrt{||\rho_G^{-1}||}e^{-\lambda t}$. Since the Davies generator converges to the Gibbs state $\rho_G = Z^{-1}\exp(-\beta H)$ we find $||\rho_G^{-1}|| = O(\exp(c_0\beta N))$, with some model specific constant c_0. Given a lower bound $0 < \mu \leq \lambda$ to the spectral gap, this bound would immediately imply an upper bound to the mixing time given by

$$t_{\text{mix}} \leq \mathcal{O}(\beta N \lambda^{-1}) \leq \mathcal{O}(\beta N \mu^{-1}). \tag{2.43}$$

To arrive at a lower bound to the spectral gap of the generator $\mathcal{L}$, we can make use of a variational expression for the spectral gap λ. Since the fixed point of $\mathcal{L}$ is the Gibbs state, and we furthermore know that the Davies generator is Hermitian with respect to a weighted Hilbert-Schmidt inner product [57, 58], we can express the the gap in terms of two quadratic forms. We define the Dirichlet form, $\mathcal{E}(f,f) = -\langle f, \mathcal{L}^*(f)\rangle_\beta = -tr[\rho_G f^\dagger \mathcal{L}^*(f)]$ and the variance, $Var(f,f) = tr[\rho_G f^\dagger f] - |tr[\rho_G f]|^2$. With these two quadratic forms we can express the spectral gap as

$$\lambda = \min_{f \in \mathcal{M}_{d^N}} \frac{\mathcal{E}(f,f)}{Var(f,f)}. \tag{2.44}$$

For a simple proof of this identity the reader is referred to [61–63]. Hence any constant $\mu > 0$ serves as a lower bound to the spectral gap if for all $f \in \mathcal{M}_{d^N}$ the Poincare inequality, $\mu Var(f,f) \leq \mathcal{E}(f,f)$, holds. Naturally, the largest possible μ coincides with λ. We will now use this inequality to derive a lower bound to the spectral gap. Note that this problem can be rephrased as an inequality for positive semi definite matrices. Since both $\mathcal{E}(f,f)$ as well as $Var(f,f)$ are quadratic forms in f, we can define two matrices, $\hat{\mathcal{E}}$ and $\hat{\mathcal{V}}$ that correspond to the matrix representations of these forms. Further using the detailed balance condition we express $\mathcal{E}(f,f) = \text{tr}\left[f^\dagger \hat{\mathcal{E}}(f)\right]$ and $Var(f,f) = \text{tr}\left[f^\dagger \hat{\mathcal{V}}(f)\right]$, where we have now interpreted $\mathcal{M}_{d^N}$ as a Hilbert space with the canonical inner product. In this case the spectral gap can be defined as $\tau = \lambda^{-1}$, where τ is the smallest positive number so that $\tau\hat{\mathcal{E}} - \hat{\mathcal{V}} \geq 0$, here any upper bound to τ constitutes a lower bound to the spectral gap. We perform the following steps to find such an upper bound to τ and in turn the lower bound $\mu = \tau^{-1}$ to the gap. Due to the similarity to the $\mathbb{Z}_2$ case, the reader is referred to a [3] for a more detailed exposition of the steps and proofs of the lemmata we need. We discuss only the particular differences to the binary case in detail here.

2.5.1 Diagonalizing the Hamiltonian, Jump operators

Since the quantum double model is comprised of commuting projectors, it is straight forward to diagonalize the full Hamiltonian (2.9). We diagonalize the pure system Hamiltonian by labeling the projectors for every subspace in terms of the error syndromes assigned to different error configurations introduced in Sec. 2.2.1. In order

to be able to encode quantum information into the ground state of this Hamiltonian, a degeneracy of ground states is required. This can be achieved by defining the square lattice on a surface with non-zero genus or by special boundary conditions.

The diagonalized Hamiltonian can be written as

$$H = \sum_{(\mathrm{a,b})} \epsilon(\mathbf{a},\mathbf{b})\Pi(\mathbf{a},\mathbf{b}), \tag{2.45}$$

with projectors and energies

$$\Pi(\mathbf{a},\mathbf{b}) = \left(\prod_v P_v^{a(v)}\right)\left(\prod_p Q_p^{b(p)}\right), \tag{2.46}$$

$$\epsilon(\mathbf{a},\mathbf{b}) = \sum_v J_v^{a(v)} + \sum_p J_p^{b(p)}, \tag{2.47}$$

where $P_v^{a(v)}$ and $Q_p^{b(p)}$ are the projectors onto different chargeons and fluxons at vertex v and plaquette p introduced before, $J_v^{a(v)}$ and $J_p^{b(p)}$ are the masses corresponding to these anyons. The eigenstates of this Hamiltonian thus correspond to different anyon configurations on the lattice, and the states can be labeled by syndromes of the form $(\mathbf{a},\mathbf{b}) = (a_1, a_2, \ldots a_N, b_1, b_2, \ldots b_N) \in Z_d^{N+N}$.

The diagonalization of H implies that we can write the Gibbs state of the system as

$$\rho_G = \sum_{(\mathbf{a},\mathbf{b})} \rho_{\mathbf{ab}}\Pi(\mathbf{a},\mathbf{b}), \quad \text{where} \quad \rho_{\mathbf{ab}} = \frac{e^{-\beta\epsilon(\mathbf{a},\mathbf{b})}}{Z}. \tag{2.48}$$

Note that the Projectors $\Pi(\mathbf{a},\mathbf{b})$ are obtained as a $\mathbb{Z}_d$ Fourier transform of powers of the star $A(v)$ and plaquette $B(p)$ terms as defined in Fig. 2.1 (a). We can write

$$\Pi(\mathbf{a},\mathbf{b}) = \frac{1}{d^{2N}} \sum_{(\mathbf{x},\mathbf{y})} e^{\frac{2\pi i}{d}(<\mathbf{a},\mathbf{x}>+<\mathbf{b},\mathbf{y}>)} \sigma_{\bar{\mathbf{x}}}\bar{\sigma}_{\bar{\mathbf{y}}}, \tag{2.49}$$

where $\sigma_{\bar{\mathbf{x}}} = A^{x_1}(1)A^{x_2}(2)\cdots A^{x_N}(N)$ and $\bar{\sigma}_{\bar{\mathbf{y}}} = B^{y_1}(1)B^{y_2}(2)\cdots B^{y_N}(N)$. Observe that we have introduced new labels $\bar{\mathbf{x}}$ and $\bar{\mathbf{y}}$, which are linear functions of $\mathbf{x}$ and $\mathbf{y}$ respectively and are defined by the decomposition of $\{A^{x_i}(i)\}$ and $\{B^{y_i}(i)\}$ (which act on vertices and plaquettes) into generalized Pauli operators, i.e., the $\{X_j^{\bar{x}_j}\}$'s and $\{Z_j^{\bar{y}_j}\}$, which act on edges of the model, so that $A^{x_1}(1)A^{x_2}(2)\cdots A^{x_N}(N) = X_1^{\bar{x}_1}X_2^{\bar{x}_2}\cdots X_{2N}^{\bar{x}_{2N}} = \sigma_{\bar{\mathbf{x}}}$ and $B^{y_1}(1)B^{y_2}(2)\cdots B^{y_N}(N) = Z_1^{\bar{y}_1}Z_2^{\bar{y}_2}\cdots Z_{2N}^{\bar{y}_{2N}} = \bar{\sigma}_{\bar{\mathbf{y}}}$.

The jump operators of the Davies generator are generated by generalized Pauli errors acting on a single spin. The commutation relations of single generalized Pauli's with the Hamiltonian projectors (2.46) is given by

$$Z_j^{l_j} X_j^{m_j} \Pi(\mathbf{a}, \mathbf{b}) = \Pi(\mathbf{a} \oplus \mathbf{e}(l_j), \mathbf{b} \oplus \mathbf{e}(m_j)) Z_j^{l_j} X_j^{m_j}, \tag{2.50}$$

where $\mathbf{e}(l_j) = (0, \ldots 0, l_j, -l_j, 0 \ldots 0)$ and $\mathbf{e}(m_j) = (0, \ldots 0, m_j, -m_j, 0 \ldots 0)$ are length N vectors whose only nonzero elements correspond to the vertices at the ends of edge $j = (v, v')$ and the plaquettes (p, p') which contain edge j. Alternatively, $\mathbf{e}(l_j)$ ($\mathbf{e}(m_j)$) is the syndrome of the excited state created by applying the error $Z_j^{l_j}$ ($X_j^{m_j}$) to the vacuum state. That excited state contains two conjugate anyons of charges $\pm l_j$ (of fluxes $\pm m_j$) located on the vertices v and v' (plaquettes (p, p') that contain the edge j).

Star and plaquette operators have one east edge E, one south edge S, one west edge W and one north edge N. Due to the construction of these operators: $A(v) = \{X_E \otimes X_S \otimes X_W^\dagger \otimes X_N^\dagger; (E, S, W, N) \in star(v)\}$ for star operators and $B(p) = \{Z_E \otimes Z_S^\dagger \otimes Z_W^\dagger \otimes Z_N; (E, S, W, N) \subset plaquette(p)\}$ for plaquette operators, a horizontal edge $j = (v, v')$ overlaps with the X operator of the star operator $A(v)$ west of edge j and the $X^\dagger$ operator of the star operator $A(v')$ east of j. (Similarly, a horizontal edge j overlaps with the $Z^\dagger$ operator of the plaquette operator north of j, and Z operator of the plaquette operator south j.) Therefore, one of the nonzero elements in $\mathbf{e}(l_j)$ is $+l_j$ and the other is $-l_j$ ($+m_j$ and $-m_j$ in $\mathbf{e}(m_j)$).

Since the generalized Pauli basis is a complete matrix basis, any one local operator at edge j can be decomposed as $S_{j,(l_j',m_j')} = \sum_{(l_j,m_j)} [s]_{(l_j,m_j)}^{(l_j',m_j')} Z_j^{l_j} X_j^{m_j}$. In order to obtain the jump operators from Eqn. (2.22), we use the commutation relations (2.50) and obtain

$$\begin{aligned} S_{j,(l_j',m_j')}(\omega) \quad = \quad & \sum_{(\mathrm{a,b})} \sum_{(l_j,m_j)} Z_j^{l_j} X_j^{m_j} [s]_{(l_j,m_j)}^{(l_j',m_j')} \Pi(\mathbf{a}, \mathbf{b}) \\ & \times \delta[\omega - \epsilon(\mathbf{a} \oplus \mathbf{e}(l_j), \mathbf{b} \oplus \mathbf{e}(m_j)) + \epsilon(\mathbf{a}, \mathbf{b})], \end{aligned} \tag{2.51}$$

where $\epsilon(\mathbf{a}, \mathbf{b})$ is the energy of the system before, while $\epsilon(\mathbf{a} \oplus \mathbf{e}(l_j), \mathbf{b} \oplus \mathbf{e}(m_j))$ is the energy configuration of the system after applying the thermal errors. Note that for ease of notation we have defined $\delta[x] = 1$, whenever $x = 0$ and $\delta[x] = 0$ otherwise.

We point out a couple of significant differences from the $\mathbb{Z}_2$ case. First, much like the standard Pauli operators the generalized $Z_j^{l_j}$ and $X_j^{m_j}$ generate a complete

local unitary matrix basis, so that any local error can be expressed as a sum of their products. However, these matrices are not Hermitian. This means that the coefficients $[s]^{(l'_j,m'_j)}_{(l_j,m_j)}$ need to obey special constraints to ensure Hermiticity of the coupling operators $S_{j,(l'_j,m'_j)}$. As discussed before we make the particular choice that $S_{j,(l_j,m_j)} = 2^{-1/2}(Z_j^{l_j} X_j^{m_j} + h.c.)$. As we will see, this will eventually result in terms appearing in the Liouvillian that are proportional to $\mathbb{1}_j \Pi(\mathbf{a}, \mathbf{b})$ and terms that are proportional to $Z_j^{2l_j} X_j^{2m_j} \Pi(\mathbf{a}, \mathbf{b})$. We are familiar with the first kind of term from the case of $\mathbb{Z}_2$ -stabilizers. However, the cross terms $Z_j^{2l_j} X_j^{2m_j} \Pi(\mathbf{a}, \mathbf{b})$ do not vanish automatically unless we consider a small lift of the accidental degeneracy in the Hamiltonian spectrum. They disappear when introducing a small spatial perturbation in the masses of different particles, since the delta function $\delta[x]$ vanishes on the slightly perturbed spectrum.

With these derivations for $S_{j,(l'_j,m'_j)}(\omega)$ it is in principle possible to state the Davies generator from Eqn. (2.21) explicitly. Since the Hamiltonian is comprised of only local commuting terms, one can verify that after performing the sum over ω in Eqn (2.21), one is left with a Lindbladian that can be written as the sum of local terms, as done, e.g., in Ref. [64]. Note, however, that we're taking another approach, as the representation mentioned above is not particularly helpful for our derivation of the spectral gap as it obfuscates the underlying general algebraic structure. This structure is best understood in terms of the action of the generator $\mathcal{L}$ on a suitable matrix basis.

2.5.2 Construction of the Dirichlet matrix and the variance matrix

In order to get a good handle on the matrix pair $(\hat{\mathcal{E}}, \hat{\mathcal{V}})$, we need to choose a suitable matrix basis of the space $\mathcal{M}_{d^N}$. It turns out that the canonical choice is also the most suitable. We define the tensor product of the generalized Pauli matrices as our basis through

$$\bar{\sigma}_{\mathbf{k}}\sigma_{\mathbf{p}} = Z_1^{k_1} Z_2^{k_2} \ldots Z_{2N}^{k_{2N}} X_1^{p_1} X_2^{p_2} \ldots X_{2N}^{p_{2N}}, \tag{2.52}$$

where $Z_j^{k_j}$ and $X_j^{p_j}$ are the generalized Pauli matrices introduced in Eqn. (2.2). This matrix basis is orthogonal with respect to the Hilbert-Schmidt inner product, i.e., $\left(\bar{\sigma}_{\mathbf{k}}\sigma_{\mathbf{p}} | \bar{\sigma}_{\mathbf{k}'}\sigma_{\mathbf{p}'}\right) \propto \delta_{k,k'}\delta_{p,p'}$. Here we denote the vectorization of $\bar{\sigma}_{\mathbf{k}}\sigma_{\mathbf{p}}$ by $\left|\bar{\sigma}_{\mathbf{k}}\sigma_{\mathbf{p}}\right)$.

Dirichlet matrix

We first turn to the derivation of the Dirichlet matrix $\hat{\mathcal{E}}$, since this matrix proves to be more challenging. Recall the definition of $\mathcal{E}(f, f) = -tr[\rho_G f^\dagger \mathcal{L}^*(f)]$. Due to

detailed balance, it turns out to be very useful to investigate the action of the map $-\rho_G\mathcal{L}(\cdot)$ on $\bar{\sigma}_{\mathbf{k}}\sigma_{\mathbf{p}}$.

Before we state the action of the generator on a basis element, we need to introduce some shorthand notation. For the syndrome vectors $(\mathbf{a},\mathbf{b})$ and $(\mathbf{c},\mathbf{f})$ and for the error vector $(\mathbf{k},\mathbf{p})$, corresponding to applying the operator $\bar{\sigma}_{\mathbf{k}}\sigma_{\mathbf{p}}$ to the system, we define the functions:

$$\begin{aligned} H^{(\mathbf{k},\mathbf{p})}_{(\mathbf{a},\mathbf{b}),(\mathbf{c},\mathbf{f})} &= \gamma(\omega^{(\mathbf{k},\mathbf{p})}(\mathbf{a},\mathbf{b})\delta[\omega^{(\mathbf{k},\mathbf{p})}(\mathbf{a},\mathbf{b})-\omega^{(\mathbf{k},\mathbf{p})}(\mathbf{c},\mathbf{f})], \\ \tilde{H}^{(\mathbf{k},\mathbf{p})}_{(\mathbf{a},\mathbf{b}),(\mathbf{c},\mathbf{f})} &= \gamma(\omega^{(\mathbf{k},\mathbf{p})}(\mathbf{a},\mathbf{b}))+\gamma(\omega^{(-\mathbf{k},-\mathbf{p})}(\mathbf{a},\mathbf{b}))+\gamma(\omega^{(\mathbf{k},\mathbf{p})}(\mathbf{c},\mathbf{f}))+\gamma(\omega^{(-\mathbf{k},-\mathbf{p})}(\mathbf{c},\mathbf{f})). \end{aligned}$$

We have introduced the Bohr frequencies $\omega^{(\mathbf{k},\mathbf{p})}(\mathbf{a},\mathbf{b}) = \epsilon(\mathbf{a}\oplus\mathbf{e}(\mathbf{k}),\mathbf{b}\oplus\mathbf{e}(\mathbf{p}))-\epsilon(\mathbf{a},\mathbf{b})$. Moreover, it proves convenient to introduce an additional short hand for syndromes that are modified by an additional error as $(\mathbf{a},\mathbf{b})^{(\mathbf{k},\mathbf{p})} = (\mathbf{a}\ominus\mathbf{e}(\mathbf{k}),\mathbf{b}\ominus\mathbf{e}(\mathbf{p}))$.

With this notation at hand, we can state an explicit representation of the action of the generator on the generalized Pauli basis element, so that

$$\begin{aligned} -\rho_G\mathcal{L}(\bar{\sigma}_{\mathbf{k}}\sigma_{\mathbf{p}}) &= \sum_{(\mathbf{a},\mathbf{b})}\sum_{j,(l_j,m_j)}\rho_{\mathbf{ab}}\frac{1}{2}\Pi(\mathbf{a},\mathbf{b})\bar{\sigma}_{\mathbf{k}}\sigma_{\mathbf{p}} \\ &\times \left(H^{(-l_j,-m_j)}_{(\mathbf{a},\mathbf{b})^{(\mathbf{k},\mathbf{p})},(\mathbf{a},\mathbf{b})}e^{\frac{2\pi i}{d}(p_jl_j-k_jm_j)}+H^{(l_j,m_j)}_{(\mathbf{a},\mathbf{b})^{(\mathbf{k},\mathbf{p})},(\mathbf{a},\mathbf{b})}e^{\frac{2\pi i}{d}(k_jm_j-p_jl_j)}-\frac{1}{2}\tilde{H}^{(l_j,m_j)}_{(\mathbf{a},\mathbf{b})^{(\mathbf{k},\mathbf{p})},(\mathbf{a},\mathbf{b})}\right). \end{aligned} \tag{2.53}$$

Recall that we can express the projector $\Pi(\mathbf{a},\mathbf{b})$ in terms of a $\mathbb{Z}_d$ Fourier transform over a particular subset of generalized Pauli operators. This in particular means, that we can express the action of $\mathcal{L}$ on any generalized Pauli again as a linear combination of the same basis elements. Hence, we can read off the matrix elements in this basis directly. Since the Dirichlet matrix is essentially given by $-\rho_G\mathcal{L}$, we can state it directly in the basis $\{|\bar{\sigma}_{\mathbf{k}}\sigma_{\mathbf{p}})\}$ and obtain

$$\begin{aligned} \hat{\mathcal{E}} &= \frac{1}{d^{2N}}\sum_{j,(l_j,m_j)}\sum_{(\mathbf{a},\mathbf{b})}\sum_{(\mathbf{k},\mathbf{p})}\sum_{(\mathbf{x},\mathbf{y})}e^{\frac{2\pi i}{d}(<\mathbf{a},\mathbf{x}>+<\mathbf{b},\mathbf{y}>)}e^{-\frac{2\pi i}{d}<\mathbf{k},\bar{\mathbf{x}}>}\,|\bar{\mathbf{y}}\oplus\mathbf{k},\bar{\mathbf{x}}\oplus\mathbf{p})\,(\mathbf{k},\mathbf{p}| \\ &\times \frac{1}{2}\left(\frac{1}{2}\tilde{H}^{(l_j,m_j)}_{(\mathbf{a},\mathbf{b})^{(\mathbf{k},\mathbf{p})},(\mathbf{a},\mathbf{b})}-H^{(l_j,m_j)}_{(\mathbf{a},\mathbf{b})^{(\mathbf{k},\mathbf{p})},(\mathbf{a},\mathbf{b})}\theta_{(\mathbf{k},\mathbf{p}),(l_j,m_j)}-H^{(-l_j,-m_j)}_{(\mathbf{a},\mathbf{b})^{(\mathbf{k},\mathbf{p})},(\mathbf{a},\mathbf{b})}\theta_{(\mathbf{k},\mathbf{p}),(-l_j,-m_j)}\right)\rho_{\mathbf{ab}}, \end{aligned} \tag{2.54}$$

where $\theta_{(\mathbf{k},\mathbf{p}),(l_j,m_j)} = e^{\frac{2\pi i}{d}(k_jm_j-p_jl_j)}$.

Variance matrix

If we now turn to the second matrix $\hat{\mathcal{V}}$, note that the variance $Var(f,f)$ can be interpreted as the Dirichlet form of a completely depolarizing semi-group on $\mathcal{M}_{d^N}$. That is we can introduce the depolarizing generator $\mathcal{D}(f) = \rho_G tr[f] - f$. So that we can write $Var(f,f) = -\mathrm{t}r\left[\rho_G f^\dagger \mathcal{D}(f)\right]$. Recall that the trace can be expressed as a twirl over generalized Pauli matrices as $tr[f] = d^{-N}\sum_{\mathbf{kp}}(\bar{\sigma}_{\mathbf{k}}\sigma_{\mathbf{p}})^\dagger f \bar{\sigma}_{\mathbf{k}}\sigma_{\mathbf{p}}$. This identity proves quite useful in the derivation of the matrix representation of $Var(f,f)$. Following the same approach, as outlined in [3], we can derive the matrix representation $\hat{\mathcal{V}}$ of the variance much like the Dirichlet matrix and obtain

$$\begin{aligned}\hat{\mathcal{V}} &= \frac{1}{d^N}\frac{1}{d^{2N}}\sum_{(\nu,\kappa)}\sum_{(\mathbf{a},\mathbf{b})}\sum_{(\mathbf{k},\mathbf{p})}\sum_{(\mathbf{x},\mathbf{y})} e^{\frac{2\pi i}{d}(<\mathbf{a},\mathbf{x}>+<\mathbf{b},\mathbf{y}>)} \\ &\times \left(\rho_{\mathbf{ab}}\rho_{(\mathbf{a},\mathbf{b})^{(-\nu,-\kappa)}} - \rho_{\mathbf{ab}}\rho_{(\mathbf{a},\mathbf{b})^{(-\nu,-\kappa)}}\theta_{(\mathbf{k},\mathbf{p}),(\nu,\kappa)}\right)|\bar{\mathbf{y}}\oplus\mathbf{k},\bar{\mathbf{x}}\oplus\mathbf{p})(\mathbf{k},\mathbf{p}|\,.\end{aligned} \tag{2.55}$$

Dirichlet and variance matrices in the dual basis

Note that the Dirichlet matrix and the Variance matrix are formally very similar. A central difference however is that the sum over (ν,κ) in the definition of $\hat{\mathcal{V}}$ is taken over the full matrix basis $\bar{\sigma}_\nu\sigma_\kappa = Z_1^{\nu_1}Z_2^{\nu_2}\cdots Z_{2N}^{\nu_{2N}}X_1^{\kappa_1}X_2^{\kappa_2}\cdots X_{2N}^{\kappa_{2N}}$. This is considerably different from the sum over $(j,(l_j,m_j))$ in the Dirichlet matrix $\hat{\mathcal{E}}$. This sum is constrained to run only over all local operators acting only on a single site. Hence $\hat{\mathcal{V}}$ contains considerably more summands than $\hat{\mathcal{E}}$. It is now the central challenge to show that despite this larger number of summands the span of $\hat{\mathcal{V}}$ lies well within the span of $\hat{\mathcal{E}}$ and the matrix can be supported with a small τ. The structural similarity becomes even more evident, when we perform a convenient basis transformation. We consider the dual basis of the commuting subgroup generated by the projectors in the quantum double Hamiltonian:

$$\left|(\mathbf{a},\mathbf{b})_{(\mathbf{k}_0,\mathbf{p}_0)}\right) = \frac{1}{d^N}\sum_{(\mathbf{x},\mathbf{y})} e^{\frac{2\pi i}{d}(<\mathbf{a},\mathbf{x}>+<\mathbf{b},\mathbf{y}>)}e^{-\frac{2\pi i}{d}<\mathbf{k}_0,\bar{\mathbf{x}}>}|\bar{\mathbf{y}}\oplus\mathbf{k}_0,\bar{\mathbf{x}}\oplus\mathbf{p}_0)\,. \tag{2.56}$$

Note that every dual vector that starts from some particular reference state labeled by $(\mathbf{k},\mathbf{p})$, is orthogonal to all other dual states which is not contained within the left action of the commuting generator group of the Hamiltonian. That is, every dual space spanned $\left|(\mathbf{a},\mathbf{b})_{(\mathbf{k}_0,\mathbf{p}_0)}\right)$ is orthogonal to the one spanned by $\left|(\mathbf{a},\mathbf{b})_{(\mathbf{k}_0',\mathbf{p}_0')}\right)$ if we can't find a $\bar{\sigma}_{\bar{\mathbf{y}}}\sigma_{\bar{\mathbf{x}}}$ so that $\bar{\sigma}_{\mathbf{k}_0'}\sigma_{\mathbf{p}_0'} \propto \bar{\sigma}_{\bar{\mathbf{y}}}\sigma_{\bar{\mathbf{x}}}\bar{\sigma}_{\mathbf{k}_0}\sigma_{\mathbf{p}_0}$. Hence we have a natural

decomposition of the matrix algebra into dual basis sets. Now, we furthermore introduce the states

$$\left|-^{(\nu,\kappa)}_{\mathbf{ab}_{(\mathbf{kp})_0}}\right) = \frac{1}{\sqrt{2}}\left(\left|(\mathbf{a},\mathbf{b})_{(\mathbf{k}_0,\mathbf{p}_0)}\right) - \theta_{(\mathbf{k}_0,\mathbf{p}_0),(-\nu,-\kappa)}\left|(\mathbf{a},\mathbf{b})^{(-\nu,-\kappa)}_{(\mathbf{k}_0,\mathbf{p}_0)}\right)\right), \tag{2.57}$$

where $\theta_{(\mathbf{k}_0,\mathbf{p}_0),(\nu,\kappa)} = e^{\frac{2\pi i}{d}(<\mathbf{k}_0,\kappa>-<\mathbf{p}_0,\nu>)}$, and recall the short hand notation $(\mathbf{a}\oplus\mathbf{e}(\nu),\mathbf{b}\oplus\mathbf{e}(\kappa)) = (\mathbf{a},\mathbf{b})^{(-\nu,-\kappa)}$.

With these vectors at hand, we can write the variance matrix as the direct sum over the orthogonal sets of the dual basis vectors as $\hat{\mathcal{V}} = \bigoplus_{(\mathbf{kp})_0}\hat{\mathcal{V}}_{(\mathbf{kp})_0}$, where every summand is positively weighted sum of projectors on to the $\left|-^{(\nu,\kappa)}_{\mathbf{ab}_{(\mathbf{kp})_0}}\right)$ so that

$$\hat{\mathcal{V}}_{(\mathbf{kp})_0} = \frac{1}{d^N}\sum_{(\nu,\kappa)}\sum_{(\mathbf{a},\mathbf{b})}\rho_{\mathbf{ab}}\rho_{(\mathbf{a},\mathbf{b})^{(-\nu,-\kappa)}}\left|-^{(\nu,\kappa)}_{\mathbf{ab}_{(\mathbf{kp})_0}}\right)\left(-^{(\nu,\kappa)}_{\mathbf{ab}_{(\mathbf{kp})_0}}\right|. \tag{2.58}$$

If we transform the Dirichlet matrix into the same dual basis, we observe the same block diagonal structure over $\hat{\mathcal{E}} = \bigoplus_{(\mathbf{kp})_0}\hat{\mathcal{E}}_{(\mathbf{kp})_0}$. One central difference to the variance is that the resulting matrices $\hat{\mathcal{E}}_{(\mathbf{kp})_0}$ cannot always be expressed as a sum of projectors. The resulting matrices $\hat{\mathcal{E}}_{(\mathbf{kp})_0}$ have more weight on the diagonal. However, we can find other matrices that lower bound them in a semi-definite sense so that $\hat{\mathcal{E}}_{(\mathbf{kp})_0} \geq \hat{\mathcal{E}}'_{(\mathbf{kp})_0}$, where $\hat{\mathcal{E}}'_{(\mathbf{kp})_0}$ is a sum of projectors. Note that when employing this bound we only worsen our estimate of τ. The lower bound $\hat{\mathcal{E}}'_{(\mathbf{kp})_0}$ is now of the desired form so that we can write after a similar calculation:

$$\hat{\mathcal{E}}'_{(\mathbf{kp})_0} = \frac{1}{4}\sum_{j,(l_j,m_j)}\sum_{(\mathbf{a},\mathbf{b})}\rho_{\mathbf{ab}}\gamma(\omega^{(l_j,m_j)}(\mathbf{a},\mathbf{b}))\left|-^{(l_j,m_j)}_{\mathbf{ab}_{(\mathbf{kp})_0}}\right)\left(-^{(l_j,m_j)}_{\mathbf{ab}_{(\mathbf{kp})_0}}\right|. \tag{2.59}$$

2.5.3 Bounds on the gap (comparison theorem and canonical paths)

We have constructed the pair $(\hat{\mathcal{E}}',\hat{\mathcal{V}})$ in a suitable basis. It is our goal to find a sufficiently small constant τ so that the positive semi-definite matrix inequality $\tau\hat{\mathcal{E}}'-\hat{\mathcal{V}}\geq 0$ holds. Since both matrices are jointly block diagonal, we can compare them block-by-block, i.e., find $\tau_{(\mathbf{kp})_0}$ for every $(\mathbf{k}_0,\mathbf{p}_0)$ so that $\tau_{(\mathbf{kp})_0}\hat{\mathcal{E}}'_{(\mathbf{kp})_0}-\hat{\mathcal{V}}_{(\mathbf{kp})_0}\geq 0$ and simply choose τ to be the largest $\tau_{(\mathbf{kp})_0}$. This problem can be solved using a framework which is called support theory [65, 66]. This framework was used in Ref. [3], to derive an upper bound on τ for a matrix pair, which is very similar to the one presented here. The fact that we can generalize theorem 11 in [3] to quantum

doubles is a consequence of the following observation:

We have pointed out earlier that $\hat{\mathcal{E}}'_{(\mathbf{kp})_0}$ and $\hat{\mathcal{V}}_{(\mathbf{kp})_0}$ are structurally very similar in that both matrices are positively weighted sums of rank one projectors $|-^{(\nu,\kappa)}_{\mathbf{ab}_{(\mathbf{kp})_0}})(-^{(\nu,\kappa)}_{\mathbf{ab}_{(\mathbf{kp})_0}}|$. The difference, however, lies in the fact that for $\hat{\mathcal{E}}'_{(\mathbf{kp})_0}$ we only sum over projectors that stem from single site Pauli operators labeled by (l_j, m_j) for $j = 1 \dots N$, whereas in $\hat{\mathcal{V}}_{(\mathbf{kp})_0}$ we sum over projectors that come from the full generalized Pauli algebra. The sum in $\hat{\mathcal{V}}_{(\mathbf{kp})_0}$ is therefore significantly bigger. However, the algebra that can be constructed in both cases is the same. We can construct every generalized Pauli $\bar{\sigma}_\nu \sigma_\kappa$ from the the product of single site generalized Pauli so that $\bar{\sigma}_\nu \sigma_\kappa = \bar{\sigma}_{l^1} \dots \bar{\sigma}_{l^{|\nu|}} \sigma_{m^1} \dots \sigma_{m^{|\kappa|}}$. A local error path for a generalized Pauli $\bar{\sigma}_\nu \sigma_\kappa$ is a sequence of generalized Pauli operators starting from the identity $(\nu^0, \kappa^0) = 0$ with $((\nu^0, \kappa^0), (\nu^1, \kappa^1), \dots, (\nu^t, \kappa^t), \dots, (\nu, \kappa))$ and terminating in (ν, κ), so that any subsequent configurations along the path (ν^t, κ^t) and $(\nu^{t+1}, \kappa^{t+1})$ only differ by a single site generalized Pauli operator (see 2.1). With such a decomposition of generalized Pauli operators at hand, observe that any vector $|-^{(\nu,\kappa)}_{\mathbf{ab}_{(\mathbf{kp})_0}})$ can be decomposed in single site vectors $\left|-^{(l_j,m_j)}_{\mathbf{ab}_{(\mathbf{kp})_0}}\right)$ as

$$|-^{(\nu,\kappa)}_{\mathbf{ab}_{(\mathbf{kp})_0}}) = \sum_{t=0}^{t_{max}-1} \theta_{(\mathbf{k}_0,\mathbf{p}_0),(-\nu^{t+1},-\kappa^{t+1})} |-^{(l^{t+1},m^{t+1})}_{(\mathbf{a},\mathbf{b})^{(-\nu^t,-\kappa^t)}_{(\mathbf{kp})_0}}), \tag{2.60}$$

where the labels $(\nu^{t+1}, \kappa^{t+1})$ and (ν^t, κ^t) differ by the single site labels (l^{t+1}, m^{t+1}). This decomposition lies at the center of the comparison theorem 11 in Ref. [3].

In order to state the result of this comparison theorem, we need to define quantum canonical paths. Observe that the decomposition in Eqn. (2.60) not only depends on the partially constructed Pauli, but also on the syndromes, or the excitations the path starts from initially. To obtain a valid decomposition we need to keep track of the excitations as well. We therefore define a *q*uantum canonical path to consist of a series of labels

$$\hat{\eta}_{(\mathbf{a},\mathbf{b})} = [\{(\mathbf{a}, \mathbf{b}), 0\}, \{(\mathbf{a}, \mathbf{b})^{(-\nu^1,-\kappa^1)}, (\nu^1, \kappa^1)\}, \dots \{(\mathbf{a}, \mathbf{b})^{-\boldsymbol{\eta}}, \boldsymbol{\eta}\}], \tag{2.61}$$

where the first of the labels $(\mathbf{a}, \mathbf{b})$ correspond to syndromes (excitations) and the second label $\boldsymbol{\eta} = (\nu, \kappa)$ corresponds to a partially constructed generalized Pauli operator. While edges correspond to single qudit errors present in the Dirichlet

form, the whole path corresponds to a general error appearing in the variance. That is, at each link $\hat{\xi} = [\{(\mathbf{a},\mathbf{b})^{(-\nu^k,-\kappa^k)}, (\nu^k,\kappa^k)\}, \{(\mathbf{a},\mathbf{b})^{-(\nu^k\oplus l^{k+1},\kappa^k\oplus m^{k+1})}, (\nu^k\oplus l^{k+1}, \kappa^k \oplus m^{k+1})\}]$ two subsequent Pauli operators differ only by a single site operator. Assume now we choose for every syndrome (set of excitations) $(\mathbf{a},\mathbf{b})$ and every generalized Pauli $\boldsymbol{\eta}$ a canonical path $\hat{\eta}_{(\mathbf{a},\mathbf{b})}$. Even though the quality of the bound strongly depends on the particular choice of this decomposition, we acquire valid bounds for any choice of $\hat{\eta}_{(\mathbf{a},\mathbf{b})}$. We have now all components in place to follow the proof of theorem 11 in Ref. [3]. With a simple additional bound on the maximum length of canonical paths we obtain the upper bound on τ as:

$$\tau \leq \max_{\hat{\xi}} \frac{4\mu(N)}{d^N \rho_{\mathbf{ab}} \gamma(\omega^{(l,m)}(\mathbf{a},\mathbf{b}))} \sum_{\hat{\eta}_{(\mathbf{a}',\mathbf{b}')} \ni \hat{\xi}} \rho_{\mathbf{a}'\mathbf{b}'} \rho_{(\mathbf{a}',\mathbf{b}')^{-\boldsymbol{\eta}}}. \tag{2.62}$$

The maximum is taken over all possible edges $\hat{\xi}$. The sum is taken over all canonical paths $\hat{\eta}_{(\mathbf{a}',\mathbf{b}')}$ that traverse the edge $\hat{\xi}$. That is we sum over syndromes $(\mathbf{a}',\mathbf{b}')$ and errors η that contain the edge $\hat{\xi}$ in their canonical path $\hat{\eta}_{(\mathbf{a}',\mathbf{b}')}$. Moreover observe that the bound also depends on the length $\mu(N)$ of the largest canonical path which has been analyzed in section 2.3.4. We pause to observe that this bound is very similar to the canonical paths bound for graph Laplacians as given derived in [62, 63, 67]. However this bound has been obtained for a full quantum mechanical semi-group and the paths are constructed from the multiplication rules of a matrix algebra.

2.5.4 Evaluation of the bound and the generalized energy barrier

The similarity of this bound to the classical canonical paths gives rise to a convenient way of evaluating the upper bound in Eqn. (2.62). We use the approach introduced in Ref. [67]. To evaluate the bound we need to introduce a map Φ_ξ that maps any $\hat{\eta}_{(\mathbf{a},\mathbf{b})}$ that makes use of the link $\hat{\xi} = [\{(\mathbf{a},\mathbf{b})^{-\boldsymbol{\xi}}, \boldsymbol{\xi}\}, \{(\mathbf{a},\mathbf{b})^{-(\boldsymbol{\xi}\oplus(l,m))}, \boldsymbol{\xi}\oplus(l,m)\}]$ to a corresponding Pauli. We define this map through

$$\Phi_\xi(\hat{\eta}_{(\mathbf{a},\mathbf{b})}) = \boldsymbol{\eta} \ominus \boldsymbol{\xi}. \tag{2.63}$$

Note that this map from the set of paths into the set of generalized Paulis is injective. This means that given the edge $\hat{\xi}$ and the image $\Phi_\xi(\hat{\eta}_{(\mathbf{a},\mathbf{b})})$ we can trivially recover the path through $\boldsymbol{\eta} = \Phi_\xi(\hat{\eta}_{(\mathbf{a},\mathbf{b})}) \oplus \boldsymbol{\xi}$ and the error syndrome $(\mathbf{a},\mathbf{b})$, since this pair uniquely identifies a path. We can now apply the argument of Ref. [67], and try to find a constant $\overline{\epsilon}$ so that for all edges $\hat{\xi}$ and all paths $\hat{\eta}_{(\mathbf{a},\mathbf{b})}$ the following inequality

holds

$$\frac{\rho_{\mathbf{a}'\mathbf{b}'}\rho_{(\mathbf{a}',\mathbf{b}')^{-\boldsymbol{\eta}}}}{\gamma(\omega^{(l,m)}(\mathbf{a},\mathbf{b}))\rho_{\mathbf{ab}}} \leq \frac{\exp(2\beta\bar{\epsilon})}{\gamma^*}\rho_{(\mathbf{a}',\mathbf{b}')^{\Phi_{\hat{\xi}}(\hat{\eta}_{(\mathbf{a}',\mathbf{b}')})}}. \tag{2.64}$$

We have denoted γ^* to correspond to the smallest value of $\gamma(\omega^{(l,m)}(\mathbf{a},\mathbf{b}))$ over all permitted transitions. Such a constant can be found and we define

$$\bar{\epsilon} = \max_{\hat{\eta}_{(\mathbf{a}',\mathbf{b}')}} \bar{\epsilon}(\hat{\eta}_{(\mathbf{a}',\mathbf{b}')}), \tag{2.65}$$

where for every error we have that

$$\bar{\epsilon}(\hat{\eta}_{(\mathbf{a}',\mathbf{b}')}) = \max_{\hat{\xi}\in\hat{\eta}_{(\mathbf{a}',\mathbf{b}')}} \left(\epsilon((\mathbf{a}',\mathbf{b}')^{-\boldsymbol{\xi}}) + \epsilon((\mathbf{a}',\mathbf{b}')^{\boldsymbol{\xi}\ominus\boldsymbol{\eta}}) - \epsilon((\mathbf{a}',\mathbf{b}')) - \epsilon((\mathbf{a}',\mathbf{b}')^{-\boldsymbol{\eta}})\right).$$

In fact, the constant $\bar{\epsilon}$ was chosen directly so that the inequality above is satisfied for all paths and all edges. This inequality can be now used to estimate an upper bound to Eqn. (2.62), and we find that for all $\hat{\xi}$

$$\tau \leq \frac{4\mu(N)}{\gamma^*}\exp(2\beta\bar{\epsilon})\max_{\hat{\xi}}\sum_{\hat{\eta}_{(\mathbf{a}'\mathbf{b}')}\ni\hat{\xi}}\frac{\rho_{(\mathbf{a}',\mathbf{b}')^{-\Phi_{\hat{\xi}}(\hat{\eta}_{(\mathbf{a}'\mathbf{b}')})}}}{d^N}. \tag{2.66}$$

Since the map Φ_{ξ} is injective for every edge $\hat{\xi}$, we can only reach a subset of all generalized Pauli operators. Hence, we may bound the sum over this subset by summing over every generalized Pauli, so that we may bound

$$\sum_{\hat{\eta}_{(\mathbf{a}'\mathbf{b}')}\ni\hat{\xi}}\frac{1}{d^N}\rho_{(\mathbf{a}',\mathbf{b}')^{-\Phi_{\hat{\xi}}(\hat{\eta}_{(\mathbf{a}'\mathbf{b}')})}} \leq \sum_{\text{every}\eta}\frac{1}{d^N}\rho_{(\mathbf{a}',\mathbf{b}')^{-\boldsymbol{\eta}}} = 1. \tag{2.67}$$

The last equality follows from the representation of the trace, as presented in step 2. of this section and an argument taken from [3], section IV. Since this bound is independent of the choice of edge $\hat{\xi}$ we obtain the convenient bound on τ that only depends on the generalized energy barrier and the length of the longest path,

$$\tau \leq \frac{4\mu(N)}{\gamma^*}\exp(2\beta\bar{\epsilon}). \tag{2.68}$$

On first sight, this bound looks identical to the bound that was obtained for $\mathbb{Z}_2$ - stabilizers. However, the generalized energy barrier is quite different. It does reduce

to the one defined in [3], when we set $d = 2$, but the advance is that it now holds for all possible Abelian quantum double models. If we substitute the energies $\epsilon((\mathbf{a}, \mathbf{b}))$ as defined in Eq. (2.47), we obtain

$$\overline{\epsilon}(\hat{\eta}_{(\mathbf{a}',\mathbf{b}')}) = \max_{\hat{\xi}\in\hat{\eta}_{(\mathbf{a}',\mathbf{b}')}} \left(\sum_v \left(J_v^{\mathbf{a}'^{-\xi_{el}}} + J_v^{\mathbf{a}'^{\xi_{el}\ominus\eta_{el}}} - J_v^{\mathbf{a}'} - J_v^{\mathbf{a}'^{-\eta_{el}}} \right) + \sum_p \left(J_p^{\mathbf{b}'^{-\xi_f}} + J_p^{\mathbf{b}'^{\xi_f\ominus\eta_f}} - J_p^{\mathbf{b}'} - J_p^{\mathbf{b}'^{-\eta_f}} \right) \right). \tag{2.69}$$

We can write $(\mathbf{a}', \mathbf{b}') = (\mathbf{a}, \mathbf{b}) \ominus e(\boldsymbol{\xi})$ and similarly $\mathbf{a}' = \mathbf{a} \ominus e(\xi_{el})$, $\mathbf{b}' = \mathbf{b} \ominus e(\xi_f)$, where ξ_{el}, η_{el}, ξ_f, η_f are the electric/magnetic part of the errors: $\boldsymbol{\xi} = (\xi_{el}, \xi_f)$ and $\boldsymbol{\eta} = (\eta_{el}, \eta_f)$. ξ_{el} (η_{el}) is understood as $\bar{\sigma}_{\xi_{el}}$ ($\bar{\sigma}_{\eta_{el}}$) error applied to a state, while ξ_f (η_f) stands for applying the σ_{ξ_f} (σ_{η_f}) error. This is a direct consequence of the charge flux duality. We observe that the charge / flux contributions behave formally identical and the contribution to the energy barrier can be seen as the sum of both these contributions, i.e., $\overline{\epsilon}(\hat{\eta}_{(\mathbf{a}',\mathbf{b}')}) = \overline{\epsilon}^{\mathbf{a}}(\hat{\eta}_{(\mathbf{a}',\mathbf{b}')}) + \overline{\epsilon}^{\mathbf{b}}(\hat{\eta}_{(\mathbf{a}',\mathbf{b}')})$. It therefore suffices to only discuss one sector, i.e., either the chargeon of the fluxon part of the model from now on, and we write:

$$\overline{\epsilon}^{\mathbf{a}}(\hat{\eta}_{(\mathbf{a}',\mathbf{b}')}) = \max_{\hat{\xi}\in\hat{\eta}_{(\mathbf{a}',\mathbf{b}')}} \sum_v \left(J_v^{\mathbf{a}'^{-\xi_{el}}} + J_v^{\mathbf{a}'^{\xi_{el}\ominus\eta_{el}}} - J_v^{\mathbf{a}'} - J_v^{\mathbf{a}'^{-\eta_{el}}} \right). \tag{2.70}$$

We can evaluate this barrier as follows: we can write $J_v^{\alpha} = \sum_z J_v^z \delta_{z,\alpha}$ for convenience. To this end we can express Eq. (2.70) as

$$\overline{\epsilon}^{\mathbf{a}}(\hat{\eta}_{\mathbf{ab}}) = \max_{\xi} \sum_{v\,:\,z=0}^{d-1} J_v^z \left(\delta_{z,a_v\oplus e_v(\xi)} - \delta_{z,a_v} + \delta_{z,a_v\oplus e_v(\eta)\ominus e_v(\xi)} - \delta_{z,a_v\oplus e_v(\eta)} \right). \tag{2.71}$$

Even though this expression (and the following expressions) directly only incorporates the electric sector, i.e., $\xi = \xi_{el}$ and $\eta = \eta_{el}$ above, it is still the complete energy barrier. Due to the charge-flux duality, we can construct the electric and magnetic errors one after the other, therefore at any time we need only to look at one of the sectors.

In order to evaluate this barrier, we need to consider several different scenarios in order to express this equation more conveniently. The different cases correspond to different values of $e_v(\xi)$ and $e_v(\eta)$ and are summarized in the table. The value inside the parentheses of course depends on the relative value of a_v and z. Our goal is to get a bound that holds for all possible a_v starting configurations, thus we maximize expression (2.71) as a function of a_v. In order to achieve that maximum, we have

chosen the relative value of a_v and z such that it gives the highest possible value in each case.

$e_v(\xi)$	$e_v(\eta)$	Sum of δ's	z
0	0	0	any
p	p	0	any
0	p	0	any
p	0	1	$a_v \oplus e_v(\xi)$ or $a_v \ominus e_v(\xi)$
p	q	1	$a_v \oplus e_v(\xi)$ or $a_v \ominus e_v(\xi) \oplus e_v(\eta)$

Table 2.1: Here $p \neq q$, $p \neq 0$, $q \neq 0$.

The case-to-case scenario shown in the table can be summarized in one simple formula, and we can rewrite the sum of the Kronecker symbols as the more convenient expression:

$$\overline{\delta_{e_v(\xi),0}} \cdot \overline{\delta_{e_v(\xi),e_v(\eta)}} \left(\delta_{z,a_v \oplus e_v(\xi)} + \delta_{z,a_v \ominus e_v(\xi) \oplus e_v(\eta)}\right), \tag{2.72}$$

where $\overline{\delta_{x,y}} = 1 - \delta_{x,y} = \{0 \text{ if } x = y; 1 \text{ if } x \neq y\}$.

Using this formula considering that for a canonical path $\hat{\eta}_a$ we can consider the edge $\xi = \eta^t$ as the partially constructed Pauli operator at some step t. To this end we need to consider for every $\hat{\eta}_a$ the largest contribution along the path and therefore have to maximize this value for the largest value t. With this substitution, the contribution $\overline{\epsilon}^{\mathbf{a}}(\hat{\eta})$ looks like

$$\overline{\epsilon}(\hat{\eta}) = \max_t \left(\max_{z,v'} J^z_{v'} \right) \sum_v \overline{\delta_{e_v(\bar{\eta}^t),0}} \cdot \overline{\delta_{e_v(\bar{\eta}^t),e_v(\eta)}}, \tag{2.73}$$

i.e., the energy barrier is the maximum energy cost the environment has to provide to the system during any canonical path which constructs the error configuration η. However, since this energy barrier upper bounds the mixing time, in order to get a better upper bound we may choose the canonical path wisely, i.e., so it gives a smaller energy barrier. The reader will observe, that this energy barrier corresponds exactly to the one that was analyzed in detail in section 2.3 of this paper. We point to a notable difference to the analysis of only $\mathbb{Z}_2$ models. In these models only those sites contribute where the charge disappeared to vacuum, while for the $d > 2$ general cases a site contributes even if the anyon doesn't completely disappear at the end of the canonical path, but it changes to an anyon characterized by a different syndrome, be it the vacuum or anything else.

This energy barrier gives a valid bound on the mixing time for all choices of

canonical paths we can make, but the quality of the bound depends on the choice of the canonical path. To this end, when evaluating the bound, we follow the decomposition into single site Paulis as it was amply discussed in section 2.3.3.

2.6 Conclusions

We have established a strict Arrhenius law upper bound for the memory time of all quantum doubles based on an Abelian group and gave a mathematically proper definition for the energy barrier. We have also seen that the energy barrier is a constant for these models. We may apply our results to the model introduced in Ref. [48] to evaluate whether entropic protection is possible for such models.

Even though our bound on the mixing time is quite general in the sense that it applies to any Abelian quantum double, there are a variety of models to which our analysis doesn't apply. For these models the possibility of entropy protection is not yet excluded. One of the possible directions one can go is to invent different kind of defects, other than the type referred to here as "consistent" (defects that allow a consistent labeling of anyons based on the region they stay at) and "permuting"-type (which only apply a permutation to any particle crossing a defect line). We investigated Hamiltonians with consistent defect lines. However, interesting constructions use non-consistent defect lines to introduce topological defects, such as the construction of Bombin for the toric code with twists [68]. Another possibility we can't exclude is to assume a different thermal environment, and thus use a different noise model for this analysis. This might result in the simple permuting-type defect lines introducing entropic protection to Abelian systems. Our analysis only applies to Abelian quantum doubles, i.e., qudit stabilizer codes, and therefore entropic protection of quantum doubles based on non-Abelian groups (or of models that are not quantum doubles of any group) is not ruled out, especially since one can think of a variety of defect lines which can arise in such models [69]. One can also consider constructions where lower dimensional topological systems are coupled to an ancillary system, and this coupling modifies the dynamics of the original model [53, 70].

2.A Maximum cardinality and sum of multisets without a zero-sum subset

In this section, we derive elementary facts about multisets of $\mathbb{Z}_d$ without any subset sum equal to zero. This is motivated by the problem of fusing anyons in a $\mathbb{Z}_d$ quantum double. Indeed, consider a set of anyons labeled by their anyonic charge. Since there can be several anyons of the same anyonic charge, we are interested in set-like mathematical objects where multiplicity is explicit. For instance, for a set of two anyons of type 1 and one anyon of type 3, we would like to write $\{1, 1, 3\}$.

The formal mathematical object for this intuitive notion are called multisets. In our simple case, they are simply a multiplicity function

$$f : \mathbb{Z}_d \to \mathbb{N}, \tag{2.74}$$

where $f(k)$ is the multiplicity of k in the multiset. For instance, for $d = 5$, the multiset $\{1, 1, 3\}$ is equivalent to $\{(1, 2), (2, 0), (3, 1), (4, 0), (5, 0)\}$ which is the graph of the multiplicity function.

The cardinality of a multiset $|f|$ is the total number of elements, taking multiplicity into account, i.e.,

$$|f| = \sum_{k \in \mathbb{Z}_d} f(k) \in \mathbb{N}. \tag{2.75}$$

The sum of a multiset $s(f)$ is the sum of all its elements, taking multiplicity into account, i.e.,

$$s(f) = \sum_{k \in \mathbb{Z}_d} k f(k) \in \mathbb{Z}_d. \tag{2.76}$$

Note that $|f|$ is an integer whereas $s(f)$ is defined modulo d. Physically, the sum $s(f)$ is the anyon type resulting from fusing all anyons in the multiset. Moreover, one defines the sum $f + g$ of two multisets f and g

$$(f + g)(k) = f(x) + g(x). \tag{2.77}$$

It corresponds to the intuitive idea of adding the elements of f and g. For instance, $\{1, 1, 3\} + \{1, 2, 4\} = \{1, 1, 3, 1, 2, 4\} = \{1, 1, 1, 2, 3, 4\}$. Finally, one defines a (multi)subset by

$$f \subseteq g \Leftrightarrow \forall k \in \mathbb{Z}_d \quad f(k) \leq g(k). \tag{2.78}$$

Given a multiset of anyons, we would like to know whether it contains subsets which fuse to the vacuum. Mathematically, given a multiset f, we are interested in the sum of its subsets $s(f')$ where $f' \subseteq f$. More precisely, we want to know if a subset sums to zero modulo d. We define the spectrum of a multiset

$$\mathrm{sp}(f) = \bigcup_{f' \subseteq f, f' \neq \emptyset} s(f'), \tag{2.79}$$

and say that a multiset is *zero-sum free* if 0 is not in its spectrum, i.e., no non-empty subset sums to 0 modulo d. We aim to determine the largest possible cardinality and sum of a zero-sum free multiset. This is related to a well-studied problem in complexity theory and cryptography, called the subset sum problem [71].

First, we want to understand what happens to the spectrum when we add a singleton to the multiset, i.e., we consider the operation $f \longrightarrow f + \{x\}$. The non-empty subsets of $f + \{x\}$ are $\{x\}$, the subsets of f and the subsets of f to which we add the element x. Thus, we have

$$\mathrm{sp}(f + \{x\}) = \{x\} \cup \mathrm{sp}(f) \cup (\mathrm{sp}(f) + x)\,. \tag{2.80}$$

We can then prove the following lemma

Lemma 2.7. *The spectrum of a zero-sum free multiset strictly increases when adding any singleton, i.e.,*

$$f \textit{ is zero-sum free} \Rightarrow sp(f) \subsetneq sp(f + \{x\}). \tag{2.81}$$

Proof: We prove the contrapositive of Eq. (2.81), i.e., we consider a multiset f for which $\mathrm{sp}(f) = \mathrm{sp}(f + \{x\})$ and we will prove that it contains a zero-sum subset. Using Eq. (2.80), the equality of spectra implies that i) x is an element of $\mathrm{sp}(f)$ and ii) $\mathrm{sp}(f) \subseteq \mathrm{sp}(f) + \{x\}$. Since the addition by x only shifts the spectrum the two sets have the same cardinality and $\mathrm{sp}(f) = \mathrm{sp}(f) + \{x\}$. In particular, since x is an element of $\mathrm{sp}(f)$, there exists a subset $f^\star \subseteq f$ for which the following equality holds modulo d: $x = \mathrm{sp}(f^\star) + x$. Thus, the sum of $f^\star$ is zero. □

Using lemma 2.7, we can deduce the maximal cardinality of a zero-sum free multiset. Indeed, consider a zero-sum multiset by sequentially adding its elements to the empty set. The spectrum will increase at each addition of a singleton by at least 1. However, a spectrum is contained in $\mathbb{Z}_d$ and thus has at most $d - 1$ elements. Hence, we have proven that

Theorem 2.8.

$$f \textit{ is zero-sum free} \Rightarrow |f| \leq (d - 1) \tag{2.82}$$

In fact, we can saturate the bound. Any multiset of an integer k co-prime with d and multiplicity $d - 1$ is zero-sum free. In particular, the multiset containing $d - 1$ with multiplicity $d - 1$ maximizes the sum of any zero-sum free multiset.

Theorem 2.9.

$$\max_{\textit{zero-sum free } f} |f| = d - 1 \tag{2.83}$$

$$\max_{\textit{zero-sum free } f} s(f) = (d-1)^2 \tag{2.84}$$

Chapter 3

ANYONS ARE NOT ENERGY EIGENSPACES OF QUANTUM DOUBLE HAMILTONIANS

Anna Kómár, and Olivier Landon-Cardinal. Anyons are not energy eigenspaces of quantum double Hamiltonians. *Physical Review B*, 96(19):195150, 2017.

Abstract

Kitaev's quantum double models, including the toric code, are canonical examples of quantum topological models on a 2D spin lattice. Their Hamiltonian defines the ground space by imposing an energy penalty to any nontrivial flux or charge, but does not distinguish among those. We generalize this construction by introducing a novel family of Hamiltonians made of commuting four-body projectors that provide an intricate splitting of the Hilbert space by discriminating among non-trivial charges and fluxes. Our construction highlights that anyons are not in one-to-one correspondence with energy eigenspaces, a feature already present in Kitaev's construction. This discrepancy is due to the presence of local degrees of freedom in addition to topological ones on a lattice.

3.1 Introduction

Interacting topological spin models are of interest in the field of condensed matter theory and quantum information due to their promising properties to encode quantum information into their degenerate ground space. The different ground states can be labeled through a topological property of the system, e.g., by the equivalency classes of the different non-contractible loops on a torus. The quantum information encoded into a ground state can be recovered by performing error correction, even after a long time provided only local coherent errors are introduced by the environment. In this sense, topological systems are inherently robust to decoherence.

One of the first proposals for a topological quantum code is the *toric code* by Kitaev [4]. This is a two-dimensional system with periodic boundary conditions, i.e., with a toroidal geometry, where physical spin-1/2 particles or *qubits* live on edges of a 2D square lattice. This model has a four-fold degenerate ground space, thus the ground space encodes two logical qubits. Any local operator acts trivially within the ground space whereas operators acting on a large number of qubits residing on

a non-contractible loop going around the torus act non-trivially. An experimentally more feasible version of the toric code is the *surface code* [37, 39], which is a two-dimensional system with physical qubits still placed on edges of a lattice, but the boundaries are now open. Several experimental groups currently pursue the physical realization of surface codes [40, 72] with the goal to use them as building blocks in a quantum computer.

The toric code belongs to a more general class of topological systems known as *quantum doubles*, introduced by Kitaev [4]. These are spin systems on a 2D lattice whose excitations are point-like, and they correspond to (non-Abelian) anyons. Excitations of the quantum double of group G correspond to the anyons described by the mathematical construction [73] known as the Drinfeld double $\mathcal{D}(G)$. For instance, the toric code is the quantum double $\mathcal{D}(\mathbb{Z}_2)$ based on the group $\mathbb{Z}_2$.

The excitations of a topological quantum field theories are indistinguishable quasi-particles called anyons: *Abelian* if taking anyons around each other modifies their wave function by only a phase, and *non-Abelian* if taking certain anyons around one another applies a nontrivial unitary operation to their wave function. In topological quantum field theories (TQFT), anyons carry a (nontrivial) charge or flux and are accordingly grouped into *chargeons*, *fluxons*, and *dyons* when they carry both a (nontrivial) charge and a (nontrivial) flux.

Quantum double models were introduced by Kitaev as a lattice realization of topological quantum field theories [4]. Those models are defined by a Hamiltonian whose ground space is spanned by vacuum states, i.e., states with no flux nor charge present. More precisely, the Hamiltonian imposes an energy penalty equal to the number of nontrivial charges or fluxes present.

Anyons are point-like excitations that appear on a site of the lattice. They are labeled by irreducible representations (irreps) of the Drinfeld double $\mathcal{D}(G)$. However, the spatial scale inherent to the lattice breaks the purely topological properties of the model and introduces *local degrees of freedom*. In particular, anyon types are not in one-to-one correspondence with energy eigenspaces. Indeed, two anyons of the same type can have different energies depending on the local degrees of freedom. This peculiar feature is already present in Kitaev's original Hamiltonian but is more explicit in the family of Hamiltonians we introduce in this paper. Those novel Hamiltonians generalize Kitaev's original proposal since they have additional local terms which allow them to distinguish among the different nontrivial fluxes and charges.

In this paper, we introduce a family of Hamiltonians that assigns different ener-

gies to the different nontrivial fluxes and charges of non-Abelian quantum doubles $\mathcal{D}(G)$. In these *refined Hamiltonian*, each term only acts on four neighboring higher-dimensional spins (a.k.a qudits in the quantum information jargon). Moreover, each 4-local terms commute pairwise, resulting in a Hamiltonian which can be solved explicitly. Our construction is qualitatively different than the 6-local terms introduced in [74] since our family of Hamiltonian maintain the feature that Hamiltonian term are either related to the charges or to the fluxes. We then show how the 4-local charge and flux projectors assign different energies to excitations by partitioning the Hilbert space of excitations according to charge and flux labels related to the representation theory of the group G. Our construction emphasizes a feature already present in Kitaev's original proposal that anyons are not in one-to-one correspondence with energy eigenspaces of the Hamiltonian due to the presence of local degrees of freedom.

Throughout the paper, we illustrate the notions we introduced by analyzing the quantum double for the smallest non-Abelian group S_3, the symmetry group of order 3, whose quantum double structure was explored in [51, 69]. We explicitly write down the 4-local refined Hamiltonian for this theory, see Eq. (3.47).

The paper is organized as follows. First, in Sec. 3.2 we review the most important properties of non-Abelian anyons, and introduce the quantum double construction. Second, in Sec. 3.3 we introduce the general charge and flux projectors and construct the 4-local refined Hamiltonian, see Theorem 3.8. We analyze how these projectors partition the Hilbert space of each site in Sec. 3.4 and introduce a diagrammatic representation to visualize this partitioning, see Fig. 3.6. This diagrammatic representation reveals that anyons are not in one-to-one correspondence with energy eigenspaces of the Hamiltonian due to the presence of local degrees of freedom. We explore how those local degrees of freedom arise out of the spatial scale introduced by the lattice in Sec. 3.5. Finally, we conclude our findings and point out future directions in Sec. 3.6.

3.2 The Drinfeld double construction and the quantum double models

The quantum double construction realizes topological lattice spin models whose anyonic excitations are described mathematically by the Drinfeld double of a group. To better appreciate the quantum double construction, we first review the properties and mathematical formalism of non-Abelian anyons in general. First, in Sec. 3.2.1 we give an overview of the anyon labels and the most important braiding properties. This pedagogical exposition is largely inspired from John Preskill's lecture notes [33] and the reader is encouraged to consult those notes for more detail. Then we introduce

the quantum double construction on a lattice in Sec. 3.2.2.

3.2.1 Non-Abelian Aharonov-Bohm effect

Anyons can be understood by analogy to the Aharonov-Bohm effect: taking a charge q around a flux tube with flux Φ results in the wave function acquiring a phase $\exp(iq\Phi)$.

$$|\psi\rangle \to \exp(iq\Phi)|\psi\rangle. \tag{3.1}$$

Non-Abelian anyons can be qualitatively understood by generalizing the Aharonov-Bohm effect to fluxes whose possible values correspond to the elements g of a group G and the charge possible values are the irreducible representations (irreps) Γ of G. In other words, the Hilbert space of each quasi-particle is spanned either by the flux orthonormal basis

$$\mathcal{H} = \text{span}\{|g\rangle\}_{g\in G}, \tag{3.2}$$

or in a conjugate charge orthonormal basis

$$\mathcal{H} = \text{span}\{|\Gamma, i\rangle\}_{\text{irrep}\Gamma, i=1\ldots|\Gamma|} \tag{3.3}$$

in which we chose an (arbitrary) orthonormal basis $\{|\Gamma, i\rangle_{i=1\ldots|\Gamma|}\}$ for every module of each irrep Γ.

Labeling fluxons

To identify a fluxon, we can check how the basis transforms when a charge Γ is transported around the fluxon

$$|\Gamma, j\rangle \to \sum_{i=1}^{|\Gamma|} \Gamma_{ij}(a)|\Gamma, i\rangle. \tag{3.4}$$

Since the matrix elements $\Gamma_{ij}(a)$ can in principle be measured by interferometry [75], performing this for every charge type $|\Gamma, j\rangle$ will reveal the flux $a \in G$.

However, labeling fluxons by group elements is not gauge-invariant since another observer could choose another orthonormal basis for the module of the irrep Γ. In fact, the correct gauge-invariant quantity to label fluxons is the *conjugacy class*:

Definition 3.1 (Conjugacy class)**.**

$$C_a = \{gag^{-1}|g \in G\}. \tag{3.5}$$

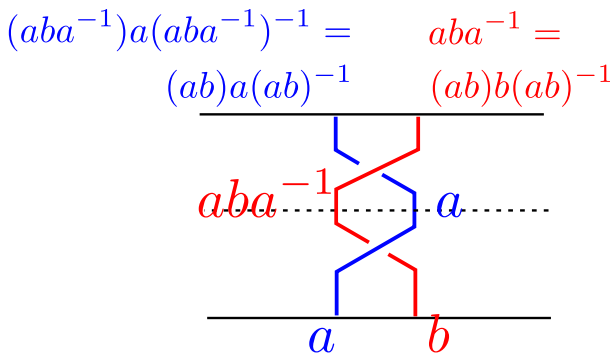

Figure 3.1: Braiding of two anyons, a and b: applying a counterclockwise exchange of the particles, resulting in conjugacy of the original wave function.

Indeed, two observers will agree on the conjugacy class of a fluxon even if they probably would disagree on the representative group element within the conjugacy class.

Braiding of fluxons

We now want to understand what happens when braiding fluxons. Let's consider two fluxons side by side. The left fluxon has flux a while the right fluxon has flux b (locally, flux types are well defined). Let's now counterclockwise exchange the fluxons, resulting in an operator R_{ab}. One can prove that the resulting effect is

$$R_{ab} \ : |\, a, b\rangle \mapsto |\, aba^{-1}, a\rangle, \tag{3.6}$$

i.e., the right flux has been conjugated by the left flux. See Fig. 3.1 for a pictorial representation.

Note that two successive counterclockwise exchange is equivalent to having the rightmost flux going around the leftmost flux counterclockwise, see Fig. 3.1. The net result of that operation is

$$R_{ab}^2 \ : |\, a, b\rangle \mapsto |\, (ab)a(ab)^{-1}, (ab)b(ab)^{-1}\rangle, \tag{3.7}$$

which is coherent with the claim that the conjugacy class of a fluxon is gauge-invariant but the representative is ambiguous since it can change by an arbitrarily far away fluxon moving around it.

Dyon: anyon with nontrivial flux and nontrivial charge

While we have discussed how to label a chargeon (by an irrep) and a fluxon (by a conjugacy class), we have yet to discuss anyons that exhibit both a nontrivial charge and a nontrivial flux. Such an anyon is called a *dyon*. Suppose we wanted to measure the charge of a dyon. We could set up an interferometric experiment. We could place the dyon behind the slits in a double slit experiment and measure the interferometry pattern for any incoming test fluxon. However, since the dyon also carries flux, subtleties arise. Indeed, the passage of the test fluxon either to the left or the right of the dyon will modify the flux of the dyon. Thus, interference will only occur if the flux a of the dyon commutes with the flux b of the test fluxon, i.e., if $ab = ba$. In other words, the charge Γ of the dyon can be determined only if the probe fluxon has a flux among the elements b commuting with a, i.e., within the *normalizer* of a

Definition 3.2 (Normalizer)**.**

$$\mathcal{N}_a = \{b \in G | ab = ba\}. \tag{3.8}$$

Note that a normalizer is always a subgroup of the group G. We thus conclude that the charge Γ of a dyon carrying flux a is not an irrep of the full G, but rather an irrep of the normalizer $\mathcal{N}_a$.

The mathematical structure corresponding to an anyon model is the Drinfeld double of a group which is a quasi-triangular Hopf algebra. Anyon types are in one-to-one correspondence with the irreps of that operator algebra. Working out the irreps of the Drinfeld double only requires knowledge of the representation theory of the underlying group, since a key mathematical result is that irreps of a Drinfeld double are labeled by i) a conjugacy class and ii) an irrep of the normalizer of any element of the conjugacy class (which are all isomorphic).

Quantum dimension of an anyon

In a Drinfeld double, the quantum dimension d_a associated to every anyon type a is the dimension of the vector subspace associated to that anyon. It is thus an integer. Given an anyon type (C_g, Γ), its quantum dimension is

$$d_{(C_g,\Gamma)} = |C_g||\Gamma|. \tag{3.9}$$

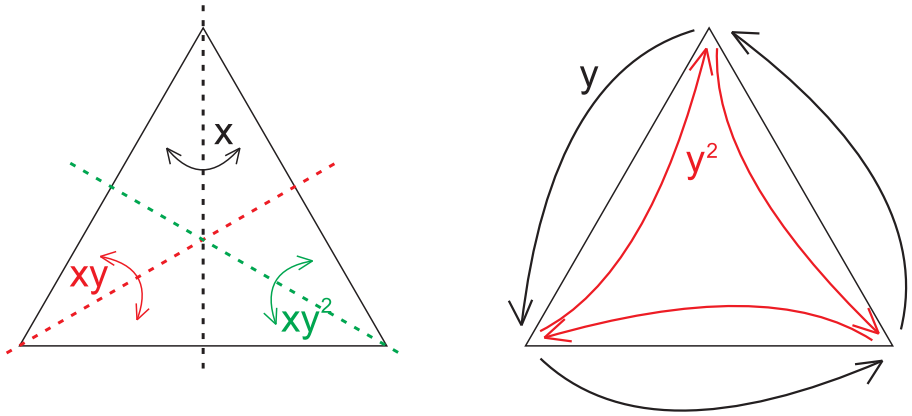

Figure 3.2: Symmetries of an equilateral triangle, or elements of the group S_3.

Moreover, another quantity of interest is the total quantum dimension $\mathcal{D}$ of the model, which is related to the quantum dimension of every anyon type by

$$\mathcal{D}^2 = \sum_{\text{anyons } k} d_k^2. \tag{3.10}$$

In the case of a quantum double, the total quantum dimension is related to the cardinality of the group

$$\mathcal{D}^2 = |G|^2. \tag{3.11}$$

This result might appear as mysterious: we will give an interpretation of this result in Sec. 3.4.3.

Example of $\mathcal{D}(S_3)$

As a more elaborate example of the above quantum double structure, let's look at the quantum double of the smallest non-Abelian group, $\mathcal{D}(S_3)$. The group S_3 is isomorphic to the symmetry transformations of an equilateral triangle (see Fig. 3.2):

- identity: e,
- rotations by $\pi/3$ and $2\pi/3$: y, y^2,
- mirrorings to the three different axes: x, xy, xy^2 .

Because of the nature of these symmetries, $y^3 = e$ and $x^2 = (xy)^2 = (xy^2)^2 = e$. The non-Abelianity of $\mathcal{S}_3$ is summed up by the commutation relation $xy = y^2x$.

S_3	e	y	y^2	x	xy	xy^2
$\Gamma_1^{S_3}$	1	1	1	1	1	1
$\Gamma_{-1}^{S_3}$	1	1	1	-1	-1	-1
$\Gamma_2^{S_3}$	$\begin{pmatrix}1&0\\0&1\end{pmatrix}$	$\begin{pmatrix}\bar{\omega}&0\\0&\omega\end{pmatrix}$	$\begin{pmatrix}\omega&0\\0&\bar{\omega}\end{pmatrix}$	$\begin{pmatrix}0&1\\1&0\end{pmatrix}$	$\begin{pmatrix}0&\omega\\\bar{\omega}&0\end{pmatrix}$	$\begin{pmatrix}0&\bar{\omega}\\\omega&0\end{pmatrix}$

Table 3.1: Irreducible representations of S_3, i.e., the possible charge labels with flux C_e.

$\mathbb{Z}_3$	e	y	y^2
$\Gamma_1^{\mathbb{Z}_3}$	1	1	1
$\Gamma_\omega^{\mathbb{Z}_3}$	1	ω	$\bar{\omega}$
$\Gamma_{\bar{\omega}}^{\mathbb{Z}_3}$	1	$\bar{\omega}$	ω

$\mathbb{Z}_2$	e	x
$\Gamma_1^{\mathbb{Z}_2}$	1	1
$\Gamma_{-1}^{\mathbb{Z}_2}$	1	-1

Table 3.2: Irreducible representations of (a) $\mathbb{Z}_3$ and (b) $\mathbb{Z}_2$, i.e., the possible charge labels with flux C_y and C_x.

The anyons of the Drinfeld double of S_3 are labeled by the conjugacy classes of S_3 and the irreducible representations of normalizers of conjugacy classes. There are three conjugacy classes of S_3:

$$C_e = \{e\}, \tag{3.12}$$
$$C_y = \{y, y^2\}, \tag{3.13}$$
$$C_x = \{x, xy, xy^2\}, \tag{3.14}$$

and the corresponding normalizers are

$$\mathcal{N}_e = S_3, \tag{3.15}$$
$$\mathcal{N}_y = \mathcal{N}_{y^2} = \{e, y, y^2\} \cong \mathbb{Z}_3, \tag{3.16}$$
$$\mathcal{N}_x = \{e, x\} \cong \mathcal{N}_{xy} \cong \mathcal{N}_{xy^2} \cong \mathbb{Z}_2. \tag{3.17}$$

We would like to point out here that while the normalizers $\mathcal{N}_y$ and $\mathcal{N}_{y^2}$ are the same independent of the labeling, $\mathcal{N}_x$, $\mathcal{N}_{xy}$, and $\mathcal{N}_{xy^2}$ are distinct, and only isomorphic to each other.

The irreducible representations of all these normalizers are listed in Tables 3.1-3.2. There and in the remainder of the paper $\omega = \exp(2\pi i/3)$ and $\bar{\omega} = \exp(4\pi i/3)$ are the third complex roots of unity.

In summary, this model has 8 anyons, and these are listed in Table 3.3. Anyon A is

Label	C_g	$\mathcal{N}_g$	Irrep.	Q.dim.	Type
A	C_e	S_3	$\Gamma_1^{S_3}$	1	vacuum
B	C_e	S_3	$\Gamma_{-1}^{S_3}$	1	chargeon
C	C_e	S_3	$\Gamma_2^{S_3}$	2	chargeon
D	C_x	$\mathbb{Z}_2$	$\Gamma_1^{\mathbb{Z}_2}$	3	fluxon
E	C_x	$\mathbb{Z}_2$	$\Gamma_{-1}^{\mathbb{Z}_2}$	3	dyon
F	C_y	$\mathbb{Z}_3$	$\Gamma_1^{\mathbb{Z}_3}$	2	fluxon
G	C_y	$\mathbb{Z}_3$	$\Gamma_\omega^{\mathbb{Z}_3}$	2	dyon
H	C_y	$\mathbb{Z}_3$	$\Gamma_{\bar{\omega}}^{\mathbb{Z}_3}$	2	dyon

Table 3.3: Anyons of $\mathcal{D}(S_3)$ with their charge and flux labels, quantum dimensions and type.

the vacuum since it has both trivial charge and flux. Anyons B and C are chargeons, and they correspond respectively to the signed and two-dimensional irreps of S_3. Anyons D and F are fluxons since they correspond to the trivial irrep of their respective normalizers. Other anyons are dyons.

At this point, we have defined anyons and described their braiding and fusion properties using a toy model of non-Abelian Aharonov-Bohm effect. We recovered, using a physics point of view, the key properties of the Drinfeld double of a group. In particular, we worked out in detail the anyon types of $\mathcal{D}(S_3)$. However, in this toy model, anyons are fundamental particles. We will now describe the quantum double construction by Kitaev in which those anyons appear effectively as point-like excitations on a spin lattice.

3.2.2 Kitaev's quantum double on a lattice

A way to realize the non-Abelian Aharonov-Bohm effect on a lattice is Kitaev's quantum double construction [4]. In this construction, charges reside on vertices and fluxes are on plaquettes of the lattice, however, fluxes and charges are not independent. A generic flux-charge composite particle (dyon) lives on a site: a combination of a vertex and a plaquette shown in Fig. 3.3.

This excitation structure is realized by first assigning a Hilbert space to each edge of the lattice, where the state of each edge can take any group element $z \in G$, and then defining a Hamiltonian that describes the interactions in this model. To introduce

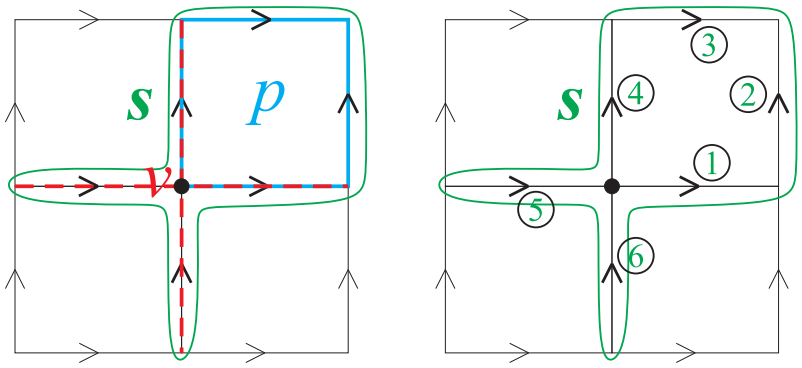

Figure 3.3: Our choice of orientation on the lattice, with (a) how a vertex v and plaquette p form a site s, and (b) the edge numbering we used to define the vertex and plaquette operators $\mathcal{A}_g^v$ and B_h^p in Eqs. (3.22)-(3.23).

the Hamiltonian, let us define the following operators:

$$L_g^+|\,z\rangle = |\,gz\rangle, \tag{3.18}$$
$$L_g^-|\,z\rangle = |\,zg^{-1}\rangle, \tag{3.19}$$
$$T_h^+|\,z\rangle = \delta_{h,z}|\,z\rangle, \tag{3.20}$$
$$T_h^-|\,z\rangle = \delta_{h^{-1},z}|\,z\rangle, \tag{3.21}$$

where L_g^+ and L_g^- are the matrices representing left- and right-multiplication operators, T_h^+ and T_h^- are diagonal operators in the flux basis.

Then, we need to assign an orientation to the edges of the lattice. We use the convention shown in Fig. 3.3 for a site, i.e., the union of a vertex and a plaquette.

Most of the definitions and arguments in this paper will be focused on quantum doubles defined on a square lattice, however, it is possible to define quantum doubles on any directed, planar lattice, see Ref. [4]. The statements in this paper, including the new charge and flux projectors, their relation and commutation should remain unchanged by considering a different lattice. The only result where we rely on the geometry of the lattice is the counting argument in Sec. 3.4.2, and this can be modified to obtain the equivalent result for other geometries.

We now introduce two families of operators, following closely the original definition of [4].

Definition 3.3 (Plaquette operators)**.** *For any element $h \in G$, we define an operator*

acting on the 4 spins around an oriented plaquette p

$$B_h^p = \sum_{h_1 h_2 h_3^{-1} h_4^{-1} = h} T_{h_1}^{+,1} \otimes T_{h_2}^{+,2} \otimes T_{h_3}^{-,3} \otimes T_{h_4}^{-,4}, \tag{3.22}$$

where the use of $T_h^{\pm}$ depends on the respective orientations of the plaquette and the edges. See Fig. 3.3 for our orientation convention and the labeling of the spins.

Definition 3.4 (Vertex operators)**.** *For any element $g \in G$, we define a vertex operator, originally called star operators in [4], acting on the 4 spins around a vertex v*

$$\mathcal{A}_g^v = L_g^{+,1} \otimes L_g^{+,4} \otimes L_g^{-,5} \otimes L_g^{-,6}, \tag{3.23}$$

where L_g^+ appears for outgoing edges and L_g^- appears for incoming edges. See Fig. 3.3 for our orientation convention and the labeling of the spins.

How these operators act on a vertex and on a plaquette is illustrated in Fig. 3.4. In order for individual B_h^p to be properly defined even for a non-Abelian group, we need to specify a starting vertex on the plaquette, then specify an orientation. Henceforth, we mark the starting vertex by a black dot in Figures 3.3-3.4 and systematically orient the plaquettes in a counterclockwise manner. Whenever the orientation of an edge is opposite to the orientation of the plaquette, a plaquette operator B_h acts on it with T_h^-, otherwise it acts with T_h^+. Similarly for the vertex operators, when the orientation of an edge points outwards from the vertex, $\mathcal{A}_g^v$ acts with L_g^+, and otherwise with L_g^- on that edge.

The projector unto the trivial flux at plaquette p is simply the plaquette operator for the trivial element B_e^p. The projector unto trivial charge A_1^v on vertex v is defined as

$$A_1^v = \frac{1}{|G|} \sum_{g \in G} \mathcal{A}_g^v = \frac{1}{|G|} \sum_{g \in G} L_g^{+,1} \otimes L_g^{+,4} \otimes L_g^{-,5} \otimes L_g^{-,6}, \tag{3.24}$$

where the use of L_g^+ vs. L_g^- again depends on the orientation of the edge with respect to the vertex. We would like to remark that this projector agrees with the original projector introduced in Ref. [4] up to normalization, which does not include the $1/|G|$ factor. The introduction of the $1/|G|$ factor does not modify either the ground state or the structure of the excited states, only rescales the characteristic energies in the model. It is less trivial to see why this operator projects to the trivial charge, i.e., corresponds to the trivial representation. One explanation is that for any $g \in G$,

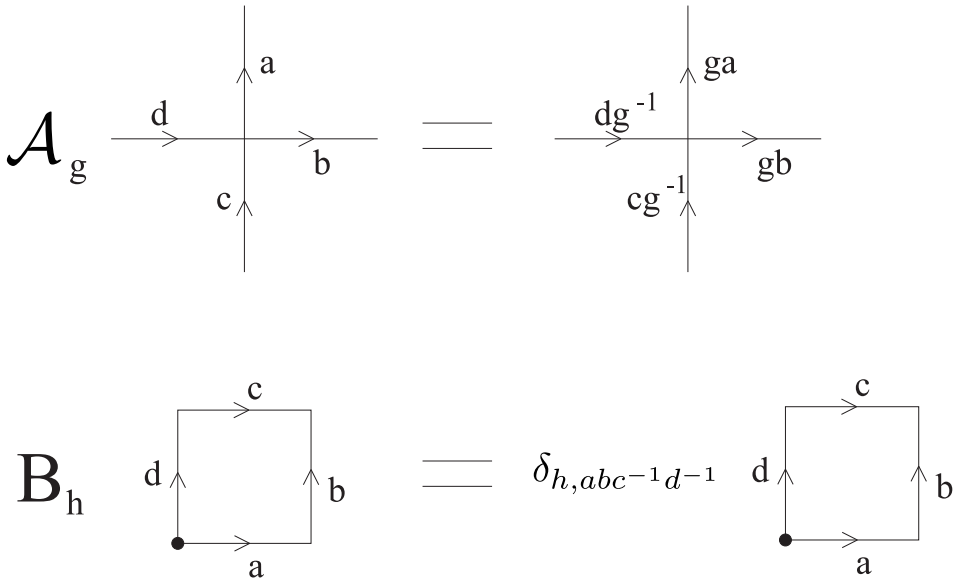

Figure 3.4: The effect of the individual projector terms ($\mathcal{A}_g$ and B_h) on a vertex and on a plaquette, respectively.

we have $A_1^v \mathcal{A}_g^v = A_1^v$. Thus, the image of A_1^v is invariant under the action of any $\mathcal{A}_g^v$, which is characteristic of the trivial representation.

Given vertex and plaquette operators, Kitaev introduced the following Hamiltonian in [4].

Definition 3.5 (Kitaev Hamiltonian)**.** *The Kitaev Hamiltonian of a quantum double* $\mathcal{D}(G)$ *is*

$$H = -\sum_v A_1^v - \sum_p B_e^p. \tag{3.25}$$

Please note that Hamiltonian (3.25) assigns an extensive energy of -2 for every site in the vacuum (ground state). Any vertex which does not carry the trivial charge receives an energy penalty. Similarly, any plaquette which does not exhibit a trivial flux receives an energy penalty.

Example: Toric code

The simplest example of the above quantum double construction is the toric code [4]. This is the quantum double of $\mathbb{Z}_2$, thus the possible group elements on an edge can be: $\{0, 1\}$, and all additions are understood modulo 2: $0 \oplus 0 = 0$, $0 \oplus 1 = 1$, $1 \oplus 1 = 0$. The corresponding spin states $|\,0\rangle$ and $|\,1\rangle$ are the usual computational basis for qubits.

In $\mathbb{Z}_2$, the left- and right-multiplication operators are the same: $L_0^+ = L_0^- = \mathbb{1}$ and $L_1^+ = L_1^- = X$, where X is the Pauli X operator. The diagonal operators are: $T_0^+ = T_0^- = (\mathbb{1} + Z)/2$ and $T_1^+ = T_1^- = (\mathbb{1} - Z)/2$, with Z being the Pauli Z operator.

The operators projecting unto trivial flux and trivial charge are (omitting the tensor product sign for simplicity, please refer to Fig. 3.3 for the labeling convention): $A^v = (\mathbb{1}^1\mathbb{1}^4\mathbb{1}^5\mathbb{1}^6 + X^1X^4X^5X^6)/2$ and $B^p = (\mathbb{1}^1\mathbb{1}^2\mathbb{1}^3\mathbb{1}^4 + Z^1Z^2Z^3Z^4)/2$, and thus the Hamiltonian is

$$H = -\sum_v \frac{1}{2}(\mathbb{1}^1\mathbb{1}^4\mathbb{1}^5\mathbb{1}^6 + X^1X^4X^5X^6) \\ -\sum_p \frac{1}{2}(\mathbb{1}^1\mathbb{1}^2\mathbb{1}^3\mathbb{1}^4 + Z^1Z^2Z^3Z^4), \tag{3.26}$$

or in its widely known form, after redefining the ground state energy:

$$H = -\sum_v X^1X^4X^5X^6 - \sum_p Z^1Z^2Z^3Z^4. \tag{3.27}$$

Similar to the general quantum double Hamiltonian of Eq. (3.25), this Hamiltonian assign an extensive energy of -2 to all sites in the vacuum state, and an energy penalty for vertices with a non-trivial charge, and for plaquettes with a non-trivial flux. (This energy penalty is now 2, while for the Hamiltonians (3.25)-(3.26) it was 1.) Having a non-trivial charge or flux at a certain vertex/plaquette is frequently referred to as "violating" that vertex/plaquette term in the Hamiltonian; the eigenvalue of each 4-body term is either $+1$ (no charge/flux) or -1 (charge/flux excitation). A violated vertex term corresponds to a charge excitation (e), while a violated plaquette term means a flux excitation is living on that plaquette (m). The four possible states of a site are thus:

$\mathbb{1}$ (vacuum)

e (charge)

m (flux)

$\epsilon = e \otimes m$ (dyon).

Further analyzing the Hamiltonian of Eq. (3.27), we can see two main features of the model. First, the charges and fluxes have decoupled from each other, which is typical of Abelian quantum doubles since any anyon type is the juxtaposition of a charge and a flux. Indeed, the only dyon is $\epsilon = e \otimes m$, which is the simple

combination of the non-trivial charge (e) and the non-trivial flux (m), and has no additional emergent properties.

Second, there is only one kind of excitation of either type (1 electric charge (e) and 1 magnetic flux (m)) in this model. Therefore, the Hamiltonian, which contains only two projectors can distinguish the four types of anyons: vacuum $\mathbb{1}$, electric chargeon e, magnetic fluxon m and the dyon $\epsilon = e \otimes m$. Introducing different coupling constants on the vertex and plaquette terms will lift the charge-flux duality and result in a 1-to-1 correspondence between energy eigenstates and anyon types. We will refer to this as the Kitaev Hamiltonian for $G = \mathbb{Z}_2$ having 1-to-1 correspondence between energy eigenstates and anyon type.

We will now generalize the Kitaev Hamiltonian for non-Abelian models by introducing local terms which project unto the different possible charges and the different possible fluxes in Sec. 3.3. We will argue that this is a natural generalization of Kitaev's Hamiltonian. However, our generalization will highlight that anyon type and energy eigenspaces are *not* in one-to-one correspondence for *non-Abelian* quantum doubles in Sec. 3.4. This peculiar feature was already present in Kitaev's original construction. This discrepancy between energy eigenspaces and anyons stems from the presence of *local degrees of freedom* that are not topological and arise from the lattice, in the case of non-Abelian models. Those will be explored in Sec. 3.5.

3.3 Refined quantum double Hamiltonian for arbitrary group

We have seen in the previous section that the Kitaev Hamiltonian given by Eq. (3.25) assigns an energy penalty to any nontrivial charge and flux. However, it does not distinguish among two distinct nontrivial charges or fluxes. It is then natural to wonder whether one can enrich the model by introducing new local terms which will introduce such a distinction? And if yes, how will that change the excitation structure of the theory?

In this section, we introduce in Sec. 3.3.1 a Hamiltonian that splits up the energies of different excitations for any quantum double, and then in Sec. 3.3.2 we work out explicitly the corresponding Hamiltonian for the quantum double of $\mathcal{D}(S_3)$.

3.3.1 Refined quantum double construction

Our aim in this section is to introduce projectors unto different nontrivial charges and fluxes. In Sec. 3.2.2 we have already given the form of the trivial flux projector B_e^p and trivial charge projector A_1^v. Even though these vacuum projectors are independent of one another, and are both 4-body operators, it is not trivial that one

could write independent 4-body charge- and flux-projectors. This is because, unlike in the case of Abelian quantum doubles, the charge and flux of a site are tied to one another when considering dyons, i.e., the charge is defined as an irreducible representation of the normalizer of the flux conjugacy class.

This section is organized as follows. We will first comment on the reasons we insist on defining a Hamiltonian whose terms are four-local in Sec. 3.3.1.1. We then outline our construction by recalling the definition of flux projectors and introducing charge projectors in Sec. 3.3.1.2. This allows us to define our family of refined Hamiltonians in Sec. 3.3.1.3. Namely, Theorem 3.8 is the novel family of Hamiltonians introduced by our work. In the following sections, we sketch the proof of Theorem 3.8 which relies on proving that the charge projectors are indeed an orthonormal family of projectors in Sec. 3.3.1.4 and then proving that they commute with the flux projectors in Sec. 3.3.1.5. Formal mathematical proofs are given in the appendix.

3.3.1.1 Locality of the Hamiltonian

A simple route to assign different masses to each anyon type would be to introduce a 6-local Hamiltonian. Indeed, each anyon lives on a site comprised of 6 spins. We can thus achieve an energy spectrum in one-to-one correspondence with anyon types by introducing 6-local projectors acting on sites, projecting unto the different anyon species defined by the combination of a flux and a charge label, $P^s_{(C_h,\Gamma^{\mathcal{N}_h})}$ where $\Gamma^{\mathcal{N}_h}$ labels irreps of the normalizer of each elements of C_h (which are isomorphic).

More precisely, we can define a massive 6-local Hamiltonian

$$H = \sum_s \sum_{C_h} \sum_{\text{irrep } \Gamma^{\mathcal{N}_h}} \alpha_{(C_h,\Gamma^{\mathcal{N}_h})} P^s_{(C_h,\Gamma^{\mathcal{N}_h})}, \tag{3.28}$$

where the projectors have been defined in [74]

$$P^{s=(p,v)}_{(C_h,\Gamma^{\mathcal{N}_h})} = \sum_{g\in C_h} \sum_{g'\in\mathcal{N}_g} \frac{d_{\Gamma^{\mathcal{N}_g}}}{|\mathcal{N}_g|} \chi_{\Gamma^{\mathcal{N}_g}}(g') \mathcal{A}^v_{g'} B^p_g, \tag{3.29}$$

where $d_{\Gamma^{\mathcal{N}_g}}$ is the dimension of irrep $\Gamma^{\mathcal{N}_g}$ (an irrep of the normalizer $\mathcal{N}_g$) and $\chi_{\Gamma^{\mathcal{N}_g}}(g') = \text{Tr}\left[\Gamma^{\mathcal{N}_g}(g')\right]$ is the character of group element g' in irrep $\Gamma^{\mathcal{N}_g}$.

Thus, each coupling constants $\alpha_{(C_h,\Gamma^{\mathcal{N}_h})}$ corresponds to the mass of an anyon type and they can be tuned independently. While this Hamiltonian offers the greatest flexibility for the energy spectrum, we will follow a different construction for three main reasons:

1. First, we aim to have the non-Abelian massive Hamiltonian be as close in form to the original Kitaev construction as possible, and we can achieve this without making our Hamiltonian more non-local.

2. The second reason for 4-local terms in the Hamiltonian is that we would like our Hamiltonian to remain local since it appears to be physically more realistic. And even though it might be possible to further decrease the degree of locality to 3-local commuting terms for non-Abelian models [76], we have arguments that indicate that 2-local commuting Hamiltonians cannot be topological in 2D [77]. Indeed, the 4-local toric code Hamiltonian can be recovered effectively in the right parameter regime of a nearest-neighbor 2-local, yet frustrated, Hamiltonian on a honeycomb lattice. More generally, there is a procedure to turn a 4-local quantum double Hamiltonian for an arbitrary group into a frustrated 2-local Hamiltonian thanks to a so-called 'gadget construction' [78].

3. Third, writing 4-local terms will allow us to underline the discrepancy between anyon types and energy eigenspaces arising from the emergence of local degrees of freedom.

3.3.1.2 Flux and charge projectors

The operators acting on a plaquette and projecting to a specific flux/specific group element have already been introduced in Eq. (3.22). However, as pointed out earlier, a group element does not provide a gauge-invariant labeling of fluxons. Thus, we are lead to define a flux projector by considering a conjugacy class C_h

Definition 3.6 (Flux projectors)**.** *The flux projector associated to a conjugacy class C_h of a group G is*

$$B_{C_h} = \sum_{h' \in C_h} B_{h'}. \tag{3.30}$$

We now introduce a family of charge projectors which generalizes the projector unto the trivial irrep introduced by Kitaev in [4]. These *charge projectors* are cornerstones of our refined quantum double construction.

Definition 3.7 (Charge projectors)**.** *The charge projector associated to an irreduci-*

ble representation Γ *of the group* G *is*

$$A_\Gamma = \frac{d_\Gamma}{|G|} \sum_{g \in G} \chi_\Gamma(g) \mathcal{A}_g, \tag{3.31}$$

where d_Γ *is the dimension of irrep* Γ *and* $\chi_\Gamma(g) = Tr\left[\Gamma(g)\right]$ *is the character of group element* g *in irrep* Γ.

These charge projectors can be thought of as a special case of the 6-body projector introduced in [74] given by Eq. (3.29), with $C_h = C_e$. Using only the set of projectors defined in (3.30) and in (3.31) will lead to a different partitioning of the Hilbert space than by using the 6-body projectors of (3.29). This will be further explored in Secs. 3.4-3.5.

We defer a sketch of the proof that those operators are indeed orthogonal projectors to Sec. 3.3.1.4. One can check that for Abelian groups, our charge projectors reduce to those introduced in Refs. [48, 50]. Our charge projectors are reminiscent of similar objects introduced in [51, 52] using the representations themselves rather than the characters in the specific case of $\mathcal{D}(S_3)$.

3.3.1.3 Definition of the refined quantum double Hamiltonian

Having defined flux projectors by Eq. (3.30) and charge projectors by Eq. (3.31), we are now in a position to introduce our novel family of commuting Hamiltonians which assign different mass to different anyons.

Theorem 3.8. *The following family of topological Hamiltonians have commuting projector 4-local terms*

$$H = \sum_v \sum_{irrep\ \Gamma^G} \alpha_{\Gamma^G} A^v_{\Gamma^G} + \sum_p \sum_{C_g \subset G} \beta_{C_g} B^p_{C_g}. \tag{3.32}$$

This family of commuting Hamiltonians is a central contribution of the paper. They are a new family of topological spin Hamiltonians made out of commuting projectors, similar to well-known families of topological models such as the Levin-Wen string-net models [29] and the Turaev-Viro codes [79]. Compared to the Kitaev original quantum double Hamiltonians, they present the new feature of having tunable coupling constants that allow the discrimination of non-trivial charges and fluxes while preserving the useful mathematical properties of quantum doubles. In particular, the coupling constants can be chosen so that the ground space is identical

to the Kitaev Hamiltonian. Note that, for simplicity, we assumed the coupling coefficients to be independent of the vertices and the plaquettes, although they need not be.

We will now prove in Sec. 3.3.1.4 that the operators defined by Eq. (3.31) are indeed projectors and then in Sec. 3.3.1.5 that the charge and the flux projectors are pairwise commuting.

3.3.1.4 Orthonormality of the charge projectors

Theorem 3.9 (Orthogonality of charge projectors)**.** *The operators defined by Eq.* (3.31) *are orthonormal projectors*

$$A_\Gamma A_\Lambda = \delta_{\Gamma\Lambda} A_\Gamma. \tag{3.33}$$

Proof: This is a non-trivial consequence of the Great Orthogonality Theorem (GOT), see Fact 3.10. To prove this theorem, we will first prove a basis-independent statement of the GOT (Lemma 3.11). The full proof is deferred to the appendix in Sec. 3.A.2.

Fact 3.10 (Great Orthogonality Theorem)**.**

$$\sum_{g\in G} (\Gamma(g))_{ij} \overline{(\Lambda(g))_{i'j'}} = \frac{|G|}{d_\Gamma} \delta_{\Gamma\Lambda} \delta_{ii'} \delta_{jj'}, \tag{3.34}$$

where $\overline{a}$ is the complex conjugate of $a \in \mathbb{C}$.

The Great Orthogonality Theorem is a strong result in representation theory, usually stated at the level of matrix elements of two representations Γ and Λ of a group G [80]. In the proof of Theorem 3.9 we utilize the following basis-independent version of the Great Orthogonality Theorem. To our knowledge, this operator restatement of the GOT is novel and could prove to be a useful tool in operator theory.

Lemma 3.11 (Basis-independent GOT)**.**

$$\sum_{g\in G} \Gamma(g) \otimes \Lambda(g^{-1}) = \frac{|G|}{d_\Gamma} \delta_{\Gamma\Lambda} S, \tag{3.35}$$

where S is the swap operator, i.e., $S : \mathbb{C}^d \times \mathbb{C}^d \to \mathbb{C}^d \times \mathbb{C}^d$ is defined by $S(|i\rangle \otimes |j\rangle) = |j\rangle \otimes |i\rangle$.

Proof: The proof is deferred to the appendix in Sec. 3.A.1.

3.3.1.5 Commutation of flux and charge projectors

We now prove that the flux projectors defined by Eq. (3.30) and charge projectors defined by Eq. (3.31) are pairwise commuting. This commutation is key since it entails that the two families of projectors split the Hilbert space in a consistent way, and states can be labeled by their common eigenstates.

Lemma 3.12 (Flux permutation by vertex operators)**.** *For a plaquette p and vertex v that form a site, $(p, v) = s$*

$$B_g^{(p)} = \mathcal{A}_{h^{-1}}^{(v)} B_{hgh^{-1}}^{(p)} \mathcal{A}_h^{(v)}; \tag{3.36}$$

for a plaquette p and vertex v that are parts of different sites, $p \in s_1$, $v \in s_2$, $s_1 \neq s_2$

$$B_g^{(p)} = \mathcal{A}_{h^{-1}}^{(v)} B_g^{(p)} \mathcal{A}_h^{(v)}. \tag{3.37}$$

Proof: The proof is deferred to the appendix in Sec. 3.A.3.

Based on Lemma 3.12 we can prove that vertex operators commute with flux projectors (although they do not commute with plaquette operators in general).

Theorem 3.13.

$$[B_{C_g}, \mathcal{A}_h] = 0 \tag{3.38}$$

Proof: Lemma 3.12 shows that the vertex operators $\mathcal{A}_h$ map the states belonging to one flux sector to another flux sector. Note however that the new flux sector is in the same conjugacy class as the original flux. More formally, we have

$$\mathcal{A}_{h^{-1}} B_{C_g} \mathcal{A}_h \quad = \quad \sum_{f \in C_g} \mathcal{A}_{h^{-1}} B_f \mathcal{A}_h = \sum_{f \in C_g} B_{h^{-1} f h} = B_{C_g}. \tag{3.39}$$

The commutation relation (3.38) follows by noting that $\mathcal{A}_{h^{-1}} = (\mathcal{A}_h)^{-1}$ since vertex operators are a representation of G. □

The immediate corollary is that charge projectors also commute with flux projectors since they are linear combination of vertex operators.

Corollary 3.14.

$$[A_{\Gamma G}, B_{C_g}] = 0 \tag{3.40}$$

We can interpret the commutation of the 4-body projectors as a decoupling of the charges from the fluxes. However, there's an apparent catch with both this statement and this formalism: all the A_{Γ^G} charge projectors project unto an irreducible representation of the full group G, rather than the appropriate normalizer subgroups $\mathcal{N}_h$ to which the charges are actually assigned. This hints at the fact that excitations of distinct energy in our family of Hamiltonians are not precisely anyons. Indeed, the internal states of some anyon types will now be split into two different energy eigenspaces. We will see how this manifests itself on the example of $\mathcal{D}(S_3)$, in Secs. 3.4-3.5. Let's start by working out in details the flux and charge projectors of $\mathcal{D}(S_3)$.

3.3.2 Example of $G = S_3$

The flux projectors (3.30) in the case of $G = S_3$ are

$$B_{C_e} = B_e, \tag{3.41}$$
$$B_{C_y} = B_y + B_{y^2}, \tag{3.42}$$
$$B_{C_x} = B_x + B_{xy} + B_{xy^2}. \tag{3.43}$$

The 4-body charge projectors (3.31) for S_3 are

$$A_{\Gamma_1} = \frac{1}{6}(\mathcal{A}_e + \mathcal{A}_y + \mathcal{A}_{y^2} + \mathcal{A}_x + \mathcal{A}_{xy} + \mathcal{A}_{xy^2}), \tag{3.44}$$
$$A_{\Gamma_{-1}} = \frac{1}{6}(\mathcal{A}_e + \mathcal{A}_y + \mathcal{A}_{y^2} - \mathcal{A}_x - \mathcal{A}_{xy} - \mathcal{A}_{xy^2}), \tag{3.45}$$
$$A_{\Gamma_2} = \frac{1}{3}(2\mathcal{A}_e - \mathcal{A}_y - \mathcal{A}_{y^2}), \tag{3.46}$$

since they are based on the characters of the irreducible representations of S_3 (see Table 3.1 for the irreps of S_3).

The refined Hamiltonian (3.32) is then

$$H = \sum_v (\alpha A^v_{\Gamma_1} + \beta A^v_{\Gamma_{-1}} + \gamma A^v_{\Gamma_2}) + \sum_p (\delta B^p_{C_e} + \epsilon B^p_{C_x} + \nu B^p_{C_y}). \tag{3.47}$$

In contrast, the 6-body projectors (3.29) have the form (see Table 3.3 for the labeling

of anyons of $\mathcal{D}(S_3)$):

$$P_A = \frac{1}{6}(\mathcal{A}_e + \mathcal{A}_y + \mathcal{A}_{y^2} + \mathcal{A}_x + \mathcal{A}_{xy} + \mathcal{A}_{xy^2})B_{C_e}, \tag{3.48}$$

$$P_B = \frac{1}{6}(\mathcal{A}_e + \mathcal{A}_y + \mathcal{A}_{y^2} - \mathcal{A}_x - \mathcal{A}_{xy} - \mathcal{A}_{xy^2})B_{C_e}, \tag{3.49}$$

$$P_C = \frac{1}{3}(2\mathcal{A}_e - \mathcal{A}_y - \mathcal{A}_{y^2})B_{C_e}, \tag{3.50}$$

$$P_D = \frac{1}{2}(\mathcal{A}_e + \mathcal{A}_x)B_x + \frac{1}{2}(\mathcal{A}_e + \mathcal{A}_{xy})B_{xy} + \frac{1}{2}(\mathcal{A}_e + \mathcal{A}_{xy^2})B_{xy^2}, \tag{3.51}$$

$$P_E = \frac{1}{2}(\mathcal{A}_e - \mathcal{A}_x)B_x + \frac{1}{2}(\mathcal{A}_e - \mathcal{A}_{xy})B_{xy} + \frac{1}{2}(\mathcal{A}_e - \mathcal{A}_{xy^2})B_{xy^2}, \tag{3.52}$$

$$P_F = \frac{1}{3}(\mathcal{A}_e + \mathcal{A}_y + \mathcal{A}_{y^2})B_{C_y}, \tag{3.53}$$

$$P_G = \frac{1}{3}(\mathcal{A}_e + \omega\mathcal{A}_y + \bar{\omega}\mathcal{A}_{y^2})B_{C_y}, \tag{3.54}$$

$$P_H = \frac{1}{3}(\mathcal{A}_e + \bar{\omega}\mathcal{A}_y + \omega\mathcal{A}_{y^2})B_{C_y}. \tag{3.55}$$

The corresponding 6-local Hamiltonian (3.28) would allow to freely tune the masses of the anyons, albeit at a cost of a more non-local Hamiltonian.

3.4 Hilbert space splitting

In this Section, we elaborate on the way the charge and flux projectors split up the Hilbert space of a site. Indeed, we will see in Sec. 3.4.1 that both the charge and flux family of projectors provide a distinct way to split the Hilbert space unto which they are acting non-trivially. Moreover, since those projectors commute, those two splittings are consistent over the Hilbert space unto which they both act non-trivially, i.e., the Hilbert space of 2 spins which has dimension $|G|^2$.

We will argue that the splitting of the common Hilbert space of charge and flux operators induces a splitting of the proper Hilbert space of a site. Because sites overlap, the dimension of the proper Hilbert space of a single site is smaller than the Hilbert space of the 6 spins forming the site. We prove in Sec. 3.4.2 that this proper Hilbert space also has dimension $|G|^2$. In Sec. 3.4.3, we introduce a diagrammatic representation of this splitting. This diagram encapsulates all the results of this paper about the structure of refined quantum double models.

3.4.1 Two distinct yet consistent ways to split the Hilbert space

We first prove that the charge and flux projectors, which respectively act non-trivially on four spins, add up to the identity operator on the Hilbert space of dimension $|G|^4$

of the four spins. Since they are orthogonal projectors, charge (resp. flux) projectors provide an orthogonal resolution of the identity, i.e., the direct sum of their images amounts to the full Hilbert space.

Resolution of the identity for charge projectors

Lemma 3.15. *The dimension of the image of the charge projector for the irreducible representation* Γ *is*

$$Tr\left[A_\Gamma\right] = |G|^3 \, d_\Gamma^2, \tag{3.56}$$

where d_Γ *is the dimension of the irrep* Γ.

Proof: Recall that the vertex operators $\mathcal{A}_g$ are tensor products of 4 copies of the (left) regular representation L. $L(g)$ matrices are permutations with no fixed points, unless $g = e$. Since the trace of a tensor product is the product of the trace, $A(g)$ is traceless unless $g = e$. The vertex operator $\mathcal{A}_e$ is nothing but the identity matrix on a space of dimension $|G|^4$. Thus,

$$\mathrm{Tr}\mathcal{A}_g = |G|^4 \, \delta_{ge}. \tag{3.57}$$

Simple calculation yields

$$\mathrm{Tr}\left[A_\Gamma\right] \;=\; \frac{d_\Gamma}{|G|} \sum_{g\in G} \chi_\Gamma(g)\mathrm{Tr}\mathcal{A}_g = |G|^3 \, d_\Gamma \chi_\Gamma(e) = |G|^3 \, d_\Gamma^2. \tag{3.58}$$

□

To see that the charge projectors add up to the identity on the Hilbert space of the 4 spins, we use a well-known fact from representation theory

$$\sum_\Gamma d_\Gamma^2 = |G|. \tag{3.59}$$

Dimension counting and the fact that charge projectors are orthogonal allows us to conclude that

$$\sum_\Gamma A_\Gamma = \mathbb{1}_{|G|^4}, \tag{3.60}$$

i.e., the charge projectors are an orthogonal resolution of the identity for the Hilbert space of the 4 spins neighboring a vertex.

Resolution of the identity for flux projectors

Lemma 3.16. *The dimension of the image of the flux projector for the conjugacy class $C_g \subset G$ is*

$$Tr\left[B_{C_g}\right] = |C_g||G|^3, \tag{3.61}$$

where $|C_g|$ is the cardinality of the conjugacy class.

Proof: Flux projectors are sum of rank-one projectors unto fluxes that belong to the same conjugacy class C_g. Thus, to compute the dimension of the image of the flux projectors, one needs to compute how many terms appear in the sum, i.e., how many ways 4 group elements can be multiplied such that their product belongs to the conjugacy class C_g. The first three group elements a, b, c can be chosen arbitrarily in $|G|^3$ distinct ways. Then the fourth group element d is chosen such that the product belongs to the conjugacy class C_g, i.e., $d \in (abc)^{-1}C_g$. Thus, there are $|C_g|$ choices for d. This concludes the proof. □

Moreover, since every group element belongs to one and only one conjugacy class, we know that

$$\sum_{C_g \subset G} \left|C_g\right| = |G|. \tag{3.62}$$

Dimension counting and the fact that flux projectors are orthogonal allows us to conclude that

$$\sum_{C_g \subset G} B_{C_g} = \mathbb{1}_{|G|^4}, \tag{3.63}$$

i.e., the flux projectors are an orthogonal resolution of the identity for the Hilbert space of the 4 spins of a plaquette.

3.4.2 Dimension of the proper Hilbert space of a site

Since the flux and charge projectors pairwise commute (see Sec. 3.3.1.5), they provide a consistent splitting of the Hilbert space unto which they both act non-trivially in the sense that a basis of this Hilbert space is spanned by common eigenstates. It is clear that the intersection of their geometric support is two spins. The corresponding Hilbert space has dimension $|G|^2$.

Here we want to argue that this splitting of Hilbert space induces a splitting of the Hilbert space of a site. Naively, a site is made of 6 spins but since spins are shared by many sites, the dimension of its proper Hilbert space is smaller than $|G|^6$. We

will show that it is $|G|^2$, the same as the common Hilbert space of flux and charge projectors.

To determine the dimension of this proper Hilbert space, first recall that a site is the union of the four spins around a plaquette and the four spins around a neighboring vertex. Since 2 spins are shared, a site consists of 6 spins. However, each spin belongs to three distinct sites: one site in which it belongs to both the vertex and the plaquette, one site for the other vertex and one site for the other plaquette, see Fig. 3.5. Thus, the dimension of the (proper) Hilbert space associated to every site is

$$d\left(\mathcal{H}_{\text{site}}\right) = \sqrt[3]{|G|^6} = |G|^2 \tag{3.64}$$

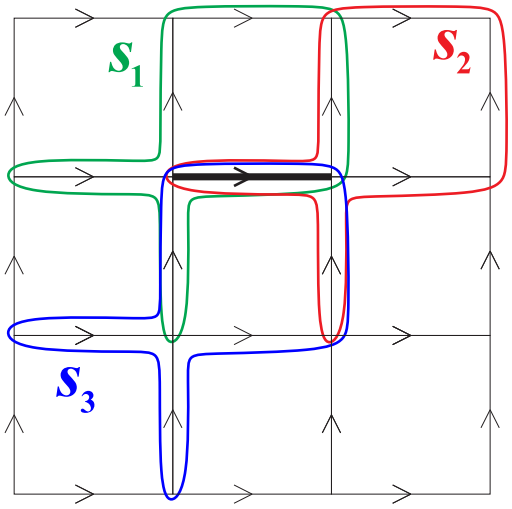

Figure 3.5: Illustration of the fact that every edge belongs to exactly 3 sites. For the thick edge in the figure the 3 sites are s_1, s_2 and s_3.

A simple way to think about this is that for every site, the two spins shared between the vertex and the plaquette are assigned to this site while other spins of the site are assigned to other neighboring sites.

This argument is only valid for square lattices. While a similar argument should hold for arbitrary local planar graph, we leave the general case for future work and focus on the case of a square lattice.

3.4.3 Diagrammatic representation and energy sectors

We now introduce a diagrammatic representation of the splitting of the proper Hilbert space of a site, which we consider to be a very useful tool to better understand the

structure of quantum double models.

The diagram, represented on Fig. 3.6 for the case of $\mathcal{D}(S_3)$, is a square of size $|G|$. Each column is indexed by an irrep Γ of G and its width is the squared dimension of the irrep d_Γ^2. Columns thus correspond to the splitting of the Hilbert space induced by the charge projectors. Similarly, each row is indexed by a conjugacy class C_g of G and its width is the cardinality of the conjugacy class $|C_g|$. Rows correspond to the splitting induced by the flux projectors.

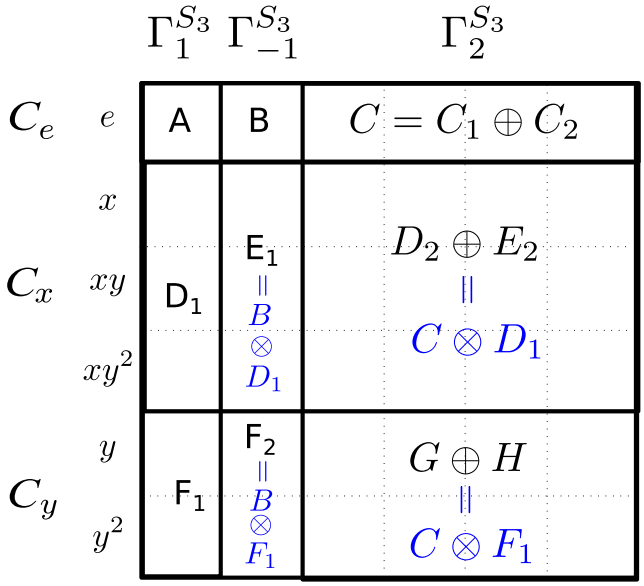

Figure 3.6: The flux and charge projectors of $\mathcal{D}(S_3)$ partition the Hilbert space of dimension $|S_3|^2 = 36$ unto which both family of operators act non-trivially. The charge projector splitting defines columns. The flux projectors, corresponding to conjugacy classes, define rows (each row between dotted lines corresponds to a group element). The 9 energy sectors are represented $\{A, B, C = C_1 \oplus C_2, D_1, E_1, D_2 \oplus E_2, F_1, F_2, G \oplus H\}$. The labels are chosen to reflect the relation of the excitations with the 8 anyon types of $\mathcal{D}(S_3)$. In particular, anyons D, E and F appear in two distinct energy sectors and there are two copies of the chargeon C, labeled C_1 and C_2. Note that the area of the surface attributed to each anyon is equal to the square of its quantum dimension. Areas of cells shared by more than one anyon are distributed among those anyons according to the corresponding irrep split-ups (Eqs. (3.69)-(3.70)), in this case equally. Labels in blue correspond to the reinterpretation of certain excitations as a combination of other excitations (see Sec. 3.5.2).

Labeling of the energy sectors

Each intersection is now labeled by a conjugacy class and an irrep. Notice that every such intersection will have a well-defined energy (see our Hamiltonian, Eq. (3.47)),

we will call these intersections *energy sectors*. However, these energy sectors do not correspond directly to anyon types since an irrep of the full group G can split into the direct sum of irreps of the normalizer of the conjugacy class. Let's explore this on the example of $G = S_3$.

Trivial representation: D_1 and F_1 Restricting the trivial representation of S_3 to the normalizer subgroup $\mathcal{N}_x$ or $\mathcal{N}_y$ will correspond to the trivial representation of both of those subgroups, i.e.,

$$\Gamma_1^{S_3}|_{\mathcal{N}_x} = \Gamma_1^{\mathbb{Z}_2} \tag{3.65}$$
$$\Gamma_1^{S_3}|_{\mathcal{N}_y} = \Gamma_1^{\mathbb{Z}_3}. \tag{3.66}$$

Thus, the energy sectors in the first column, corresponding to the trivial irrep of S_3, correspond to anyon types A, D and F (please refer to Table 3.3 for anyon labels for S_3) depending on their row, i.e., their conjugacy class. For the non-Abelian anyons D and F, we will label those energy sectors D_1 and F_1 since we will see shortly that other energy sectors correspond to those anyon types as well.

Alternating representation: E_1 and F_2 Similarly, restricting the alternating representation of S_3 to $\mathcal{N}_x$ corresponds to the alternating representation of $\mathcal{N}_x$ (excitation E_1), and restricting it to N_y will give the trivial representation of $\mathcal{N}_y$ (excitation F_2). Thus, we have already uncovered two energy sectors for anyon F.

$$\Gamma_{-1}^{S_3}|_{\mathcal{N}_x} = \Gamma_{-1}^{\mathbb{Z}_2} \tag{3.67}$$
$$\Gamma_{-1}^{S_3}|_{\mathcal{N}_y} = \Gamma_1^{\mathbb{Z}_3}. \tag{3.68}$$

Two-dimensional representation: $D_2 \oplus E_2$ and $G \oplus H$ Finally, the two-dimensional representation, restricted to $\mathcal{N}_x$ or $\mathcal{N}_y$ will break up to two 1-dimensional representations on the subgroups. These 1-dimensional representations will be the trivial and the alternating of $\mathcal{N}_x$ (dyons D_2, E_2), and the two nontrivial representations of $\mathcal{N}_y$ (dyons G and H).

$$\Gamma_2^{S_3}|_{\mathcal{N}_x} = \Gamma_1^{\mathbb{Z}_2} \oplus \Gamma_{-1}^{\mathbb{Z}_2} \tag{3.69}$$
$$\Gamma_2^{S_3}|_{\mathcal{N}_y} = \Gamma_\omega^{\mathbb{Z}_3} \oplus \Gamma_{\bar{\omega}}^{\mathbb{Z}_2}. \tag{3.70}$$

We refer the reader to Tables 3.1-3.2 to check these relations between the representations of S_3 and its subgroups. The breaking of irreps of the full group $G = S_3$ into

irreps of its subgroups $\mathbb{Z}_2$ and $\mathbb{Z}_3$ explains how our refined Hamiltonian correctly accounts for anyons D, E, F, G and H although the irreps of the normalizers $\mathbb{Z}_2$ and $\mathbb{Z}_3$ do not have an associated Hamiltonian term. This property can be made general for an arbitrary group G by discussing *induced* representations, which we do in Appendix 3.B.

Even in the smallest non-Abelian example (quantum double of S_3), irrep breaking leads to a very intricate splitting of the Hilbert space. Consider the rectangle labeled by C_x and $\Gamma_2^{S_3}$. The two-dimensional irrep will split into the sum of two one-dimensional irreps of $\mathbb{Z}_2$. However, the splitting is slightly different since the normalizers $\mathcal{N}_x$, $\mathcal{N}_{xy}$, and $\mathcal{N}_{xy^2}$, while isomorphic, are not equal.

Energies

Recall the Hamiltonian given by Eq. (3.47). We can compute the energy associated to each energy eigenspace (energy sector), which we denote J to avoid confusion with anyon type E. This Hamiltonian assigns the following energies to the excitations: $J_A = \alpha + \delta$, $J_B = \beta + \delta$, $J_{C_1} = J_{C_2} = \gamma + \delta$, $J_{D_1} = \alpha + \epsilon$, $J_{D_2} = J_{E_2} = \gamma + \epsilon$, $J_{E_1} = \beta + \epsilon$, $J_{F_1} = \alpha + \nu$, and $J_{F_2} = \beta + \nu$, $J_G = J_H = \gamma + \nu$. Thus, we see that anyon types D, E and F, can be in different energy eigenspaces. This is surprising and should not be possible from a topological point of view. However, anyons in a quantum double are not fundamental particles, rather emergent quasi-particles on a *lattice* model. We will now explore further this discrepancy and see that the existence of local degrees of freedom on a lattice explains the different energies attributed to states corresponding to the same anyon at the mesoscopic level.

Dimension and area of the diagram

Finally, note that the area of the rectangle (or the sum of the areas of distinct rectangles when an anyon occupies different energy sectors) is exactly the squared quantum dimension of that anyon $(d_k)^2$. Since the area of the whole square is $|G|^2$, we recover the well-known result

$$\mathcal{D}^2 \equiv \sum_k (d_k)^2 = |G|^2. \tag{3.71}$$

We will see that the topological degrees of freedom of an anyon have dimension d_k while the local degrees of freedom have also dimension d_k, which results in a dimension $(d_k)^2$ for each anyon.

3.5 Local degrees of freedom

We now elucidate the fact that anyon types are not in one-to-one correspondence with energy sectors. We will argue that anyon types are labels that are topological at the mesoscopic level, in the sense that they cannot be changed locally. However, additional *local* degrees of freedom, which can be modified by local unitary transformations acting close to the excitations, also arise. We explore the complex interplay of those different types of degrees of freedom.

3.5.1 Disagreement between anyons and energy sectors

The way the Hilbert space of a site is split up by the charge and flux projectors, detailed in Sec. 3.4, leads to a disagreement between energy sectors of our Hamiltonian and anyon labels. Here, we will explain in detail what we mean by this disagreement.

First, chargeons appear in multiple copies. For $G = S_3$, the chargeon C corresponding to the non-trivial 2D irrep appears in 2 copies, labeled C_1 and C_2. In general, an irrep Γ^G will result in a number of copies equal to its dimension d_{Γ^G}. This simply reflects that the multiplicity of the irrep in the regular representation is equal to its dimension.

Second, some anyons appear in multiple energy sectors. As an example, let's look at anyon D, which appears in two distinct energy sectors of the diagram since the trivial irrep of $\mathbb{Z}_2$ can be obtained from the trivial irrep of S_3, see Eq. (3.65), or from the two-dimensional irrep of S_3, see Eq. (3.69). We say that anyon D comes in two distinct *charge flavors*. Each charge flavor is an eigenspace of the Hamiltonian. D_1 labels a subspace with dimension three and is within the image of the trivial irrep of S_3 whereas the label D_2 labels a subspace of dimension six and is within the image of the two-dim irrep of S_3. The same phenomenon relates E_1 to E_2 and F_1 to F_2.

It seems peculiar that a local observable allows to distinguish two subspaces of internal states of anyon D (i.e., the two charge flavors). This even seems like a violation of anyonic properties of D, since by simply applying the local operators $A_{\Gamma_1^{S_3}}$ and $A_{\Gamma_2^{S_3}}$ we can establish a global labeling that differentiates between the two charge flavors based on their energies. How is that possible if both those charge flavors of D are just subspaces of one and the same anyon? We will argue that the anyon labeling corresponds to degrees of freedom that cannot be changed locally whereas there exist *local degrees of freedom* that can be changed locally. The charge projectors discriminate among those local degrees of freedom.

The surprising property that site excitations corresponding to the same anyon type

can have different energies is not a peculiarity of our family of Hamiltonians. In fact, this property was already present in Kitaev's original Hamiltonian. Indeed, in the original quantum double construction, the pairs $(D_1,\ D_2)$ and $(F_1,\ F_2)$ would have different energy. Our family of Hamiltonian simply highlights this property.

3.5.2 The role of finite lattice spacing

The charge projectors act on the four spins around a vertex, and not on the remaining two spins of a site, see Fig. 3.4. They can be interpreted as operators that coherently move all fluxon types and check that they transform according to the correct irrep [74]. In particular, note that those test fluxons do not enclose the flux content of the *site*.

Now, let us recall the interference experiment described in Sec. 3.2.1, that allows us to determine the charge of a dyon by having test fluxons undergo a double slit experiment with the dyon located behind the slits. It was key in that experiment that the flux of the test fluxon (a) and the flux of the measured dyon (b) have commuting labels, i.e., $ab = ba$, in order to have interference. The consequence of this requirement was that the charge of the measured dyon was labeled by an irrep of the normalizer $\mathcal{N}_b$ rather than an irrep of the full group G. However, this requirement stemmed from the fact that in a topological quantum field theory, to determine the charge of a dyon, one cannot avoid enclosing the flux of the dyon as well. But does that fact still hold in our *lattice* model?

Indeed, in the quantum double construction, the charge of a dyon is located on a vertex whereas its flux is located on a plaquette, see Fig. 3.7. In other words, the lattice separates charge and flux. This separation then allows something that would be impossible in a field theory: to braid the test fluxon with the charge part of a dyon without enclosing its flux. The corresponding worldline for the text fluxon is represented in purple on Fig. 3.7 (worldline 1), whereas the worldline allowed by field theory is represented in black (worldline 2). Consequently, this experiment discriminates different *charge flavors* of a dyon.

Interpreting charge flavors in $\mathcal{D}(S_3)$

Based on the arguments above, we can understand better the meaning of the charge flavors D_1 vs D_2, E_1 vs E_2 or F_1 vs F_2. For instance, for anyon F, F_1 is a pure fluxon since its charge is the trivial irrep of S_3, while F_2 has the non-trivial alternating charge (see Fig. 3.6). They both correspond to anyon F since the alternating charge becomes trivial when restricted to the normalizer $\mathcal{N}_y$ as indicated by Eq. (3.68).

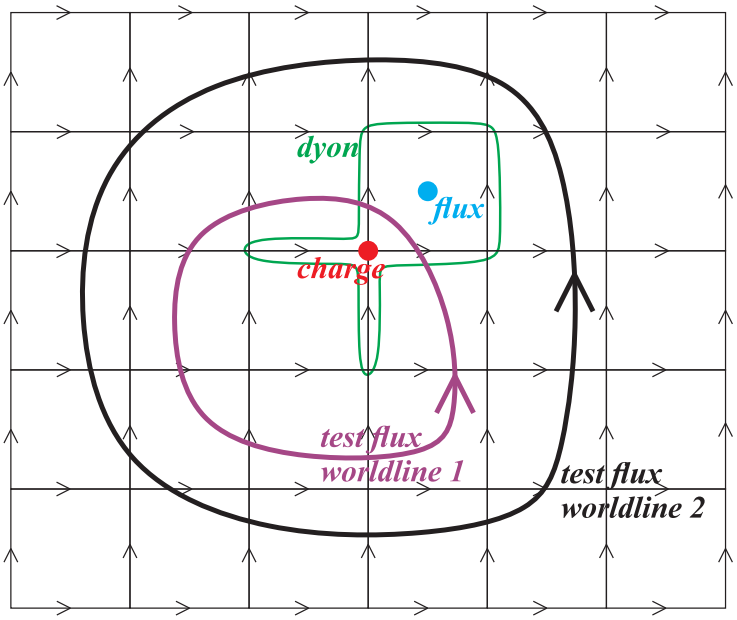

Figure 3.7: Spatial separation of charge and flux of a dyon on the lattice: the charge is located on a vertex, while the flux is on the plaquette. This allows one to take a test flux around *only the charge part* of a dyon following the test fluxon worldline 1. Such interferometric experiment allows to determine not only its charge but also its charge flavor since it is unaffected by the flux of the dyon. On the contrary, topological quantum field theory only allows for test fluxon worldline 2 which encloses both the charge and flux of the dyon.

One way to interpret this result is that F_2 is an excitation on a site which contains both a fluxon F_1 on the plaquette and a chargeon B on the vertex. Thus,

$$F_2 = B \otimes F_1, \tag{3.72}$$

which agrees with the known fusion rules of $\mathcal{D}(S_3)$ which state that $B \otimes F = F$ [69]. In terms of masses, one can notice that $M_{F_2} = M_{F_1} + M_B$, where for anyon X: $M_X = J_X - J_A$, i.e., mass is the energy penalty of anyon X compared to vacuum. Thus, one can think of F_2 as a composite anyon made of F_1 and B. We will see that a similar relation between masses will be true for the following examples as well.

Similarly, the anyon E_1 is a composite anyon made of the fluxon D_1 with the chargeon B

$$E_1 = B \otimes D_1, \tag{3.73}$$

as well as the fusion rules state $B \otimes D = E$ [69].

The other case of energy sector–anyon disagreement is slightly more involved since it involves a direct sum:

$$D_2 \oplus E_2 = C \otimes D_1, \tag{3.74}$$

i.e., the combination of the chargeon C (either from the C_1 or C_2 copies) with a fluxon D_1 is a superposition of anyon D and E with a charge corresponding to the two-dimensional irrep of S_3. The Hamiltonian doesn't distinguish D_2 from E_2 since they have the same energy. The fusion rules are again in agreement with this statement: $C \otimes D = D \oplus E$ [69]. Similarly, the energy sector $G \oplus H$ results from the combination of a chargeon C and a fluxon F_1:

$$G \oplus H = C \otimes F_1, \tag{3.75}$$

which agrees with the fusion rule $C \otimes F = G \oplus H$ [69].

We can relabel the energy sectors of Fig. 3.6 based on those combinations of flux and charge. The new labels are indicated in blue.

3.5.3 Local vs. global degrees of freedom

We now argue that charge flavor is a local degree of freedom which can be transformed by a local unitary whereas anyon labels cannot be changed locally. We present an intuitive argument and refer to [74] for a formal, yet distinct, argument.

The charge flavor cannot be discriminated by any operator that encloses the whole site $s = (v, p)$, since it requires enclosing the vertex v without enclosing the plaquette p (see Fig. 3.7). This means that two distinct charge flavors, say D_1 and D_2, have the same reduced density matrix outside the site, i.e., on the set of spins that do not belong to that site s. Yet, they correspond to distinct global states $|\psi_1\rangle$ and $|\psi_2\rangle$ on the whole lattice. Since those states are purifications of the same reduced density matrix, there exists a local unitary transformation U_s acting only on the site s such that $U_s|\psi_1\rangle = |\psi_2\rangle$. A similar statement holds for different copies of a chargeon such as C_1 and C_2.

The presence of local degrees of freedom explains that the dimension of the subspace associated with an anyon labeled by the conjugacy class C_g and the irrep Γ of its normalizer is

$$d^2 = \left(|C_g||d_\Gamma|\right)^2 \tag{3.76}$$

rather than d, which we expect from topological quantum field theory [33]. The dimension of the anyon is the product of the dimensions of its local and topological degrees of freedom. It turns out that for quantum double models there are as many

local degrees of freedom as global topological degrees of freedom [74], i.e.,

$$d_{\text{local}} = d_{\text{topo}} = d, \tag{3.77}$$

however, the number of local degrees of freedom appears to be tied to the specific lattice configuration, in our case the square lattice; see Sec. 3.4.2 for more details.

Thus, in a quantum double model, due to the lattice, each anyon corresponds to a subspace of dimension

$$d_{\text{local}} \times d_{\text{global}} = d^2. \tag{3.78}$$

This result confirms the observation made on the anyon splitting diagram of Fig. 3.6 in which each anyon corresponds to a surface of area d^2. Moreover, the total area $|G|^2 = \sum_k d_k^2$ is a graphical representation of the identity given by Eq. (3.71).

3.6 Discussion

In this paper, we introduced a new family of 2D topological spin lattice models which generalize Kitaev's quantum double construction. The Hamiltonian of this new class of topological models is given by a translation-invariant sum of local commuting terms acting each on 4 neighboring spins.

We provided a proof on the commutation of those operators which is based on a basis-independent reformulation of the Great Orthogonality Theorem.

Each local term of that refined Hamiltonian can be multiplied by a coupling constant which makes the energy spectrum of those models richer than the original Kitaev quantum double construction. Moreover, the new Hamiltonian highlights the feature that point-like excitations on a site corresponding to the same anyon can have different energies. This feature arises because the lattice introduces local degrees of freedom in addition to topological degrees of freedom. The interplay between those degrees of freedom might lead to surprising consequences.

3.6.1 Consequences for quantum computation

The disagreement between anyons and energy sectors is already present in the original quantum double construction, since Kitaev's Hamiltonian would give different masses to D_1 which is a fluxon than D_2 which is a dyon (from the point of view of irreps of S_3). Similar properties hold for the two charge flavors of anyon F, labeled F_1 and F_2, as well as anyon E, labeled E_1 and E_2, the latter would however not be distinguished by Kitaev's Hamiltonian. This leads us to the troubling question of what (if any) consequences will arise in quantum computation with non-Abelian

anyons when performing them on a lattice?

As the disagreement between anyons and energy sectors arises due to the finite separation between flux and charge of a dyon, one would have to be careful to perform every braiding procedure on a large scale, making sure to always braid with both flux and charge of a dyon. On a large enough lattice system, we can imagine the spacing will become insignificant, and no consequences will arise. On the other hand, the environment could introduce local noise that will project out one or the other charge flavor of a dyon, possibly resulting in unexpected processes, if for example, the local degrees of freedom entangle with the topological degrees of freedom. It is possible that this will not create problem for topological quantum computation since it occurs in fusion space. Nonetheless, clarifying those consequences needs careful consideration, and is the scope of future work.

3.6.2 Consequences for quantum memories

Using our family of Hamiltonians allows for tuning the masses of excitations, which will modify both the coherent dynamics and the incoherent dynamics of the topological model in the presence of a (thermal) environment. Thus, our family of Hamiltonian opens a new possibility for quantum self-correcting models based on topological models. Indeed, our models generalize the Abelian construction in Ref. [48] where a parameter regime interesting for quantum self-correction was identified. In that regime, it was argued that entropic effects lead to a different scaling of the memory time. While that improvement was shown to not carry over in the low temperature regime [50], a non-Abelian model might yield a different result or, at least, allow for a better understanding of entropic effects in quantum double models.

3.6.3 Holography between local, topological, and fusion degrees of freedom?

The fact that local degrees of freedom and topological degrees of freedom have the same dimension d_k (where k labels the anyon types) might be a clue pointing to an underlying holography. Moreover, the dimension of the subspace associated to an anyon on a site is $(d_k)^2$, which is the same dimension as the fusion space of two anyons of type k. We wonder whether this also hints at a deeper mathematical/physical connection.

Finally, it seems that local degrees of freedom are somehow unavoidable in a quantum double construction. Indeed, anyons live on a site, whose proper Hilbert space dimension is $|G|^2$. In the absence of local degrees of freedom, the direct sum of every anyon subspace would have dimension $\sum_k d_k$. Since this last quantity

is not simply related to the dimension of the group $|G|$, local degrees of freedom have to account for the dimension mismatch. The emergence of local degrees of freedom, considered here for quantum double models, could be very different in other topological models, such as Levin-Wen models [29]. We leave this question for future work.

3.A Mathematical proofs

We now detail the mathematical proofs of Sec. 3.3.

3.A.1 Proof of Lemma 3.11

To prove Theorem 3.9, we need to first prove Lemma 3.11, which is a restatement of the Great Orthogonality theorem, Fact 3.10.

Lemma (Basis-independent GOT)**.**

$$\sum_{g\in G} \Gamma(g) \otimes \Lambda(g^{-1}) = \frac{|G|}{d_\Gamma} \delta_{\Gamma\Lambda} S, \tag{3.79}$$

where S is the swap operator, i.e., $S : \mathbb{C}^d \times \mathbb{C}^d \to \mathbb{C}^d \times \mathbb{C}^d$ is defined by $S(|i\rangle \otimes |j\rangle) = |j\rangle \otimes |i\rangle$.

Proof: The proof is a sequence of simplifications. The GOT is specifically used to simplify Eq. (3.83):

$$\sum_{g\in G} \Gamma(g) \otimes \Lambda(g^{-1}) \tag{3.80}$$

$$= \sum_{g\in G} \sum_{ij} (\Gamma(g))_{ij} |i\rangle\langle j| \otimes \sum_{k\ell} \left(\Lambda(g^{-1})\right)_{k\ell} |k\rangle\langle \ell| \tag{3.81}$$

$$= \sum_{g\in G} \sum_{ij} (\Gamma(g))_{ij} |i\rangle\langle j| \otimes \sum_{k\ell} \overline{(\Lambda(g))_{\ell k}} |k\rangle\langle \ell| \tag{3.82}$$

$$= \sum_{ijk\ell} \sum_{g\in G} (\Gamma(g))_{ij} \overline{(\Lambda(g))_{\ell k}} |i\rangle\langle j| \otimes |k\rangle\langle \ell| \tag{3.83}$$

$$= \sum_{ijk\ell} \frac{|G|}{d_\Gamma} \delta_{\Gamma\Lambda} \delta_{i\ell} \delta_{jk} |i\rangle\langle j| \otimes |k\rangle\langle \ell| \tag{3.84}$$

$$= \frac{|G|}{d_\Gamma} \delta_{\Gamma\Lambda} \sum_{ij} |i\rangle\langle j| \otimes |j\rangle\langle i| \tag{3.85}$$

$$= \frac{|G|}{d_\Gamma} \delta_{\Gamma\Lambda} S. \tag{3.86}$$

□

3.A.2 Proof of Theorem 3.9

We can now prove Theorem 3.9.

Theorem (Orthogonality of charge projectors)**.** *The operators defined by Eq.* (3.31) *are orthonormal projectors*

$$A_\Gamma A_\Lambda = \delta_{\Gamma\Lambda} A_\Gamma. \tag{3.87}$$

Proof: Simple algebra shows that

$$A^s_\Gamma A^s_\Lambda = \frac{d_\Gamma d_\Lambda}{|G|^2} \sum_{g,g' \in G} \chi_\Gamma(g)\chi_\Lambda(g') \mathcal{A}^s_g \mathcal{A}^s_{g'} \tag{3.88}$$

$$= \frac{d_\Gamma d_\Lambda}{|G|^2} \sum_{h\in G} \underbrace{\sum_{g\in G} \chi_\Gamma(g)\chi_\Lambda(g^{-1}h)}_{(*)} \mathcal{A}^s_h. \tag{3.89}$$

We thus would like to prove that the $(*)$ term is proportional to $\delta_{\Gamma\Lambda} \cdot \chi_\Lambda(h)$.

Using the fact that $\mathrm{Tr}\,[A \otimes B] = \mathrm{Tr}\,[A]\,\mathrm{Tr}\,[B]$, one can rewrite the $(*)$ term as

$$(*) = \mathrm{Tr}\left[\left(\sum_{g\in G} \Gamma(g) \otimes \Lambda(g)^\dagger\right)(\mathbb{I} \otimes \Lambda(h))\right]. \tag{3.90}$$

We can now use Lemma 3.11 to express the trace as

$$(*) = \delta_{\Gamma\Lambda} \frac{|G|}{d_\Gamma} \mathrm{Tr}\left[\sum_{ij} (|i\rangle\langle j| \otimes (|j\rangle\langle i|)\,\Lambda(h)\right] \tag{3.91}$$

$$= \delta_{\Gamma\Lambda} \frac{|G|}{d_\Gamma} \sum_{ij} \delta_{ij} \langle i|\Lambda(h)|j\rangle \tag{3.92}$$

$$= \delta_{\Gamma\Lambda} \frac{|G|}{d_\Gamma} \sum_{i} (\Lambda(h))_{ii} \tag{3.93}$$

$$= \delta_{\Gamma\Lambda} \frac{|G|}{d_\Gamma} \chi_\Lambda(h), \tag{3.94}$$

which concludes the proof of Theorem 3.9. □

3.A.3 Proof of Lemma 3.12

We prove Lemma 3.12.

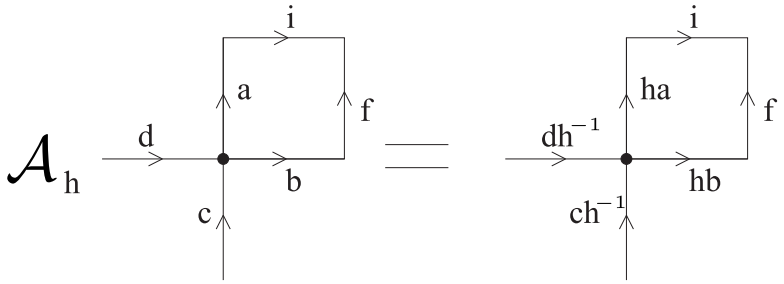

Figure 3.8: Relative configuration of a vertex and a plaquette in the case when the commutation of charge and flux projectors is nontrivial. The figure shows how a vertex operator acts on these spins. Note that the flux around the plaquette, starting from the vertex, is $g = bfi^{-1}a^{-1}$ prior to the application of $\mathcal{A}_h$. Afterward, the flux is now $g' = hbfi^{-1}(ha)^{-1} = hgh^{-1}$.

Lemma (Flux permutation by vertex operators)**.** *For a plaquette p and vertex v that form a site, $(p, v) = s$*

$$B_g^{(p)} = \mathcal{A}_{h^{-1}}^{(v)} B_{hgh^{-1}}^{(p)} \mathcal{A}_h^{(v)}; \tag{3.95}$$

for a plaquette p and vertex v that are parts of different sites, $p \in s_1$, $v \in s_2$, $s_1 \neq s_2$

$$B_g^{(p)} = \mathcal{A}_{h^{-1}}^{(v)} B_g^{(p)} \mathcal{A}_h^{(v)}. \tag{3.96}$$

Proof: We will check the operator equality for an arbitrary state in which each spin is in a flux state (such states span the full (Hilbert) space). Note that the plaquette operator B_g is in fact a projector unto states with flux g threading the plaquette while states having a different flux are annihilated by B_g. Thus, the Hilbert space is split into a direct sum

$$\mathcal{H} = I_g \oplus K_g, \tag{3.97}$$

where I_g (resp. K_g) denotes the image (resp. kernel) of the projector. The image is spanned by states with flux g while states with other flux span the kernel. We will prove Eq. (3.95) first for a state in I_g and then for a state in K_g.

For a state $|\psi_g\rangle$ whose flux is g, i.e., $B_g|\psi_g\rangle = |\psi_g\rangle$ the application of the vertex operator $\mathcal{A}_h$ will act non-trivially on two spins around the plaquette and change its flux to hgh^{-1} (when the plaquette and vertex operators act on the same site, see Fig. 3.8). Thus, $\mathcal{A}_h|\psi_g\rangle$ is in the image of $B_{hgh^{-1}}$, i.e.,

$$\mathcal{A}_h|\psi_g\rangle = B_{hgh^{-1}} \mathcal{A}_h|\psi_g\rangle. \tag{3.98}$$

Finally, applying $\mathcal{A}_{h^{-1}}$ will restore the spins into their original state and, in particular, restore the flux to $h^{-1}(hgh^{-1})h = g$, so that

$$\mathcal{A}_{h^{-1}} B_{hgh^{-1}} \mathcal{A}_h |\,\psi_g\rangle = |\,\psi_g\rangle. \tag{3.99}$$

Let's now consider a state $|\,\phi\rangle$ whose flux is not g, i.e., $B_g|\,\phi\rangle = 0$. That state is a linear combination of states with flux $f \neq g$. Let's assume that $|\,\phi\rangle$ has a well-defined flux f (the general case will follow by linearity). Then, $\mathcal{A}_h|\,\phi\rangle$ will have flux hfh^{-1} and will be annihilated by $B_{hgh^{-1}}$ since $hfh^{-1} \neq hgh^{-1}$. Thus,

$$\mathcal{A}_{h^{-1}} B_{hgh^{-1}} \mathcal{A}_h |\,\phi\rangle = 0. \tag{3.100}$$

Since we checked Eq. (3.95) on the two sectors of Eq. (3.97), it is valid for any state of the Hilbert space. Please note that we proved Eq. (3.95) only for one respective position of the vertex with respect to the plaquette. For the other three respective positions one can dutifully check that the proof is also valid, resulting in Eq. (3.96). □

3.B Induced representations of an arbitrary quantum double $\mathcal{D}(G)$

A surprising feature of our refined quantum double Hamiltonian (3.47) (see Eq. (3.32) for the general form) is that irreps of normalizers that are proper subgroups of G do not have an associated Hamiltonian term. For instance, in the case of $\mathcal{D}(S_3)$, the irreps of $\mathbb{Z}_2$ and $\mathbb{Z}_3$ do not have an associated Hamiltonian term. How is it then that anyons D, E, F, G and H which are labeled by irreps of those two subgroups are correctly accounted for?

The reason they have not been forgotten is that the irreps of those subgroups appear when restricting the irrep of S_3 to the fluxes within a normalizer. For instance, if we know that a dyon has flux in the conjugacy class C_y and that the charge on the vertex corresponds to the 2-dim irrep $\Gamma_2^{S_3}$, we should consider the action of this irrep restricted to the elements of the normalizer $\mathcal{N}_y$. One can straightforwardly check that the 2-dim irrep of the group splits into two 1-dim irreps of the subgroup $\mathbb{Z}_3$, i.e., recall Eq. (3.70):

$$\Gamma_2^{S_3}|_{\mathcal{N}_y} = \Gamma_{\omega}^{\mathbb{Z}_3} \oplus \Gamma_{\bar{\omega}}^{\mathbb{Z}_3}. \tag{3.101}$$

Thus, the anyons $G = (C_y, \Gamma_{\omega}^{\mathbb{Z}_3})$ and $H = (C_y, \Gamma_{\bar{\omega}}^{\mathbb{Z}_3})$ are accounted for. However, our Hamiltonian will give them the same mass since it does not distinguish between them. This is a general feature of our construction in the sense that the splitting of irrep of the group G to recover irreps of the normalizer will happen for any group

G.

Indeed, the statements about the correspondence between representations of the group and its subgroups can be made rigorous for any group G. For any finite group G, the A_{Γ^G} charge projector corresponding to irrep Γ^G will contain in its image the particle with trivial flux and Γ^G charge, as well as all particles that have non-trivial flux C_h ($h \neq e$) and their charge corresponds to the restricted representation [80] of Γ^G onto the appropriate normalizer subgroup $\mathcal{N}_h$:

$$(C_e, \Gamma^G) \subset \mathfrak{I}[A_{\Gamma^G}] \tag{3.102}$$

$$(C_h, \Gamma^G|_{\mathcal{N}_h}) \subset \mathfrak{I}[A_{\Gamma^G}], \tag{3.103}$$

where $\mathfrak{I}[O]$ denotes the image of operator O and $\subset$ means that the anyon labeled by the pair (conjugacy class, irrep) corresponds to a subspace located within the vector space on the right hand-side.

If $\Gamma^G|_{\mathcal{N}_h}$ is reducible on $\mathcal{N}_h$, then anyons will instead correspond to the resulting irreps:

$$\Gamma^G|_{\mathcal{N}_h} = \bigoplus_i \Gamma_i^{\mathcal{N}_h} \tag{3.104}$$

$$\text{anyon label}_i = (C_h, \Gamma_i^{\mathcal{N}_h}) \tag{3.105}$$

and all such anyons ($\forall i$) will have the same energy. For example, for the group $G = S_3$, anyons G and H have the same energy.

Similarly, one might ask the converse question: if we take an anyon type $(C_h, \Gamma^{\mathcal{N}_h})$, does the 4-local Hamiltonian account for it? The answer is yes; one needs to consider the *induced* representation κ^G from $\Gamma^{\mathcal{N}_h}$ onto the full group G [80]. In the case that the induced representation is irreducible on G, then that anyon labeled $(C_h, \Gamma^{\mathcal{N}_h})$ corresponds to charge κ^G

$$\text{Ind}_{\mathcal{N}_h}^G(\Gamma^{\mathcal{N}_h}) = \kappa^G \tag{3.106}$$

$$(C_h, \Gamma^{\mathcal{N}_h}) \subset \mathfrak{I}[A_{\kappa^G}], \tag{3.107}$$

whereas, in the case the induced representation is reducible on the group G, then the anyon labeled $(C_h, \Gamma^{\mathcal{N}_h})$ corresponds to different charge flavors κ_i^G:

$$\text{Ind}_{\mathcal{N}_h}^G(\Gamma^{\mathcal{N}_h}) = \bigoplus_i \kappa_i^G \tag{3.108}$$

$$(C_h, \Gamma^{\mathcal{N}_h}) \subset \mathfrak{I}[A_{\kappa_i^G}] \quad \forall i. \tag{3.109}$$

For example, for $G = S_3$, anyon F is in the image of both $A_{\Gamma_1^{S_3}}$ and $A_{\Gamma_{-1}^{S_3}}$, as $\Gamma_1^{S_3}$ and $\Gamma_{-1}^{S_3}$ are the irreducible components of $\mathrm{Ind}_{\mathcal{N}_y}^{S_3}(\Gamma_1^{\mathcal{N}_y})$.

Chapter 4

TOPOLOGICAL PHASE DIAGRAM OF $\mathcal{D}(S_3)$ INDUCED BY FORBIDDING CHARGES AND FLUXES

Anna Kómár, and Olivier Landon-Cardinal. Topological phase diagram of $\mathcal{D}(S_3)$ induced by forbidding charges and fluxes. *arXiv preprint: 1805.00032*.

Abstract

We analyze phase transitions induced by forbidding charges and fluxes in $\mathcal{D}(S_3)$, the simplest non-Abelian model among quantum doubles, a class of 2D spin lattice topological models introduced by Kitaev. Contrary to a topological quantum field theory, the lattice degrees of freedom allow to forbid charges and fluxes independently, resulting in a non-trivial effect on dyons. Forbidding charges and fluxes leads to only a subset of the original anyons remaining, and when this subset is closed under fusion, they form a new theory. We interpret the processes the theory undergoes in terms of condensation and splitting of particles. Mapping the phase diagram of $\mathcal{D}(S_3)$, we find the emergent phase $\mathcal{D}(\mathbb{Z}_3)$, based on a subgroup of S_3, as well as that other phases, charge and flux sectors of doubles, will fully condense to the vacuum.

4.1 Introduction

Understanding phase transitions and critical phenomena of physical systems is an important step in understanding properties of physical materials and fundamental physical processes. Classical phase transitions, e.g., magnetic transitions of the Ising model are well-understood, and are described by Landau's theory, using a free-energy description of the processes [49]. Therein the free energy, a local function of the state of the system, undergoes a change where it encounters a discontinuity (first-order phase transition), or a discontinuity of a higher-order nth derivative (nth-order phase transition).

Quantum phase transitions occur as a result of a change in the Hamiltonian of a quantum system, when slowly changing from one Hamiltonian to another the system passes through a critical point of non-analiticity. This could happen at a point where the ground state and the first excited state produce a level-crossing (the gap closes), or even when the gap becomes small enough that it would close *in a limit*. The classic

description of Landau's theory can be extended to provide a faithful description of these processes as well, through a quantum-classical mapping [49].

An important concept of Landau's theory is the existence of a *local order parameter* that characterizes the state of the system. This is the main parameter of the free energy function, and the form of the function is inferred using existing symmetries of the system. However, introduce topological theories, and Landau's theory breaks down. Topological order, an inherently non-local property, can't be captured through a local order parameter. As a result, changes in the topological order of a field theory can't be described using this classic framework. An accurate description of topological phase transitions would help us understand more about the nature of topological order.

One well-known theory exhibiting topological order is the quantum double construction, introduced by Kitaev in Ref. [4]. This is a family of 2D spin theories on a lattice, with a Hamiltonian whose ground state exhibits topological order. This means that there exists no local parameter that characterizes the ground state, and as such, quantum doubles are prime candidates for storing quantum information in: information stored in their degenerate ground space won't decohere due to local noise from the environment. The specific quantum double, and thus the specific topological order such a theory realizes, depends on the group, G that is used to build the quantum double. As a result, quantum doubles built around different groups would have different topological properties.

In this work, we analyze phase transitions of quantum doubles, induced by changing the set of allowed excitations (anyons) in the theory. A correspondence between the set of anyons in a field theory, and the topological order of the ground state has been established in Ref. [81]. Therefore, anyons of a theory may be treated as a signature of topological order, a concept we will revisit in the Discussion section of this paper.

We focus our analysis on the simplest non-Abelian quantum double, $\mathcal{D}(S_3)$, and investigate what processes this double undergoes when we remove (or forbid) certain anyons from the theory, i.e., we don't allow their creation through thermal processes from the vacuum. More precisely, we forbid conjugacy classes and irreducible representations of the group, which leads to forbidding anyons. Whenever the resulting allowed set of anyons is closed under fusion, a new, consistent theory emerges. We interpret the mathematical steps of our calculations as physical processes: condensation and splitting of particles.

We make a map of the phase diagram of $\mathcal{D}(S_3)$, and find the phase $\mathcal{D}(\mathbb{Z}_3)$, an Abelian theory that is based on a subgroup of S_3. We conclude that other phases,

the charge and flux sectors of $\mathcal{D}(\mathbb{Z}_3)$ among others, will become trivial after all excitations condense to the vacuum.

This paper is organized as follows. In Sec. 4.2 we provide a general review of anyons and anyonic data (Secs. 4.2.1-4.2.2) and introduce the quantum doubles that appear in this paper (Sec. 4.2.3). Then, in Sec. 4.3 we will give an overview of the physical processes a quantum double might undergo during a phase transition; this is in fact a summary of all processes found in the later sections, with their physical interpretations. In this section, we also give a detailed description of our mathematical protocol, used to obtain the results of this paper. In Sec. 4.4, we demonstrate this protocol on four cases of phase transitions: one transition yields $\mathcal{D}(\mathbb{Z}_3)$, two others yield the charge and flux sectors of $\mathcal{D}(\mathbb{Z}_3)$ that won't live on their own and will fully condense to the vacuum, and the last one yields the charge sector $\mathbb{Z}_2$, which again will become trivial after its single excitation condenses to the vacuum. Until this point our analysis focuses only on the anyons, and the field theory aspects of quantum doubles. In Sec. 4.5 we investigate possible ways to realize these phase transitions, using the standard lattice description. We argue that while strictly speaking a global projection might be necessary to induce a phase transition, this can be approximated by adding local terms to the topological Hamiltonian of the model. Sec. 4.6 is a summary of our results and further directions. Finally, the appendix contains additional mathematical properties of the doubles discussed in this paper (Appendix 4.A).

4.2 Anyons in Drinfeld doubles

We start by introducing the concept of anyons, and that of non-Abelian anyons (Sec. 4.2.1). Anyons can emerge as excitations of two-dimensional field theories, their exchange statistics differ from the trivial statistics of bosons and fermions. In Sec. 4.2.2 we will present the mathematical framework for the description of anyons, including the concept of the braiding S-matrices and fusion rules. Then, in Sec. 4.2.3 we introduce a few examples of Drinfeld doubles, which have anyonic excitations. We provide three examples: Abelian doubles $\mathcal{D}(\mathbb{Z}_2)$, widely known as the toric code, and $\mathcal{D}(\mathbb{Z}_3)$, as well as the non-Abelian double $\mathcal{D}(S_3)$, which is the central object of this paper.

4.2.1 Anyons and labeling

In two-dimensional field theories, excitations can have esoteric exchange statistics, unlike those of bosons and fermions. Denoting the (counterclockwise) exchange operation of particles a and b by R_{ab}, doubly exchanging said particles of a two-

dimensional theory in general can yield

$$R^2_{ab}|\,a,b\rangle = U_{a,b}|\,a,b\rangle, \tag{4.1}$$

where $U_{a,b}$ is a unitary transformation acting on the joint wave function. If the effect of $U_{a,b}$ is a simple (non-trivial) phase, $\exp(i\varphi)$, then we call a and b *Abelian anyons*, otherwise they are *non-Abelian*.

Following Ref. [33], we can introduce flux- and charge-labels for the anyons. The flux labels are elements of a group $g \in G$, and the charge labels are irreducible representations, or *irreps* of the same group G. These two labellings, in fact, provide two complementary resolutions of the Hilbert space of an anyon:

$$\mathcal{H} = \text{span}\,\{|\,g\rangle \mid g \in G\} \tag{4.2}$$

$$\mathcal{H} = \text{span}\,\{|\,\Gamma, i\rangle \mid \Gamma \text{ irrep of } G,\ i \in \{1, ...|\Gamma|\}\}\,. \tag{4.3}$$

Anyons that only have a non-trivial flux, or a non-trivial charge label, are called *fluxons* or *chargeons*, while their other label is trivial. Anyons with both a non-trivial flux and charge label are called *dyons*.

Due to the transformations fluxons undergo when braided with each other, it is not possible to use a group element g as a globally agreed upon label for a fluxon [33]. Rather, the gauge-invariant flux labels are conjugacy classes C_g of G:

Definition 4.1 (Conjugacy class)**.**

$$C_g = \{zgz^{-1}|g, z \in G\}. \tag{4.4}$$

We can find this flux label of an anyon by braiding the unknown anyon with known chargeons (labeled by irreps of G), i.e., transporting known chargeons around the unknown fluxon (see Fig. 4.1). We can similarly find the charge label of an anyon by braiding it with known fluxons. However, when we try to find the charge label of a dyon this way, we don't have access to the specific label Γ^G (an irrep of G) [33]. Rather, the gauge-invariant charge label of a dyon that has flux g: is an irrep of the normalizer group of g.

Definition 4.2 (Normalizer)**.**

$$N_h = \{z \in G|zh = hz\}. \tag{4.5}$$

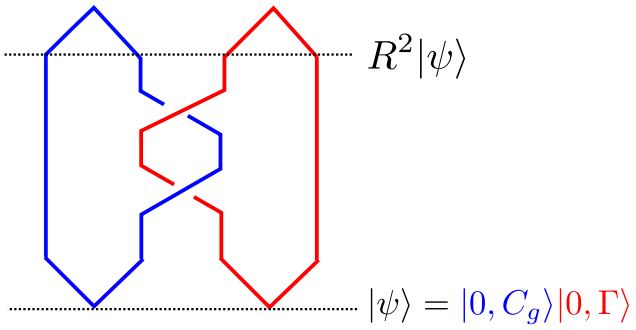

Figure 4.1: Braiding fluxon C_g with chargeon Γ.

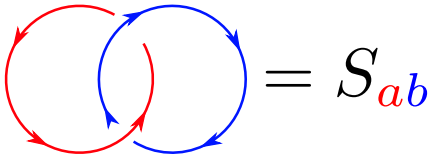

Figure 4.2: Definition of the S-matrix element S_{ab} where a and b label different anyon types. S_{ab} is the probability amplitude associated to the braiding described by the figure.

The normalizer of an element of G is always a subgroup of G. Furthermore, even though the exact normalizer group will depend on the specific choice of element z, the normalizer groups $\mathcal{N}_z$ are isomorphic to each other for all $z \in C_g$.

4.2.2 Anyonic data

Having reviewed how to label anyons, we would like to introduce the mathematical objects which encode the information about the anyon model, in particular the S-matrix, the fusion rules and the quantum dimensions.

S-matrix

The S-matrix encapsulates the braiding relations of the different anyons. Formally, the S-matrix elements are the amplitude probabilities of braiding events described in Fig. 4.2.

The S-matrix is unitary and for the models in the focus of this paper (quantum doubles) it can be computed from the representation theory of the underlying group thanks to the formula [69, 82]

$$S_{(C_g,\Gamma),(C_{g'},\Gamma')} = \frac{1}{|\mathcal{N}(g)|\,|\mathcal{N}(g')|} \sum_{h:hg'h^{-1}\in\mathcal{N}(g)} \chi_\Gamma(hg'h^{-1})\chi_{\Gamma'}(h^{-1}g^{-1}h), \qquad (4.6)$$

where $\chi_\Gamma(z) = \mathrm{Tr}(\Gamma(z))$ is the character of representation Γ.

For completeness, let us state that the S-matrix is not sufficient to uniquely identify an anyon model. For instance, the quantum double of the dihedral group of degree 4, D_4 and the quantum double of the quaternion group Q have the same S-matrices yet different anyon models. The S-matrix of $\mathcal{D}(D_4)$ is worked out in [83] while the S-matrix of $\mathcal{D}(Q)$ is worked out in [84]. One also needs to provide the T-matrix which encapsulates the topological spin of each anyon. For quantum doubles, i.e., most theories appearing in this paper, the T-matrix can be computed thanks to

$$T_{(C_g,\Gamma),(C_{g'},\Gamma')} = \delta_{C_g C_{g'}} \delta_{\Gamma\Gamma'} \frac{\chi_\Gamma(g)}{\chi_\Gamma(e)}, \tag{4.7}$$

where e is the identity element of group G. We will use the notation $t_{(C_g,\Gamma)} = T_{(C_g,\Gamma),(C_g,\Gamma)}$ for the topological spin of an anyon.

Fusion rules

In addition to braiding, fusing two anyons is an essential feature of an anyon model. Suppose two anyons are next to one another. One would like to treat them as a single anyon, and identify the properties of this resulting anyon. The resulting anyon is the *fusion* of the two original anyons. In the absence of information about the particular state of the two original anyons, the best description of the fusion state is summarized by listing the allowed fusion channels. This information is captured in the N-symbols:

$$a \times b = \sum_c N_{ab}^c c, \tag{4.8}$$

where N_{ab}^c is the multiplicity of particle c when fusing anyon a with anyon b. In a non-Abelian theory, at least one fusion has two (or more) possible fusion channels, making the result of that fusion non-deterministic.

An important feature of the fusion rules is that for any anyon type a there exists a unique anyon type a^{-1} such that the vacuum is a possible fusion outcome. The corresponding anyon is called the antiparticle of a.

Having defined an antiparticle, one can capture all the information about the braiding of anyons into the topological S-matrix whose elements are the amplitudes of the different braiding processes:

$$S_{ab} = \mathrm{Tr}(R_{b^{-1}a} R_{ab^{-1}})/\mathcal{D}, \tag{4.9}$$

where b^{-1} is the antiparticle of anyon b. Eq. (4.6) in the previous section was a special case of this formula.

Fusing and braiding are not independent but related by the Verlinde-formula:

$$N_{ab}^{c} = \sum_{z} \frac{S_{az} S_{bz} S_{c^{-1}z}}{S_{1z}}, \tag{4.10}$$

where 1 is the trivial anyon (vacuum). This relates the S-matrix to the N-symbols.

Quantum dimensions

The quantum dimension d_a of anyon a is the dimension of the space of anyon a, and is related to the number of internal degrees of freedom the anyon has. The fact that an anyon might have more than one internal degree of freedom, we will refer to as that anyon having different *flavors*. Abelian anyons necessarily have $d_a = 1$, while non-Abelian anyons have quantum dimension $d_a > 1$.

The definition of quantum dimensions is through the fusion rules: the fusion space of a pair of anyons needs to be equal to the combined space of the outcome-anyons, taking their multiplicity into account, i.e., a fusion of anyons a and b in the form of Eq. (4.8) means the quantum dimensions of participating anyons are [34]:

$$d_a \cdot d_b = \sum_{c} N_{ab}^{c} d_c. \tag{4.11}$$

Quantum dimensions need not be integers.

The total quantum dimension of a topological theory is then the square-sum of the quantum dimensions of all anyon species in the theory:

$$\mathcal{D}^2 = \sum_{\text{anyons } k} d_k^2. \tag{4.12}$$

4.2.3 Drinfeld doubles

In this section we will review the theories that appear in this paper. We discuss two Abelian doubles: $\mathcal{D}(\mathbb{Z}_2)$ and $\mathcal{D}(\mathbb{Z}_3)$, as well as the simplest non-Abelian double $\mathcal{D}(S_3)$, which is the focus of this paper.

One algebraic model that produces anyons is the Drinfeld double. The Drinfeld double of group G, $\mathcal{D}(G)$ is a quasi-triangular Hopf-algebra [73], with elements in the form of pairs of $g, h \in G$: (g, h), hence the name "double" for this theory. The

irreducible representations of this algebra describe anyons: Abelian anyons if the group G is Abelian, and non-Abelian anyons if G is non-Abelian.

Anyons in Drinfeld doubles have *flux* and *charge* labels, just as the anyons of Sec. 4.2.1. The flux labels are conjugacy classes of G. Charge labels of anyons are either irreps of G (for chargeons), or irreps of normalizer subgroups of G (for dyons).

$\mathcal{D}(\mathbb{Z}_2)$

The simplest Drinfeld double is the toric code, based on $G = \mathbb{Z}_2$: $\mathcal{D}(\mathbb{Z}_2)$; it has Abelian anyons. Let us look at this example.

The group $\mathbb{Z}_2$ has two elements: $\{e, x\}$, where e is the identity, and $x \cdot x = e$.

Then, the elements of the algebra $\mathcal{D}(\mathbb{Z}_2)$ are

$$(e, e) \tag{4.13}$$
$$(e, x) \tag{4.14}$$
$$(x, e) \tag{4.15}$$
$$(x, x). \tag{4.16}$$

Meanwhile, anyons of this theory are labeled by conjugacy classes and irreps. The conjugacy classes of $\mathbb{Z}_2$ are simply its elements:

$$C_e = e \tag{4.17}$$
$$C_x = x, \tag{4.18}$$

and these are the flux labels of the theory. The normalizers of both of these conjugacy classes/elements are the full group, $\mathbb{Z}_2$. Thus, the irreps labeling the charges are irreps of $\mathbb{Z}_2$: $\Gamma_1^{\mathbb{Z}_2}$ and $\Gamma_{-1}^{\mathbb{Z}_2}$, regardless of the flux content of the anyon. (See the appropriate subtable in Table 4.2 for these irreps.)

The traditional electric and magnetic excitations of the toric code are shown in Fig. 4.3. These anyons are the simple juxtapositions of a flux and a charge label. The chargeon $\mathbf{e}$ and the fluxon $\mathbf{m}$ inherit their fusion rules from $\mathbb{Z}_2$:

$$\mathbf{e} \times \mathbf{e} = 1 \tag{4.19}$$
$$\mathbf{m} \times \mathbf{m} = 1, \tag{4.20}$$

	Γ_1	Γ_{-1}
e	1	e
x	m	em

Figure 4.3: Anyons of $\mathcal{D}(\mathbb{Z}_2)$ in relation to their labels.

and

$$\mathbf{e} \times \mathbf{m} = \mathbf{em}. \tag{4.21}$$

Similarly, $\mathbf{em} \times \mathbf{e} = \mathbf{m}$, $\mathbf{em} \times \mathbf{m} = \mathbf{e}$, and $\mathbf{em} \times \mathbf{em} = 1$.

$\mathcal{D}(\mathbb{Z}_3)$

Another theory with Abelian anyons is $\mathcal{D}(\mathbb{Z}_3)$, the double of the cyclic group of order 3. This theory plays a role in Sec. 4.4.

The group $\mathbb{Z}_3$ has three elements: $\{e, y, y^2\}$, with $y^3 = e$. The double $\mathcal{D}(\mathbb{Z}_3)$ then has 9 distinct elements of its algebra, in the form of $\{(g, h)|g, h \in \mathbb{Z}_3\}$.

The flux part of anyons of the model are labeled by conjugacy classes of $\mathbb{Z}_3$:

$$C_e = e \text{ (trivial flux)} \tag{4.22}$$
$$C_y = y \ (m_1) \tag{4.23}$$
$$C_{y^2} = y^2 \ (m_2), \tag{4.24}$$

each corresponding to a flux label from the set $\{\text{triv}, m_1, m_2\}$.

As the normalizer subgroups of each of these conjugacy classes are $\mathbb{Z}_3$ itself, the charge content of anyons are labeled by irreps of $\mathbb{Z}_3$: Γ_1 (trivial flux), Γ_ω (e_1) and $\Gamma_{\bar{\omega}}$ (e_2) (see the appropriate subtable in Table 4.2 for these irreps, ω and $\bar{\omega} \equiv \omega^2$ are the third complex roots of unity). Each of these introduce a charge label, forming the set of charge labels: $\{\text{triv}, e_1, e_2\}$.

All 9 anyons of the theory are the simple combinations of a flux and charge label from these sets: there's the vacuum (1, it has a trivial flux and trivial charge label), there are two distinct chargeons (e_1 and e_2), two distinct fluxons (m_1 and m_2), and four dyons (e_1m_1, e_1m_2, e_2m_1, e_2m_2).

All anyons of $\mathcal{D}(\mathbb{Z}_3)$ are Abelian, and their fusion rules can be inferred from the

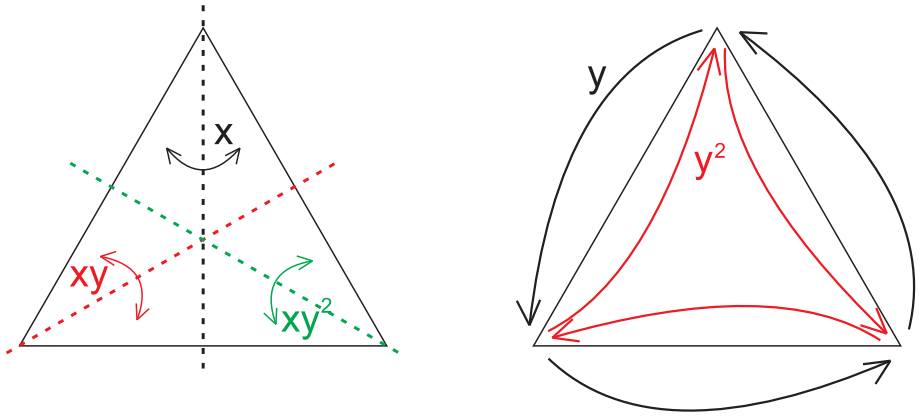

Figure 4.4: Elements of the group S_3 as symmetry transformations of an equilateral triangle: (a) mirrorings x, xy, xy^2, (b) rotations y, y^2, and the identity transformation (not shown).

fusions of pure chargeons and fluxons. For the chargeons:

$$e_1 \times e_1 = e_2 \tag{4.25}$$
$$e_1 \times e_2 = 1 \tag{4.26}$$
$$e_2 \times e_2 = e_1 \tag{4.27}$$

and the rules are identical for the fluxons. For additional details of this model, please refer to Ref. [75]. The S-matrix and T-matrix are provided in Appendix 4.A of the current paper.

$\mathcal{D}(S_3)$

The simplest double that exhibits non-Abelian anyons is $\mathcal{D}(S_3)$. It is based on the smallest non-Abelian group, the symmetry group of order 3: S_3. This group is isomorphic to the symmetry transformations of an equilateral triangle. Its elements are easily enumerated by thinking about the symmetries of this triangle (see Fig. 4.4):

$$e \quad \text{identity} \tag{4.28}$$
$$\{x, xy, xy^2\} \quad \text{mirrorings to 3 axes} \tag{4.29}$$
$$\{y, y^2\} \quad \text{rotations by } \pi/3 \text{ and } 2\pi/3. \tag{4.30}$$

Considering the double $\mathcal{D}(S_3)$, one can then dutifully enumerate all the elements of the algebra: they will be in the form of $\{(g, h)|g, h \in S_3\}$, and there will be a total of 36 of them. However, the anyons of this model, similarly to those of $\mathcal{D}(\mathbb{Z}_2)$ and

S_3	e	y	y^2	x	xy	xy^2
$\Gamma_1^{S_3}$	1	1	1	1	1	1
$\Gamma_{-1}^{S_3}$	1	1	1	-1	-1	-1
$\Gamma_2^{S_3}$	$\begin{pmatrix}1&0\\0&1\end{pmatrix}$	$\begin{pmatrix}\bar{\omega}&0\\0&\omega\end{pmatrix}$	$\begin{pmatrix}\omega&0\\0&\bar{\omega}\end{pmatrix}$	$\begin{pmatrix}0&1\\1&0\end{pmatrix}$	$\begin{pmatrix}0&\omega\\\bar{\omega}&0\end{pmatrix}$	$\begin{pmatrix}0&\bar{\omega}\\\omega&0\end{pmatrix}$

Table 4.1: Irreducible representations of $\mathcal{N}_{C_e} = S_3$.

$\mathbb{Z}_3$	e	y	y^2
$\Gamma_1^{\mathbb{Z}_3}$	1	1	1
$\Gamma_\omega^{\mathbb{Z}_3}$	1	ω	$\bar{\omega}$
$\Gamma_{\bar{\omega}}^{\mathbb{Z}_3}$	1	$\bar{\omega}$	ω

$\mathbb{Z}_2$	e	x
$\Gamma_1^{\mathbb{Z}_2}$	1	1
$\Gamma_{-1}^{\mathbb{Z}_2}$	1	-1

Table 4.2: Irreducible representations of (a) $\mathcal{N}_{C_y} = \mathbb{Z}_3$ and (b) $\mathcal{N}_{C_x} = \mathbb{Z}_2$.

$\mathcal{D}(\mathbb{Z}_3)$, will be labeled by conjugacy classes and irreps of normalizer subgroups of S_3.

Fluxes of the double are labeled by the conjugacy classes of S_3:

$$C_e = \{e\} \tag{4.31}$$
$$C_x = \{x, xy, xy^2\} \tag{4.32}$$
$$C_y = \{y, y^2\}. \tag{4.33}$$

The charge labels of $\mathcal{D}(S_3)$ will be irreps of normalizers. The normalizers of S_3 are

$$\mathcal{N}_e = S_3 \tag{4.34}$$
$$\mathcal{N}_x = \{e, x\} \cong \mathcal{N}_{xy} \cong \mathcal{N}_{xy^2} \cong \mathbb{Z}_2 \tag{4.35}$$
$$\mathcal{N}_y = \mathcal{N}_{y^2} = \{e, y, y^2\} \cong \mathbb{Z}_3. \tag{4.36}$$

Notice that sometimes normalizers of different elements of a conjugacy class differ (e.g., for elements x, xy and xy^2 above); however, as remarked in Sec. 4.2.1, these are isomorphic to each other. Thus, the irreps on them will be identical.

The irreps of each of these normalizer subgroups are listed in Tables 4.1-4.2; the irreps of $\mathcal{N}_{C_g}$ are the possible charge labels for a dyon with flux label C_g. In those tables, and for the remainder of this paper, $\omega = \exp(2\pi i/3)$ and $\bar{\omega} = \omega^2 = \exp(4\pi i/3)$ are the third complex roots of unity.

The full list of anyons of $\mathcal{D}(S_3)$ is given in Table 4.3.

Label	C_g	$\mathcal{N}_g$	Irrep.	Q.dim.	Type
A	C_e	S_3	$\Gamma_1^{S_3}$	1	vacuum
B	C_e	S_3	$\Gamma_{-1}^{S_3}$	1	chargeon
C	C_e	S_3	$\Gamma_2^{S_3}$	2	chargeon
D	C_x	$\mathbb{Z}_2$	$\Gamma_1^{\mathbb{Z}_2}$	3	fluxon
E	C_x	$\mathbb{Z}_2$	$\Gamma_{-1}^{\mathbb{Z}_2}$	3	dyon
F	C_y	$\mathbb{Z}_3$	$\Gamma_1^{\mathbb{Z}_3}$	2	fluxon
G	C_y	$\mathbb{Z}_3$	$\Gamma_\omega^{\mathbb{Z}_3}$	2	dyon
H	C_y	$\mathbb{Z}_3$	$\Gamma_{\bar{\omega}}^{\mathbb{Z}_3}$	2	dyon

Table 4.3: Anyons of $\mathcal{D}(S_3)$ with their charge and flux labels, quantum dimensions and type.

Other properties of $\mathcal{D}(S_3)$, such as the complete set of fusion rules of its anyons, its S-matrix, and T-matrix, can be found in Appendix 4.A.

Relation between anyons

One peculiar mathematical property of Drinfeld doubles $\mathcal{D}(G)$ is the relation of irreps of G to the irreps of its normalizer subgroups. It turns out that while gauge-invariant charge labels of dyons are indeed irreps of normalizers, these can be connected to irreps of the full group, G. For example, for $\mathcal{D}(S_3)$ we find that the various charge labels are related to each other through restriction of irreps. If we restrict irreps of S_3 to the normalizer group $\mathcal{N}_x$:

$$\Gamma_1^{S_3}|_{\mathcal{N}_x} = \Gamma_1^{\mathcal{N}_x} \tag{4.37}$$
$$\Gamma_{-1}^{S_3}|_{\mathcal{N}_x} = \Gamma_{-1}^{\mathcal{N}_x} \tag{4.38}$$
$$\Gamma_2^{S_3}|_{\mathcal{N}_x} = \Gamma_1^{\mathcal{N}_x} \oplus \Gamma_{-1}^{\mathcal{N}_x}. \tag{4.39}$$

Similarly, restricting irreps of S_3 to the group $\mathcal{N}_y$:

$$\Gamma_1^{S_3}|_{\mathcal{N}_y} = \Gamma_1^{\mathcal{N}_y} \tag{4.40}$$
$$\Gamma_{-1}^{S_3}|_{\mathcal{N}_y} = \Gamma_1^{\mathcal{N}_y} \tag{4.41}$$
$$\Gamma_2^{S_3}|_{\mathcal{N}_y} = \Gamma_\omega^{\mathcal{N}_y} \oplus \Gamma_{\bar{\omega}}^{\mathcal{N}_y}. \tag{4.42}$$

The diagram in Fig. 4.5, which is a generalized, non-Abelian version of Fig. 4.3, now for $\mathcal{D}(S_3)$, summarizes these connections. Rows of this diagram correspond to flux labels (conjugacy classes) of the theory, and in the rows anyons are shown

that are labeled by those flux labels. Notice that there are six rows of the diagram, while there are only three flux labels: each flux label incorporates as many rows as is the cardinality of the appropriate conjugacy class, and we may think about each individual row as labeled by a specific element of the conjugacy class.

Columns of the diagram are labeled by irreps of the group S_3: the three irreps $\Gamma_1^{S_3}$, $\Gamma_{-1}^{S_3}$, and $\Gamma_2^{S_3}$ each label as many columns as is the number of independent parameters for that irrep (1 and 1 for the one-dimensional irreps, and 4 for the two-dimensional irrep). Anyons are distributed amongst these charge labels according to their charge labels. An anyon label is shown in a certain column if and only if that anyon has *charge flavors* described by that charge label. We can deduce these relations by taking the irrep splitting relations Eqs. (4.37)-(4.42) into account.

The connection between anyon labels and irreps of S_3 detailed here will have an interesting consequence for any analysis conducted for this double. If we were to fundamentally modify all elements of the algebra related to an irrep of S_3, several anyons and anyon flavors would be affected by that: all of those related to the modified charge label through these intricate irrep-restrictions. As an example, modifying (e.g., completely removing) the charge label $\Gamma_2^{S_3}$ would not only have an effect on anyon C (the one directly labeled by $\Gamma_2^{S_3}$), but also on anyons G and H, as their charge labels are related to the modified irrep $\Gamma_2^{S_3}$ (see Fig. 4.5).

An additional useful property of the diagram in Fig. 4.5 is that the number of distinct squares corresponding to an anyon equals its squared quantum dimension [85], each distinct square of the diagram representing a different flavor of that anyon. Meanwhile, the total number of squares in the diagram (36) is exactly the square dimension of the total quantum dimension of this theory.

As a final note, we'd like to point out that such connections between irreps of the full group G and irreps of the normalizer subgroups can always be established, for any group G, and a diagram equivalent to Fig. 4.5 can always be drawn [85]. For Abelian doubles based ony cyclic groups ($G = \mathbb{Z}_d$), these connections will be trivial. The normalizer subgroups in such a case will be the full group, G, thus the irreps of G and those of the normalizers will be exactly the same. For non-Abelian doubles, the connections will be more interesting, as there will be non-trivial normalizer subgroups whose irreps will sometimes split (Eqs. (4.40)-(4.41) above), sometimes merge (Eq. (4.39), Eq. (4.42)) to yield an irrep of G.

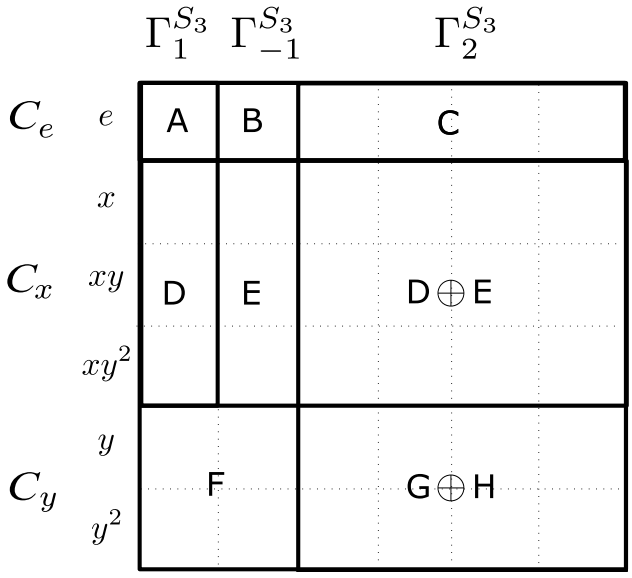

Figure 4.5: Connections between the sets of labels $\{\Gamma_1^{S_3}, \Gamma_{-1}^{S_3}, \Gamma_2^{S_3}\}$, $\{C_e, C_x, C_y\}$ and (flavors of) anyons of $\mathcal{D}(S_3)$. The number of rows and columns for each flux and charge label correspond to the number of distinct flavors that label describes. The number of squares corresponding to an anyon label is the squared dimension of that anyon.

4.3 Phase transitions in Drinfeld doubles

In this paper we analyze phase transitions in Drinfeld doubles, induced by *forbidding* one (or several) flux or charge labels. Anyons described by the forbidden label cannot be created as thermal excitations from the vacuum. Forbidding anyons in the double $\mathcal{D}(G)$ in a way that the remaining unforbidden set of anyons is closed under fusion will modify the dynamics and result in the emergence of a new theory for the unforbidden set of anyons.

In Sec. 4.3.1 we review the physical processes the double $\mathcal{D}(G)$ undergoes through these phase transitions. Then, in Sec. 4.3.2 we present the mathematical procedure for modeling the transitions, and how one can find the proper emergent theory in all cases. We will present our detailed analysis of the phase transitions in $\mathcal{D}(S_3)$ in Sec. 4.4.

4.3.1 Mechanisms of phase transition

To find the new topological theory emerging after forbidding flux and charge labels, one can picture that the original theory, i.e, $\mathcal{D}(G)$, undergoes a series of physical processes. These processes are conceptual tools to illustrate the way the topological model restructures itself. This representation of our results is complementary to

mathematical transformations on the S-matrix, a procedure described in Sec. 4.3.2.

Those processes, which we will review in details in the following paragraphs are

1. Forbiddance of certain anyons, related to the forbidden label;
2. Condensation of some particles, i.e., they become indistinguishable from the vacuum;
3. Non-Abelian anyons with quantum dimension larger than one splitting up into lower-dimensional anyons, due to their previously indistinguishable flavors becoming distinguishable in the new theory.

Forbiddance

Anyons that are never created in the new theory, because of forbidding a label (a conjugacy class or an irrep of G) they are related to, become *forbidden*. This is a fundamental process that happens in every one of the phase transitions we consider. In fact, forbiddance of these particles is what induces the other processes listed in the current section.

Forbidden anyons are not created from the vacuum. Whenever the resulting unforbidden set of anyons is closed under fusion, i.e., their fusion cannot lead to the emergence of forbidden anyons, a new consistent theory emerges for the remaining subset of anyons.

These constraints have a practical significance for our calculations, as we will use these properties to find the new theories. In particular, our findings will be justified by performing transformations on the S-matrix, a mathematical procedure described in Sec. 4.3.2.

Condensation

In certain cases the resulting set of anyons after forbiddance will not form a valid theory. In these cases, however, some particles become indistinguishable from the vacuum, and *condense* to it.

This happens when through forbiddance we remove the full set of anyons that have made the now indistinguishable anyons previously distinguishable in the original theory. For example, anyons A (the vacuum) and B of $\mathcal{D}(S_3)$ are only distinguished through their braiding relations to anyons labeled by the conjugacy class C_x (anyons

D and E). Thus, when we forbid C_x in Sec. 4.4.1, anyon B condenses to the vacuum, A.

We identify these processes through the S-matrix of the new theory: when the new S-matrix has identical (or linearly dependent) entries for two particles, that is an indicator that those two particles have become indistinguishable from each other in the new theory.

Splitting of particles

Anyons with dimension higher than 1 in the original model sometimes *split up* into two or more 1-dimensional anyons in the new theory. This splitting happens when the different flavors of the anyon in question, indistinguishable in the original model by braiding or fusion, become distinguishable in the new theory. Thus, the newly distinguishable states form separate anyons.

Mathematically, this process can be shown by relating the S-matrix of (the new) *theory A* to the S-matrix of (a different) *theory B*. If by merging anyons g and h in *theory B* we arrive to the S-matrix of *theory A*, with merged anyon gh, we conclude that the gh anyon of *theory A* could split up and become the anyons g and h in *theory B*.

An example of this is analyzed in Sec. 4.4.1. After anyon B condenses to the vacuum, we arrive at an S-matrix that is identical to the matrix we get when we merge fluxes and charges in $\mathcal{D}(\mathbb{Z}_3)$. Thus, the emergent theory of Sec. 4.4.1, and the quantum double $\mathcal{D}(\mathbb{Z}_3)$ are related through a series of condensation and splitting of anyons.

4.3.2 Our protocol

The mathematical protocol to find the new theories emerging from $\mathcal{D}(G)$ is the following. First, we forbid a (set of) conjugacy classes and irreps, i.e., all anyons and anyon flavors related to those labels. They won't be created from the vacuum.

When the resulting unforbidden set of anyons has consistent, closed fusion rules, we conclude that a new theory emerges. Then, we construct the S-matrix of this new theory, based on the fusion rules for the subset of unforbidden anyons.

Truncating fusion rules

To enforce forbiddance of anyons, we start with the original fusion rules of $\mathcal{D}(G)$ and truncate them to the subset of unforbidden anyons. In our analysis, these new fusion rules are *closed* on the considered subset.

Constructing the N-symbols

We use the remaining set of fusion rules to construct the N-symbols (see Eq. (4.8)) for each particle. In this step we can utilize an anyon-diagram of $\mathcal{D}(G)$, a generalized version of Figs. 4.3 and 4.5, that encapsulates the relation between irreps of G and irreps of its normalizer subgroups. We are guided by the assumption that the quantum dimensions of anyons are those inferred from this diagram, i.e., the quantum dimensions are unchanged from the dimensions of $\mathcal{D}(G)$.

Inverting the Verlinde-formula

We then compute the eigenvalues of the N-symbols, and use the relation between these eigenvalues and the elements of the S-matrix [26] to invert the (4.10) Verlinde-formula and reverse-engineer the S-matrix. Throughout this process, we use the symmetries of the S-matrix of the original $\mathcal{D}(G)$ model, only to make a choice between new S-matrices that otherwise equivalently reproduce the fusion rules and quantum dimensions of the new model. We find the prefactor (or the exact entries, rather than simply their relative values) of the S-matrix by enforcing that it be unitary.

If we arrive at an S-matrix that has linearly dependent entries for certain anyons (it does not recreate all the fusion rules we have started with, and is not unitary in these cases), we conclude that further physical processes will happen: condensation of some particles. For a list of the possible physical processes, see Sec. 4.3.1.

Comparing topological spins

Finally, when we arrive at an S-matrix that is our "candidate matrix" for the emergent theory, we reference the topological spins of this candidate theory with those of the original double $\mathcal{D}(G)$. It is possible to find the correspondence between labels of the original and emergent theories, and at this step we verify that the spins of anyons of $\mathcal{D}(G)$ agree with the topological spins of the new theory.

4.4 Phases of $\mathcal{D}(S_3)$

In this section we will present phases that can emerge from the theory $\mathcal{D}(S_3)$ through a series of physical processes, outlined in Sec. 4.3. We focus on $\mathcal{D}(S_3)$ as it is the simplest non-Abelian double, and as such it could undergo non-trivial processes during phase transitions.

We consider combinations of charge and flux labels of $\mathcal{D}(S_3)$, and derive the theories

that emerge as a result of forbidding sets of labels. We focus on transitions where the unforbidden set of anyons have closed fusion rules amongst them.

The exact protocol to find the emerging theories is outlined in Sec. 4.3.2. We include the phases resulting from that protocol in this section, as well as the detailed analysis of how those theories emerge from $\mathcal{D}(S_3)$.

4.4.1 Forbidding the conjugacy class C_x leads to $\mathcal{D}(\mathbb{Z}_3)$

Let us first give a high-level, intuitive overview of what happens when we forbid the conjugacy class C_x.

First, simply concentrate on the group $S_3 = \{e, x, xy, xy^2, y, y^2\}$ instead of the double $\mathcal{D}(S_3)$. Then, remove the elements $C_x = \{x, xy, xy^2\}$ from this group. The remaining set of elements is $\{e, y, y^2\}$, which themselves form a group: $\mathbb{Z}_3$.

It turns out that when we do the same procedure for $\mathcal{D}(S_3)$, and forbid the conjugacy class C_x (i.e., the elements $\{x, xy, xy^2\}$ among the flux labels), the remaining set of anyons will form the theory $\mathcal{D}(\mathbb{Z}_3)$.

However, this parallel is not at all trivial, as we have never considered the charge labels in this argument. What happens is the following process.

Step 1 — Forbidding the conjugacy class C_x confines anyons D and E of the original model, leaving the set $\{A, B, C, F, G, H\}$.

Step 2 — As anyons A and B only differ through their braiding relations with, the now forbidden, anyons D, E (see Appendix 4.A), anyons A and B will become indistinguishable in the new theory. B will condense to the vacuum, A.

This induces anyons C, F, G, H to lose their antisymmetric charge subspaces (as the fundamental antisymmetric chargeon, B disappeared).

Notice that this is the step where all antisymmetric charge flavors disappear, as is necessary for the eventual emergence of $\mathcal{D}(\mathbb{Z}_3)$. (Just as removing the C_x labels from the flux flavors was necessary.)

Step 3 — This is followed by the split-up of higher-dimensional anyons C, F, G, H into two distinct 1-dimensional, Abelian anyons each. This split-up can happen, as the fluxons previously making their flavors indistinguishable were part of the C_x conjugacy class, now forbidden.

For example, anyon F originally had two flux flavors: y and y^2, being indistinguishable due to the braiding process $xyx = y^2$, which would transform one flavor to

	1	e_1	e_2
1	A'	C_a	C_b
m_1	F_a	G_a	H_a
m_2	F_b	H_b	G_b

Table 4.4: Correspondence between standard anyon labels of $\mathcal{D}(\mathbb{Z}_3)$ and anyon labels evolved from of $\mathcal{D}(S_3)$, when forbidding the conjugacy class C_x.

	A	B	C	F	G	H
A	A	B	C	F	G	H
B	B	A	C	F	G	H
C	C	C	A ⊕ B ⊕ C	G ⊕ H	F ⊕ H	F ⊕ G
F	F	F	G ⊕ H	A ⊕ B ⊕ F	H ⊕ C	G ⊕ C
G	G	G	F ⊕ H	H ⊕ C	A ⊕ B ⊕ G	F ⊕ C
H	H	H	F ⊕ G	G ⊕ C	F ⊕ C	A ⊕ B ⊕ H

Table 4.5: Fusion rules of remaining particles after forbidding conjugacy class C_x.

the other. After forbidding the class C_x, such a process is now forbidden, and the y and y^2 flavors of F become distinguishable.

The final set of anyons is thus: $\{A', C_a, C_b, F_a, F_b, G_a, G_b, H_a, H_b\}$, which will form the quantum double $\mathcal{D}(\mathbb{Z}_3)$. Labels in the form of X_a and X_b correspond to two distinct one-dimensional flavors of anyon X, which have split up to form two separate anyons. The correspondence between standard labels of $\mathcal{D}(\mathbb{Z}_3)$ and our labels is shown in Table 4.4. The process described above is shown in Fig. 4.6.

Proof

We can prove that anyons of $\mathcal{D}(S_3)$ indeed undergo the above process by following the protocol detailed in Sec. 4.3.2. Throughout this proof, we will refer to the steps numbered in the overview given above, which coincide with the steps shown in Fig. 4.6.

Step 1 — The first step in this physical process is the forbiddance of anyons D, E. In our protocol, we truncate the fusion rules of $\mathcal{D}(S_3)$ for the remaining set of particles $\{A, B, C, F, G, H\}$, these truncated rules are shown in Table 4.5.

Using the new set of fusion rules we can construct the new S-matrix, following our

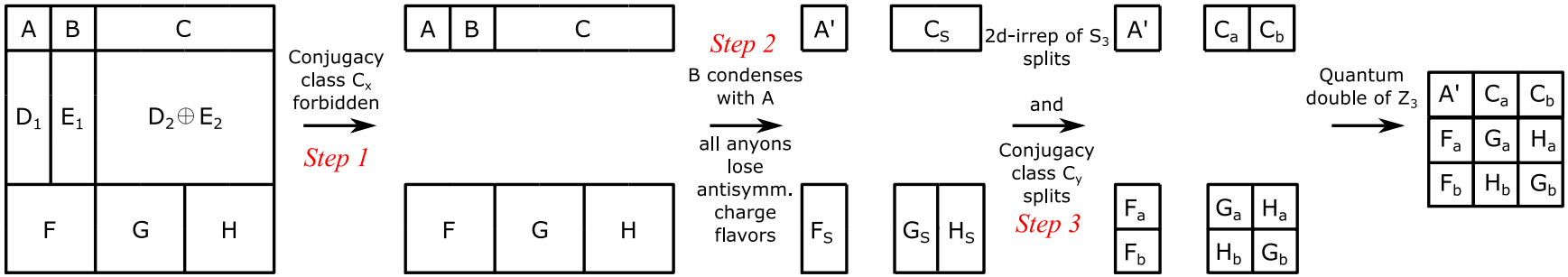

Figure 4.6: Pictorial representation of the process transforming $\mathcal{D}(S_3)$ to $\mathcal{D}(\mathbb{Z}_3)$, when we forbid conjugacy class C_x. The subscripts S denote the symmetric subspaces of anyons ($F_S \equiv F_1$ of Fig. 4.10), and subscripts a and b denote the final, 1-dimensional components of the anyons. A' is the vacuum after the condensation of B.

protocol, and we have:

$$S = \frac{1}{6}\begin{bmatrix} 1 & 1 & 2 & 2 & 2 & 2 \\ 1 & 1 & 2 & 2 & 2 & 2 \\ 2 & 2 & 4 & -2 & -2 & -2 \\ 2 & 2 & -2 & 4 & -2 & -2 \\ 2 & 2 & -2 & -2 & 4 & -2 \\ 2 & 2 & -2 & -2 & -2 & 4 \end{bmatrix}. \tag{4.43}$$

Now, we can state the following two lemmas:

Lemma 4.3 (Condensation (*Step 2*))**.** *Anyon B condenses to the vacuum, and the following S-matrix describes the emerging theory:*

$$\frac{1}{3}\begin{bmatrix} 1 & \sqrt{2} & \sqrt{2} & \sqrt{2} & \sqrt{2} \\ \sqrt{2} & 2 & -1 & -1 & -1 \\ \sqrt{2} & -1 & 2 & -1 & -1 \\ \sqrt{2} & -1 & -1 & 2 & -1 \\ \sqrt{2} & -1 & -1 & -1 & 2 \end{bmatrix}. \tag{4.44}$$

Proof: We transform the (4.43) S-matrix from its current basis

$$\{A, B, C, F, G, H\}$$

to the basis

$$\{(A+B)/\sqrt{2}, (A-B)/\sqrt{2}, C, F, G, H\}$$

in the same spirit as how Ref. [86] relates the toric code to the Ising model. The transformation applied here yields zero entries for the entire row and column corresponding to $(A-B)/\sqrt{2}$. Dropping these, we get the matrix (4.44).

Lemma 4.4 (Splitting of anyons (*Step 3*))**.** *Merging anyons of $\mathcal{D}(\mathbb{Z}_3)$ (chargeons $\{e_1, e_2\}$, fluxons $\{m_1, m_2\}$, and dyons $\{e_1m_1, e_2m_2\}$, $\{e_1m_2, e_2m_1\}$, pairwise) yields a block-diagonal S-matrix, the physical block of which is* (4.44).

Proof: We transform the matrix (4.65) from its current basis

$$\{1, e_1, e_2, m_1, m_2, e_1m_1, e_2m_1, e_1m_2, e_2m_2\}$$

to a new basis, which is

$$1/\sqrt{2}\left\{\sqrt{2}, e_1+e_2, m_1+m_2, e_1m_1+e_2m_2, e_1m_2+e_2m_1,\right.$$

$$\left. e_1-e_2, m_1-m_2, e_1m_1-e_2m_2, e_1m_2-e_2m_1\right\}.$$

In this new basis we find the S-matrix is block-diagonal, the "upper block" is formed by the first 5 anyons (symmetric block), the "lower block" is formed by the last 4 anyons (antisymmetric block).

We can drop the antisymmetric block, on the basis that it doesn't include the vacuum state, and if we were to add the vacuum to it, we would get a pathological S-matrix with all zero entries for the first row and column. This leaves us the symmetric block, whose entries are identical to those of Eq. (4.44).

Combining Lemmas 4.3 and 4.4 we can conclude that the theory emerging by forbidding the conjugacy class C_x will undergo a condensation (*Step 2*), followed by splitting of anyons (*Step 3*), and form $\mathcal{D}(\mathbb{Z}_3)$.

As a last step, we can also compare the topological spins of anyons of $\mathcal{D}(S_3)$ to their counterparts in $\mathcal{D}(\mathbb{Z}_3)$. Taking all splitting processes into account, they are in agreement:

$$t_A \cdot t_B = 1 \cdot 1 = t_1 = 1 \tag{4.45}$$

$$t_C = 1 = t_{e_1} \cdot t_{e_2} = 1 \cdot 1 \tag{4.46}$$

$$t_F = 1 = t_{m_1} \cdot t_{m_2} = 1 \cdot 1 \tag{4.47}$$

$$t_G = \omega = t_{e_1m_1} \cdot t_{e_2m_2} = \bar{\omega} \cdot \bar{\omega} \tag{4.48}$$

$$t_H = \bar{\omega} = t_{e_1m_2} \cdot t_{e_2m_1} = \omega \cdot \omega \tag{4.49}$$

□

4.4.2 Forbidding C_x and Γ_2 jointly leads to the trivial theory

The result of forbidding C_x and Γ_2 can be inferred from the results of Sec. 4.4.1. There, forbidding the C_x conjugacy class resulted in the condensation of anyon B, followed by a split-up of particles, leading to the theory $\mathcal{D}(\mathbb{Z}_3)$. If we additionally forbid the irrep Γ_2 we forbid all remaining anyons with nontrivial charge, i.e., anyons C, G, and H. The resulting theory seems to be the trivial-charge sector of $\mathcal{D}(\mathbb{Z}_3)$, i.e., the flux sector $\mathbb{Z}_3$.

However, at this point we should consider whether such a flux sector can live on its

own. In fact, the S-matrix of it is degenerate in the same way as the entries for A and B were degenerate in Sec. 4.4.1, as all fluxes have trivial braiding with each other. According to our protocol detailed in Sec. 4.3.2, anyons having degenerate entries in the S-matrix of a theory will condense. Therefore, the two non-trivial fluxes in this flux sector $\mathbb{Z}_3$ will condense to the vacuum, forming a trivial theory without excitations.

Here is a summary of this process:

Step 1 — Anyons C, D, E, G, H all become forbidden. The set $\{A, B, F\}$ remains.

Step 2 — The initial forbiddance will induce the condensation of B, which is accompanied by the anyon F losing its antisymmetric charge flavor (this is the same process as detailed in Sec. 4.4.1).

Step 3 — Then, anyon F will split up into two 1-dimensional anyons, F_a and F_b. With the label-correspondence

$$A' = 1 \tag{4.50}$$
$$F_a = m_1 \tag{4.51}$$
$$F_b = m_2 \tag{4.52}$$

this forms the flux sector of $\mathcal{D}(\mathbb{Z}_3)$: $\mathbb{Z}_3$.

Step 4 — The two fluxons, F_a and F_b, in the absence of any charges, are indistinguishable from the vacuum, and condense to it. The resulting theory is highly trivial (A only), and has no allowed excitations.

For an overview of this process, see Fig. 4.7.

Proof

We have proven that forbidding conjugacy class C_x will lead to the emergence of $\mathcal{D}(\mathbb{Z}_3)$, in Sec. 4.4.1.

It is clear that if we additionally forbid all nontrivial charges, we arrive at the flux sector of $\mathcal{D}(\mathbb{Z}_3)$: $\mathbb{Z}_3$. This is a classical theory, the S-matrix of which is

$$\frac{1}{\sqrt{3}}\begin{bmatrix} 1 & 1 & 1 \\ 1 & 1 & 1 \\ 1 & 1 & 1 \end{bmatrix}. \tag{4.53}$$

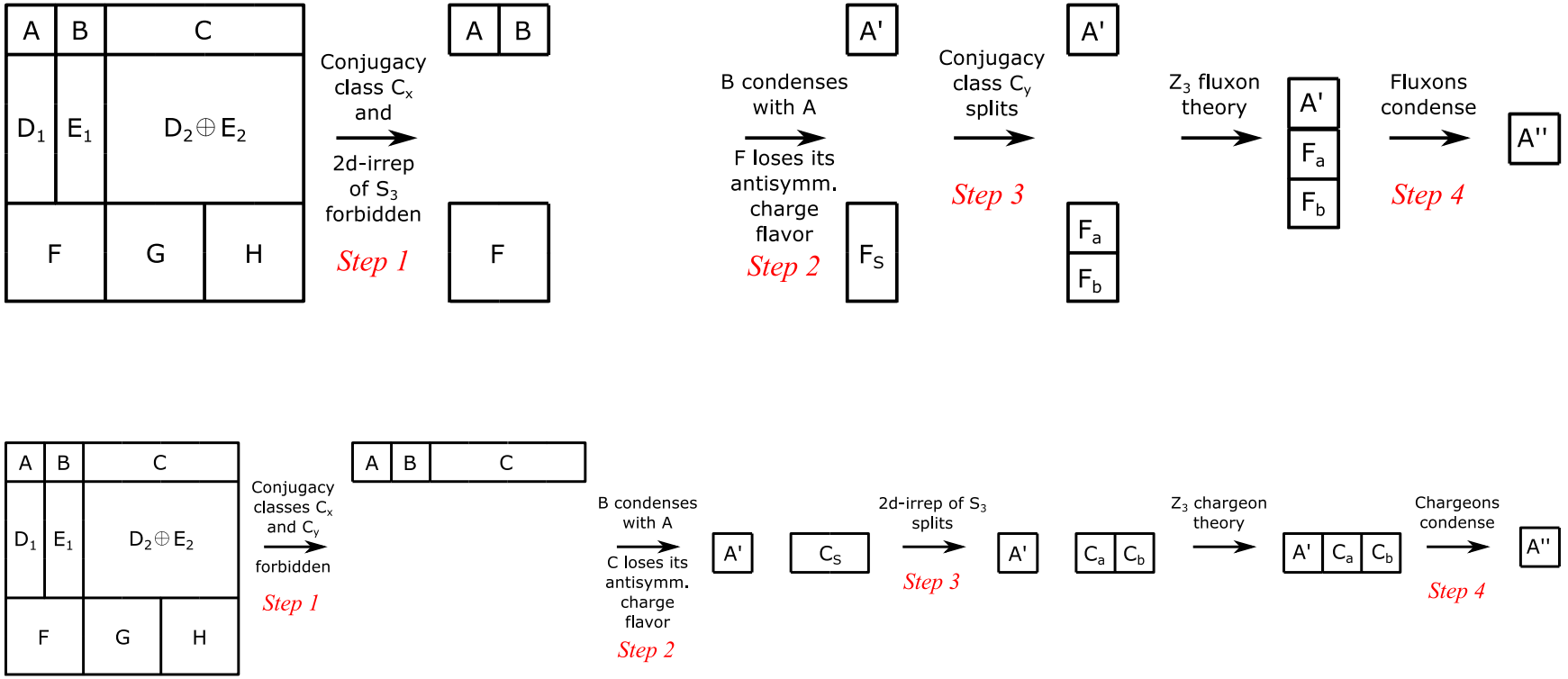

Figure 4.7: (a) Forbidding conjugacy class C_x and irrep Γ_2 of S_3 transforms $\mathcal{D}(S_3)$ to the trivial theory, (b) Forbidding conjugacy classes C_x and C_y transforms $\mathcal{D}(S_3)$ to the trivial theory. The subscripts S denote the symmetric subspaces of anyons ($F_S \equiv F_1$ of Fig. 4.10), and subscripts a and b denote the final, 1-dimensional components. A' is the vacuum after the condensation of B, A'' is the vacuum after all particles condensed.

Clearly, all entries of this S-matrix are identical, thus we conclude that the nontrivial fluxes F_a and F_b condense to the vacuum. □

4.4.3 Forbidding C_x and C_y jointly leads to the trivial theory

This transition is very similar to the one presented in Sec. 4.4.2. In fact, the physical processes this transition will follow will be identical to the ones detailed in Sec. 4.4.2, due to the original $\mathcal{D}(S_3)$ having a $C \leftrightarrow F$ exchange symmetry.

Forbidding C_x and C_y results in:

Step 1 — Anyons D, E, F, G, H become forbidden, and the set $\{A, B, C\}$ remains.

Step 2 — The condensation of B will follow, and C becomes partially forbidden.

Step 3 — Then, C splits up into two 1-dimensional anyons, which together with the vacuum will form $\mathbb{Z}_3$, the charge sector of $\mathcal{D}(\mathbb{Z}_3)$.

Step 4 — The $\mathbb{Z}_3$ charge theory can't live on its own, and its two chargeons condense to the vacuum, to give rise to a trivial theory without any excitations.

This process is shown in Fig. 4.7.

Proof

The proof is identical to the one presented in Sec. 4.4.2. □

4.4.4 Forbidding C_x, C_y, Γ_2 jointly leads to the trivial theory

In this example, anyons C, D, E, F, G, H all become forbidden, leaving the closed set $\{A, B\}$. Clearly, B will act as a single $\mathbb{Z}_2$ charge in this model. However, similar to the cases presented in Secs. 4.4.2-4.4.3, there are no nontrivial fluxes to differentiate between the B charge and the vacuum. Thus, B condenses to the vacuum, giving rise to a trivial theory, without excitations.

For a pictorial argument, see Fig. 4.8.

4.5 Lattice realization

Until this point, we have been analyzing field theories: we have started with a Drinfeld double, $\mathcal{D}(G)$, enumerated its irreps (the anyons of the model), and drawn connections between those irreps, through the usual labels (conjugacy classes and irreps of the group G). We have introduced the concept of "forbidding a label", which leads to forbidding anyons of the theory, and analyzed what other theories emerge, when the double is $\mathcal{D}(S_3)$.

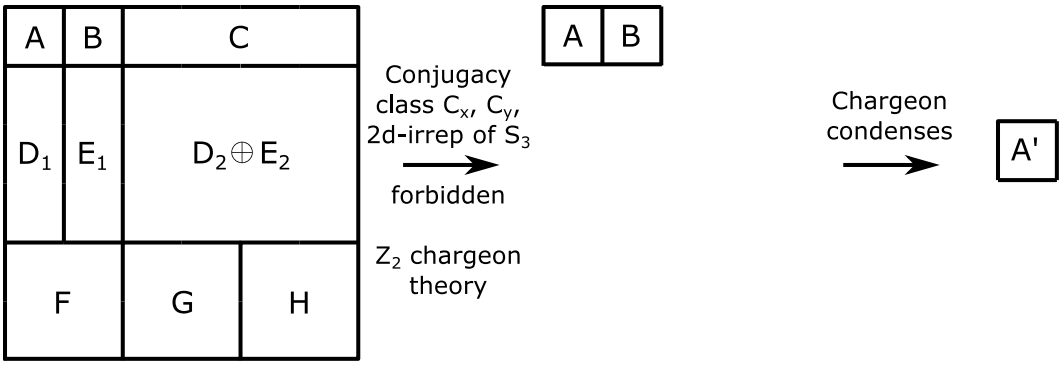

Figure 4.8: Forbidding conjugacy classes C_x and C_y, and irrep Γ_2 of S_3 transforms $\mathcal{D}(S_3)$ to the trivial theory. A' is the vacuum after the condensation of B.

In this section, we present a way to physically realize Drinfeld doubles: Kitaev's quantum double construction [4]. We introduce the physical lattice and the corresponding Hilbert space in Sec. 4.5.1, the states of which correspond to the elements of a Drinfeld double. Based on this Hilbert space we provide a high-level picture of what we meant by "forbidding labels" in Secs. 4.3-4.4. Then, in Sec. 4.5.2 we introduce a Hamiltonian to this system, the excitations of which will be the anyons, corresponding to the irreps of the algebra $\mathcal{D}(G)$. The introduction of this Hamiltonian will allow us to give a more concrete protocol to realize the phase transitions discussed in this paper.

4.5.1 Projecting out part of the Hilbert space

Quantum doubles, introduced by Kitaev [4], are a way to realize the excitations of a Drinfeld double of group G, $\mathcal{D}(G)$ in a many-body, nearest-neighbor interacting lattice system. We assign a qudit Hilbert space of dimension $|G|$ to every edge of the lattice, as well as a direction to each edge, pointing from one end of the edge towards the other.

The lattice geometry can be chosen to have an arbitrary graph structure, in this description we will focus on a square lattice. Then, anyons of this model live on sites formed by 6 qudits: the combination of the 4 qudits of a vertex and 4 qudits of a plaquette, with 2 qudits overlapping (see Fig. 4.9). The inner structure of a site, the fact that it is formed by a vertex and a plaquette, has significance, as the chargeon part of an anyon lives on the vertex, and the fluxon part lives on the plaquette.

Now, we're in a position to talk about the process of "forbidding", ubiquitously present in the current paper. In this lattice description, we can interpret the forbiddance of certain anyons or anyon labels by *projecting out part of the Hilbert space*, the

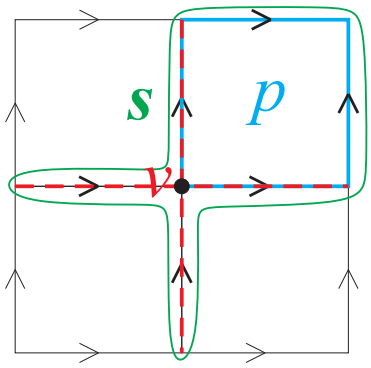

Figure 4.9: A site, formed by 6 qudits, is the combination of a vertex, v (4 qudits) and a plaquette, p (4 qudits), with 2 of the qudits overlapping.

parts that contains the forbidden labels. As a result of such a complete projection, the theory will transition to a new theory, with a Hilbert space that is a subspace of the original one:

$$\Pi_{\text{forbiddance}}: \quad \mathcal{H}_{\mathcal{D}(G)} = \text{span}\left\{ \bigotimes_{i \text{ qudits}} |\, g_i\rangle_i \right\}_{g_i \in G} \rightarrow \mathcal{H}_{\text{new}} \subset \mathcal{H}_{\mathcal{D}(G)}, \tag{4.54}$$

where $|\, g_i\rangle_i$ is the state of the qudit of edge i.

For example, when the emergent theory is a quantum double itself:

$$\mathcal{H}_{\text{new}} = \text{span}\left\{ \bigotimes_{i \text{ qudits}} |\, g_i\rangle_i \right\}_{g_i \in H}, \tag{4.55}$$

where $H \subset G$.

We can illustrate this point by considering the ground state of the Hamiltonian in a string-net representation [29]. The ground state will be the sum of distinct string-net configurations, whose terms can be grouped into two separate sets: those containing strings of the forbidden anyon(s), and those that are formed only by the (still) allowed set of anyons. In this representation, the effect of the projection (4.54) on the ground state will simply correspond to removing one set of string-net terms from this sum.

Simple as it may sound, the operation (4.54) can't be realized unitarily on the system. Furthermore, it is unclear how to build such a projector from local projections unto lattice sites. While the local operations could successfully remove the forbidden

excitations at all sites, they wouldn't remove states of the Hilbert space which have none of the forbidden excitations, but have condensation loops of the forbidden anyon (such as the string-net terms mentioned in the previous paragraph).

Instead, we will now introduce a way to approximate this projection. Here we will present this for $\mathcal{D}(S_3)$, but all facts in Sec. 4.5.2 can be stated for a quantum double of any general group, $\mathcal{D}(G)$ [85].

4.5.2 Tuning a Hamiltonian

In the previous work [85], we introduced two sets of orthogonal projectors unto the space of a single site of a quantum double: one set of charge projectors, and one set of flux projectors. The charge projectors act on vertices, the flux projectors act on plaquettes, while an anyon lives on the combination of the two (see Fig. 4.9). Hence, these projectors are all 4-local.

Charge projectors correspond to irreps of the whole group (S_3 in this case), and the flux projectors to conjugacy classes of the group. Therefore, for $\mathcal{D}(S_3)$, there are three charge projectors and three flux projectors. The two sets individually provide a full orthogonal resolution of the Hilbert space of a site. Furthermore, all those projectors commute pairwise.

Using these (or a subset of these) 4-local projectors to construct a quantum double Hamiltonian will result in a peculiar property of the resulting model: anyons of the double won't be in one-to-one correspondence with the energy eigenspaces of this Hamiltonian [85]. Depending on the exact *flavor* of an anyon, the Hamiltonian would assign a different energy to it.

In order to obtain a fully topological model, we instead need to construct a Hamiltonian with 6-local projectors, projecting unto all six qudits of a site. Then, we may utilize the 4-local projectors by adding them to a quantum double with a topological (6-local) Hamiltonian. Tuning the couplings of the newly added projectors, we can achieve phase transitions as a limit of the original double $\mathcal{D}(S_3)$.

Sets of flux and charge projectors

Let us first introduce 4-local projectors unto the sites of $\mathcal{D}(S_3)$. For $\mathcal{D}(S_3)$, the set of *flux labels* on which the flux projectors are based are the conjugacy classes of S_3 (Eqs. (4.31)-(4.33)). Then, we can introduce the projectors

$$B_{C_e},\ B_{C_x},\ B_{C_y}$$

acting on plaquettes of the model. This set of projectors spans the plaquette (flux) space of a site, the flux labels C_e, C_x, and C_y provide an orthogonal basis for all flux flavors. The rank of these projectors follow the rank of the conjugacy classes they are based on: 1, 3, and 2, in order.

The images of these projectors are straightforward:

$$\mathfrak{I}(B_{C_e}) = A \oplus B \oplus C \tag{4.56}$$
$$\mathfrak{I}(B_{C_x}) = D \oplus E \tag{4.57}$$
$$\mathfrak{I}(B_{C_y}) = F \oplus G \oplus H, \tag{4.58}$$

where the anyon labels A–H denote the subspace of a site corresponding to having that anyon present at that site. (See Table 4.3 for the list of anyons of $\mathcal{D}(S_3)$.)

The set of *charge labels* on which the charge projectors are based are the irreps of S_3 (Table 4.1). Then, we can introduce the three projectors

$$A_{\Gamma_1},\ A_{\Gamma_{-1}},\ A_{\Gamma_2}$$

acting on vertices of the model. They are of rank 1, 1 and 4, in order, following the (square) dimensionality of the irreps they are based on. These three projectors span the vertex (charge) space of a site, and the charge labels $\Gamma_1^{S_3}$, $\Gamma_{-1}^{S_3}$ and $\Gamma_2^{S_3}$ provide an orthogonal basis for all charge flavors. This resolution of the Hilbert space of a site is complementary to the resolution provided by the three flux projectors.

For non-Abelian doubles, the images of these projectors are less trivial than those of the flux projectors. For $\mathcal{D}(S_3)$ they are:

$$\mathfrak{I}(A_{\Gamma_1}) = A \oplus D_1 \oplus F_1 \tag{4.59}$$
$$\mathfrak{I}(A_{\Gamma_{-1}}) = B \oplus E_1 \oplus F_2 \tag{4.60}$$
$$\mathfrak{I}(A_{\Gamma_2}) = C \oplus D_2 \oplus E_2 \oplus G \oplus H, \tag{4.61}$$

where anyon labels with subscripts (e.g., D_1, E_1, F_2) denote orthogonal *flavors* of anyons on a site [85].

Equations (4.56)-(4.58) and (4.59)-(4.61) are summarized in Fig. 4.10.

It is key throughout these sections that (some of) the 4-local projectors presented here are *not topological*. Even though they form an orthogonal and commuting set, in their images certain anyons will split, depending on the flavor of the anyon. Physically, this means that adding such a 4-local projector to the Hamiltonian of

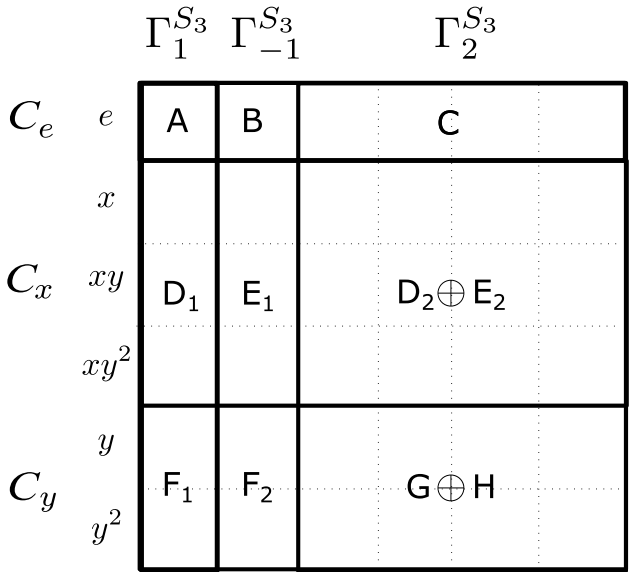

Figure 4.10: Anyon splitting diagram, based on Fig. 4.5. Here we added labels for the different charge flavors of anyons (D_1, D_2, E_1, E_2, and F_1, F_2) which are differentiated by the 4-local charge projectors (4.59)-(4.61).

$\mathcal{D}(S_3)$ will result in the new Hamiltonian distinguishing between flavors of the same anyon, i.e., yielding different energies based on the exact inner state of the anyon [85].

For example, anyon D has two flavors: D_1 and D_2. While D_1 is in the image of A_{Γ_1} (Eq. (4.59)), thus it is a chargeon, and the other flavor D_2 is in the image of the A_{Γ_2} projector (orthogonal to A_{Γ_1}) and therefore should be considered a dyon (Eq. (4.61)). The standard Hamiltonian introduced in Ref. [4]

$$H = -\sum_v A_{\Gamma_1}^{(v)} - \sum_p B_{C_e}^{(p)} \tag{4.62}$$

assigns energy -1 to the D_1 flavor, and energy 0 to the D_2 flavor of anyon D.

In contrast, the purely topological Hamiltonian is 6-local:

$$H = -\sum_{s=(v,p)} A_{\Gamma_1}^{(v)} B_{C_e}^{(p)}. \tag{4.63}$$

Notice how the only difference from the (4.62) Hamiltonian is that here we multiply the 4-local vertex and plaquette projectors to form 6-local projectors unto sites. (This is simple for this case, when we only wish to project out the vacuum, and is less trivial for other, non-vacuum states, see Ref. [85].)

The (4.63) Hamiltonian only distinguishes the single vacuum state by giving it -1 energy, while treating all states of excitations equally: it simply assigns energy 0 to all (non-vacuum) anyons.

Adding 4-local terms to the Hamiltonian

Let's take the fully topological Hamiltonian of $\mathcal{D}(S_3)$, Eq. (4.63), which doesn't distinguish between flavors of the same anyon. Now, we may add the 4-local terms introduced in the previous section, and they all commute with both the vacuum projector and each other [85]:

$$H = -\sum_{s=(v,p)} A^{(v)}_{\Gamma_1} B^{(p)}_{C_e} + \sum_v \left(\beta A^{(v)}_{\Gamma_{-1}} + \gamma A^{(v)}_{\Gamma_2}\right) + \sum_p \left(\epsilon B^{(p)}_{C_x} + \nu B^{(p)}_{C_y}\right). \tag{4.64}$$

We could also add 4-local terms for A_{Γ_1} and B_{C_e}, but as shortly demonstrated, it is not necessary for our purposes.

The prefactors in front of each projector are tunable energy parameters (the notation follows that of Ref. [85]). As long as none of the parameters are decreased below -0.5 (more precisely, no combination of charge and flux projectors together are below -1), the ground space of this Hamiltonian coincides with the vacuum state of $\mathcal{D}(S_3)$. Thus, all anyons of the Drinfeld double are excitations of the Hamiltonian (4.64).

Energy-suppression of conjugacy classes or irreps

Engineering the Hamiltonian (4.64), and then tuning some of its parameters to be very large, will practically forbid anyons and anyon flavors related to the projector (or label of) we are tuning. In an environment with finite temperature, thermal processes that cost energy $E \gg k_B T$ will be suppressed. Thus, processes leading to the creation of certain anyons would cost too much energy, and those processes become thermally forbidden. This procedure is a way to physically realize the phase transitions discussed in Sec. 4.4.

For example, tuning the parameter $\epsilon \to \infty$ in the Hamiltonian (4.64) will result in the conjugacy class C_x becoming forbidden in the theory, and lead to the analysis presented in Sec. 4.4.1. It is possible to tune any combination of the parameters in (4.64).

In certain cases, such an energy suppression of the Hamiltonian will lead to the (joint) forbiddance of labels in such a way that the unforbidden labels form a

Figure 4.11: The quantum phases along the path $\{\beta = \gamma = \nu = 0, \epsilon\}$. $\epsilon = 0$ is in the topological Hamiltonian of the $\mathcal{D}(S_3)$ state. $\epsilon \to \infty$ is the topological Hamiltonian of the quantum phase $\mathcal{D}(\mathbb{Z}_3)$. Note that every point corresponds to a frustration-free local Hamiltonian with commuting terms. Aside from the point $\epsilon \to \infty$, all other Hamiltonians are in the $\mathcal{D}(S_3)$ phase.

consistent, closed theory. These cases are investigated in Sec. 4.4. In other cases, tuning the parameters this way won't immediately induce a phase transition, as the unforbidden set of anyons can still realize some of the energetically suppressed anyons, *through fusion*. This is, in fact, a subtle difference between projection and energy suppression. We will discuss this topic more in Sec. 4.6.

Furthermore, it is key to understand that in order to induce the phase transition, we need to *completely project out* certain parts of the Hilbert space, as discussed in Sec. 4.5.1. This will only happen when the tuned parameter reaches infinity. As an example, the Hamiltonian for which $\epsilon \gg 1$ is not the same Hamiltonian as $\epsilon \to \infty$. Consider the (4.64) Hamiltonian along the path $\{\beta = \gamma = \nu = 0, \epsilon\}$ in which ϵ increases starting from 0. For $\epsilon = 0$, the Hamiltonian is the fully topological (4.63) and by definition in the $\mathcal{D}(S_3)$ phase. As ϵ increases, the Hamiltonian remains in the $\mathcal{D}(S_3)$ phase since it is connected to the $\epsilon = 0$ topological Hamiltonian by a smooth path *without closing the gap* between the ground space and first-excited states. However, the (4.64) Hamiltonian for which $\epsilon \to \infty$ is in the $\mathcal{D}(\mathbb{Z}_3)$ phase, as shown in Sec. 4.4.1. In other words, we expect the (4.64) Hamiltonian $H(\epsilon \to \infty)$ to be renormalized to the topological Hamiltonian of $\mathcal{D}(\mathbb{Z}_3)$ by an RG flow. This discussion highlights the fact that it is possible to escape from a quantum phase by taking a limit, which makes a quantum phase an open set in the mathematical sense. Our picture of the phase transition is represented on Fig. 4.11.

4.6 Discussion

In this paper we introduced a framework and tools to describe quantum phase transitions in a family of topological field theories: quantum doubles. The physical processes we found can be described using terms borrowed from Landau's theory of phase transitions. We characterized phase transitions using anyonic data: fusion rules, quantum dimensions, and the S-matrix and T-matrix of a theory.

A similar analysis can be done for any quantum double, $\mathcal{D}(G)$. As quantum doubles of (Abelian) cyclic groups, $\mathcal{D}(\mathbb{Z}_d)$ are the simple juxtaposition of $\mathbb{Z}_d$ charges and $\mathbb{Z}_d$ fluxes, with all anyons having quantum dimension 1, the theories emerging there will always be quantum doubles of subgroups, similar to the theories found in the current paper. Both in these cases and for the non-Abelian $\mathcal{D}(S_3)$, the quantum dimension of anyons only decrease or don't change, but never increase (e.g., due to two anyons combining). It is an interesting question whether for more complex Abelian doubles (e.g., for $\mathcal{D}(\mathbb{Z}_d \times \mathbb{Z}_k)$) this would still hold, or would there be processes leading to the (non-trivial) combination of Abelian anyons, resulting in the emergence of a non-Abelian theory [83, 86]. Further, it could be worthwhile to investigate whether non-Abelian doubles with more degrees of freedom than the simple $\mathcal{D}(S_3)$ model, could lead to theories that aren't based on subgroups of the original group.

4.6.1 Difference between Projection and Energy Suppression

In Sec. 4.5 we discussed how phase transitions could be realized through projecting out part of a Hilbert space vs. using a modified Hamiltonian to suppress anyons through their energy couplings. One difference between these two methods concerns the ground space of the new theory.

The projection operator will clearly change the ground space, therefore the new theory will have the correct ground state. Meanwhile, tuning the parameters of a commuting Hamiltonian, as done during the energy suppression, won't change the ground space of the model. This is especially interesting in light of Ref. [87], which establishes a connection between anyons of a model and the ground-space degeneracy, thus it hints at the fact that a different set of anyons should result in a changed ground space.

We refer to our analysis of the process of energetic suppression in Sec. 4.5.2, where we argued that energy suppression will move a theory towards a phase transition, but won't necessarily take it over the critical point. Thus, the fact that the ground space throughout this procedure remains unchanged, is in agreement with our understanding of the distinction between energetic suppression vs. projection of the Hilbert space.

Another consequence of the subtle difference between projection and energy suppression is the following. In certain sections the reader might expect our analysis to yield a different theory than the one presented, for example, in Sec. 4.4.3. There we forbid all non-trivial flux labels, and as a result we would expect that the pure

chargeon theory of $\mathcal{D}(S_3)$ will arise: the Φ–Λ theory [52]. Following our analysis instead leads us to the emergence of a trivial theory, without any excitations. Why is this?

It turns out that in some of the cases investigated in this paper, performing the projection on the Hilbert space vs. energy suppression will result in completely different theories. In the above example, energetically suppressing all anyons with non-trivial fluxes, through the Hamiltonian, will result in the Φ–Λ theory, living in the complete Hilbert space of $\mathcal{D}(S_3)$. However, when we *project out* parts of the Hilbert space related to the forbidden anyons, we will transition into a theory that needs to live in this new subspace of a Hilbert space. The Φ–Λ theory needs support on the full Hilbert space, and it can't manifest in this subspace. Therefore, the theory after the projection will instead transition into the chargeon sector of $\mathcal{D}(\mathbb{Z}_3)$ (and then the trivial theory), for which the new Hilbert space is a sufficient support. This is reminiscent of two-dimensional topological theories that can only live on boundaries of three-dimensional theories.

4.6.2 Expanding the phase diagram

It is an open question whether the phases presented in the current paper are an exhaustive list of all possible emergent theories. For example, in Sec. 4.4.1 we have found the emergence of $\mathcal{D}(\mathbb{Z}_3)$, the double based on the $\mathbb{Z}_3$ subgroup of S_3. Would it be possible to induce a phase transition that leads to the emergence of $\mathcal{D}(\mathbb{Z}_2)$, a double of the other subgroup of S_3? In order to realize e.g., $\mathcal{D}(\mathbb{Z}_2)$ we would need to induce *partial forbiddance*, a process that breaks the gauge-invariance of not only the flux labels but of the charge labels as well.

For example, we might consider energetically suppressing the conjugacy class C_y. Then, as we have changed the coupling of projector B_y, the flux labels y and y^2 become heavy. Meanwhile, the other non-trivial flux labels, all of x, xy and xy^2 will be unaffected by the energy change of projector B_y. But then we can take the far away, individual fluxes x and xy, and combine them to form a non-local flux with label y (or y^2)! Therefore, energetic suppression in this example doesn't change the theory; it doesn't undergo phase transition, but stays $\mathcal{D}(S_3)$. (This is clearly different from projecting out any and all components that could lead to the creation of y and y^2 fluxes, which by definition needs to involve projecting out two of the three elements in the C_x conjugacy class.)

However, in such cases, we could consider adding new (non-commuting) terms to the (4.64) Hamiltonian, then tuning their couplings. These new terms would be

4-local flux projectors unto specific labels of a conjugacy class, e.g., B_x, B_{xy}, and B_{xy^2}, and were first introduced in Ref. [4]. While these projectors are well-defined, they are not topological (they allow the split-up of labels inside a conjugacy class), and don't commute with all terms of the (4.64) Hamiltonian (but do commute with the 6-body vacuum projector). Therefore, while they might provide a possibility for realizing phase transitions not discussed in this paper, analyzing their effect on the $\mathcal{D}(S_3)$ theory requires more work, and is the scope of future research.

Finally, we would like to mention that it could be possible to find a complementary description to the processes presented in the current paper, in terms of bosonic condensation inducing phase transitions in quantum doubles. For example, the transition described in Sec. 4.4.1 in terms of forbidding anyons D and E, then the condensation of B, could also be described through the bosonic excitation B condensing, which induces the confinement of anyons D, E, and leads to the emergence of a new theory. It is possible that all phase transitions presented in this paper can be described in such a complementary language, wherein the transition is induced by the condensation of a boson to the vacuum, and followed by additional confinement.

4.A Additional details of quantum doubles

Here we summarize a few key properties of the theories discussed in this paper, including fusion rules, and S- and T-matrices.

4.A.1 S-matrix of $\mathcal{D}(\mathbb{Z}_3)$

The S-matrix of the theory is [75]:

$$S = \frac{1}{3}\begin{bmatrix} 1 & 1 & 1 & 1 & 1 & 1 & 1 & 1 & 1 \\ 1 & 1 & 1 & \omega & \bar{\omega} & \omega & \omega & \bar{\omega} & \bar{\omega} \\ 1 & 1 & 1 & \bar{\omega} & \omega & \bar{\omega} & \bar{\omega} & \omega & \omega \\ 1 & \bar{\omega} & \omega & 1 & 1 & \bar{\omega} & \omega & \bar{\omega} & \omega \\ 1 & \omega & \bar{\omega} & 1 & 1 & \omega & \bar{\omega} & \omega & \bar{\omega} \\ 1 & \bar{\omega} & \omega & \omega & \bar{\omega} & 1 & \bar{\omega} & \omega & 1 \\ 1 & \bar{\omega} & \omega & \bar{\omega} & \omega & \omega & 1 & 1 & \bar{\omega} \\ 1 & \omega & \bar{\omega} & \omega & \bar{\omega} & \bar{\omega} & 1 & 1 & \omega \\ 1 & \omega & \bar{\omega} & \bar{\omega} & \omega & 1 & \omega & \bar{\omega} & 1 \end{bmatrix}, \tag{4.65}$$

where rows and columns correspond to the elements in the following order:

$$\{1, e_1, e_2, m_1, m_2, e_1m_1, e_2m_1, e_1m_2, e_2m_2\}$$

	A	B	C	D	E	F	G	H
A	A	B	C	D	E	F	G	H
B	B	A	C	E	D	F	G	H
C	C	C	A ⊕ B ⊕ C	D ⊕ E	D ⊕ E	G ⊕ H	F ⊕ H	F ⊕ G
D	D	E	D ⊕ E	A ⊕ C ⊕ F ⊕ G ⊕ H	B ⊕ C ⊕ F ⊕ G ⊕ H	D ⊕ E	D ⊕ E	D ⊕ E
E	E	D	D ⊕ E	B ⊕ C ⊕ F ⊕ G ⊕ H	A ⊕ C ⊕ F ⊕ G ⊕ H	D ⊕ E	D ⊕ E	D ⊕ E
F	F	F	G ⊕ H	D ⊕ E	D ⊕ E	A ⊕ B ⊕ F	H ⊕ C	G ⊕ C
G	G	G	F ⊕ H	D ⊕ E	D ⊕ E	H ⊕ C	A ⊕ B ⊕ G	F ⊕ C
H	H	H	F ⊕ G	D ⊕ E	D ⊕ E	G ⊕ C	F ⊕ C	A ⊕ B ⊕ H

Table 4.6: Fusion rules of anyons in $\mathcal{D}(S_3)$.

The topological spin of each anyon can be computed through the formula (4.7), and are:

$$t_1 = 1 \tag{4.66}$$
$$t_{e_1} = 1 \tag{4.67}$$
$$t_{e_2} = 1 \tag{4.68}$$
$$t_{m_1} = 1 \tag{4.69}$$
$$t_{m_2} = 1 \tag{4.70}$$
$$t_{e_1 m_1} = \bar{\omega} \tag{4.71}$$
$$t_{e_1 m_2} = \omega \tag{4.72}$$
$$t_{e_2 m_1} = \omega \tag{4.73}$$
$$t_{e_2 m_2} = \bar{\omega} \tag{4.74}$$

i.e., all anyons with trivial charge and trivial flux are bosons, while the rest have neither bosonic nor fermionic spins.

4.A.2 Fusion rules, S-matrix and topological spins of $\mathcal{D}(S_3)$

The fusion rules of the 8 anyons of $\mathcal{D}(S_3)$ are shown in Table 4.6.

The S-matrix of the theory is [69]:

$$S = \frac{1}{6}\begin{bmatrix} 1 & 1 & 2 & 3 & 3 & 2 & 2 & 2 \\ 1 & 1 & 2 & -3 & -3 & 2 & 2 & 2 \\ 2 & 2 & 4 & 0 & 0 & -2 & -2 & -2 \\ 3 & -3 & 0 & 3 & -3 & 0 & 0 & 0 \\ 3 & -3 & 0 & -3 & 3 & 0 & 0 & 0 \\ 2 & 2 & -2 & 0 & 0 & 4 & -2 & -2 \\ 2 & 2 & -2 & 0 & 0 & -2 & 4 & -2 \\ 2 & 2 & -2 & 0 & 0 & -2 & -2 & 4 \end{bmatrix}. \tag{4.75}$$

The topological spin of each anyon can be computed through the formula (4.7), and they are:

$$t_A = 1 \tag{4.76}$$
$$t_B = 1 \tag{4.77}$$
$$t_C = 1 \tag{4.78}$$
$$t_D = 1 \tag{4.79}$$
$$t_E = -1 \tag{4.80}$$
$$t_F = 1 \tag{4.81}$$
$$t_G = \omega \tag{4.82}$$
$$t_H = \bar{\omega} \tag{4.83}$$

i.e., anyons A, B, C, D, F are bosons, anyon E is a fermion, and G and H are "true anyons" with spins that are neither bosonic nor fermionic.

LIST OF ILLUSTRATIONS

LIST OF TABLES

BIBLIOGRAPHY

[1] Alice in wonderland vintage book illustration. http://maxpixel.freegreatpicture.com/Alice-In-Wonderland-Vintage-Book-Illustration-1794700. CC0 Public Domain, Free for commercial use; Accessed: 2018-04-05.

[2] Lewis Carroll. *Alice in Wonderland*. Tribeca Books, 2013.

[3] Kristan Temme. Thermalization time bounds for pauli stabilizer hamiltonians. *arXiv preprint arXiv:1412.2858*, 2014.

[4] Alexei Kitaev. Fault-tolerant quantum computation by anyons. *Ann. Phys.*, 303(1):2–30, January 2003.

[5] Daniel Gottesman. *Stabilizer Codes and Quantum Error Correction*. PhD thesis, California Institute of Technology, 1997.

[6] Richard P Feynman. Simulating physics with computers. *International journal of theoretical physics*, 21(6-7):467–488, 1982.

[7] Richard P Feynman. There's plenty of room at the bottom. *Caltech Engineering and Science*, 23(5):22–35, February 1960.

[8] David Deutsch. Quantum theory, the church–turing principle and the universal quantum computer. *Proc. R. Soc. Lond. A*, 400(1818):97–117, 1985.

[9] Peter W Shor. Algorithms for quantum computation: Discrete logarithms and factoring. In *Foundations of Computer Science, 1994 Proceedings., 35th Annual Symposium on*, pages 124–134. Ieee, 1994.

[10] A Robert Calderbank and Peter W Shor. Good quantum error-correcting codes exist. *Physical Review A*, 54(2):1098, 1996.

[11] Andrew M Steane. Error correcting codes in quantum theory. *Physical Review Letters*, 77(5):793, 1996.

[12] Masoud Mohseni, Peter Read, Hartmut Neven, Sergio Boixo, Vasil Denchev, Ryan Babbush, Austin Fowler, Vadim Smelyanskiy, and John Martinis. Commercialize quantum technologies in five years. *Nature News*, 543(7644):171, 2017.

[13] Davide Castelvecchi et al. Quantum cloud goes commercial. *Nature*, 543(7644):159–159, 2017.

[14] Peter W Shor. Polynomial-time algorithms for prime factorization and discrete logarithms on a quantum computer. *SIAM review*, 41(2):303–332, 1999.

[15] Lov K Grover. A fast quantum mechanical algorithm for database search. In *Proceedings of the twenty-eighth annual ACM symposium on Theory of computing*, pages 212–219. ACM, 1996.

[16] Lov K Grover. Quantum mechanics helps in searching for a needle in a haystack. *Physical review letters*, 79(2):325, 1997.

[17] Edward Farhi, Jeffrey Goldstone, Sam Gutmann, and Michael Sipser. Quantum computation by adiabatic evolution. *arXiv preprint quant-ph/0001106*, 2000.

[18] Robert Raussendorf and Hans J Briegel. A one-way quantum computer. *Physical Review Letters*, 86(22):5188, 2001.

[19] Paolo Zanardi and Mario Rasetti. Holonomic quantum computation. *Physics Letters A*, 264(2-3):94–99, 1999.

[20] Michael A Nielsen and Isaac L Chuang. *Quantum computation and quantum information*. Cambridge: Cambridge University Press, 2000.

[21] R Walter Ogburn and John Preskill. Topological quantum computation. In *Quantum computing and quantum communications*, pages 341–356. Springer, 1999.

[22] John Preskill. Fault-tolerant quantum computation. In *Introduction to quantum computation and information*, pages 213–269. World Scientific, 1998.

[23] Michael H Freedman, Michael Larsen, and Zhenghan Wang. A modular functor which is universal for quantum computation. *Communications in Mathematical Physics*, 227(3):605–622, 2002.

[24] Sergey Bravyi and Alexei Kitaev. Universal quantum computation with ideal clifford gates and noisy ancillas. *Physical Review A*, 71(2):022316, 2005.

[25] Chetan Nayak, Steven H Simon, Ady Stern, Michael Freedman, and Sankar Das Sarma. Non-abelian anyons and topological quantum computation. *Reviews of Modern Physics*, 80(3):1083, 2008.

[26] Alexei Kitaev. Anyons in an exactly solved model and beyond. *Annals of Physics*, 321(1):2–111, 2006.

[27] Alexei Kitaev. Unpaired majorana fermions in quantum wires. *Physics-Uspekhi*, 44(10S):131, 2001.

[28] Jason Alicea. Majorana fermions in a tunable semiconductor device. *Physical Review B*, 81(12):125318, 2010.

[29] Michael Levin and Xiao-Gang Wen. String-net condensation: A physical mechanism for topological phases. *Phys. Rev. B*, 71(4):1–21, January 2005.

[30] Sergey Bravyi, Matthew B Hastings, and Spyridon Michalakis. Topological quantum order: stability under local perturbations. *Journal of Mathematical Physics*, 51:093512, 2010.

[31] R Alicki, M Fannes, and M Horodecki. On thermalization in kitaev's 2d model. *Journal of Physics A: Mathematical and Theoretical*, 42(6):065303, 2009.

[32] Robert Alicki, Michal Horodecki, Pawel Horodecki, and Ryszard Horodecki. On thermal stability of topological qubit in kitaev's 4d model. *Open Systems & Information Dynamics*, 17(01):1–20, 2010.

[33] John Preskill. Lecture notes for physics 219: Quantum information and computation. *California Institute of Technology*, 1998.

[34] Jiannis K Pachos. *Introduction to topological quantum computation*. Cambridge University Press, 2012.

[35] Courtney G Brell. A proposal for self-correcting stabilizer quantum memories in 3 dimensions (or slightly less). *arXiv preprint arXiv:1411.7046*, 2014.

[36] Eric Dennis, Alexei Kitaev, Andrew Landahl, and John Preskill. Topological quantum memory. *Journal of Mathematical Physics*, 43:4452, 2002.

[37] Sergey B Bravyi and A Yu Kitaev. Quantum codes on a lattice with boundary. *arXiv preprint quant-ph/9811052*, 1998.

[38] Austin G Fowler, Ashley M Stephens, and Peter Groszkowski. High-threshold universal quantum computation on the surface code. *Physical Review A*, 80(5):052312, 2009.

[39] Austin G Fowler, Matteo Mariantoni, John M Martinis, and Andrew N Cleland. Surface codes: Towards practical large-scale quantum computation. *Physical Review A*, 86(3):032324, 2012.

[40] R Barends, J Kelly, A Megrant, A Veitia, D Sank, E Jeffrey, TC White, J Mutus, AG Fowler, B Campbell, et al. Superconducting quantum circuits at the surface code threshold for fault tolerance. *Nature*, 508(7497):500–503, 2014.

[41] Barbara M Terhal. Quantum error correction for quantum memories. *Reviews of Modern Physics*, 87(2):307, 2015.

[42] Markus Reiher, Nathan Wiebe, Krysta M Svore, Dave Wecker, and Matthias Troyer. Elucidating reaction mechanisms on quantum computers. *Proceedings of the National Academy of Sciences*, page 201619152, 2017.

[43] Sergey Bravyi and Barbara Terhal. A no-go theorem for a two-dimensional self-correcting quantum memory based on stabilizer codes. *New J. Phys.*, 11(4):043029, 2009.

[44] Olivier Landon-Cardinal and David Poulin. Local topological order inhibits thermal stability in 2d. *Phys. Rev. Lett.*, 110:090502, Feb 2013.

[45] Benjamin J Brown, Daniel Loss, Jiannis K Pachos, Chris N Self, and James R Wootton. Quantum memories at finite temperature. *Reviews of Modern Physics*, 88(4):045005, 2016.

[46] Sergey Bravyi and Jeongwan Haah. Quantum self-correction in the 3d cubic code model. *Physical review letters*, 111(20):200501, 2013.

[47] Claudio Castelnovo and Claudio Chamon. Topological quantum glassiness. *Philosophical Magazine*, 92(1-3):304–323, 2012.

[48] Benjamin J Brown, Abbas Al-Shimary, and Jiannis K Pachos. Entropic barriers for two-dimensional quantum memories. *Physical review letters*, 112(12):120503, 2014.

[49] Subir Sachdev. *Quantum Phase Transitions*. Cambridge University Press, 2 edition, 2011.

[50] Anna Kómár, Olivier Landon-Cardinal, and Kristan Temme. Necessity of an energy barrier for self-correction of abelian quantum doubles. *Physical Review A*, 93(5):052337, 2016.

[51] GK Brennen, Miguel Aguado, and J Ignacio Cirac. Simulations of quantum double models. *New Journal of Physics*, 11(5):053009, 2009.

[52] James R Wootton, Jan Burri, Sofyan Iblisdir, and Daniel Loss. Error correction for non-abelian topological quantum computation. *Physical Review X*, 4(1):011051, 2014.

[53] FL Pedrocchi, Adrian Hutter, JR Wootton, and Daniel Loss. Enhanced thermal stability of the toric code through coupling to a bosonic bat. *arXiv preprint arXiv:1309.0621*, pages 1–14, 2013.

[54] Michael Herold, Earl T Campbell, Jens Eisert, and Michael J Kastoryano. Cellular-automaton decoders for topological quantum memories. *arXiv preprint arXiv:1406.2338*, 2014.

[55] Olivier Landon-Cardinal, Beni Yoshida, David Poulin, and John Preskill. Perturbative instability of quantum memory based on effective long-range interactions. *Physical Review A*, 91(3):032303, 2015.

[56] Jeongwan Haah. Local stabilizer codes in three dimensions without string logical operators. *Phys. Rev. A*, 83:042330, Apr 2011.

[57] Edward Brian Davies. Quantum theory of open systems. 1976.

[58] E Brian Davies. Generators of dynamical semigroups. *Journal of Functional Analysis*, 34(3):421–432, 1979.

[59] Theodore Frankel. *The geometry of physics: an introduction*. Cambridge University Press, 2011.

[60] Kamil P. Michnicki. 3d topological quantum memory with a power-law energy barrier. *Phys. Rev. Lett.*, 113:130501, Sep 2014.

[61] K Temme, Michael James Kastoryano, MB Ruskai, Michael Marc Wolf, and F Verstraete. The $\chi 2$-divergence and mixing times of quantum markov processes. *Journal of Mathematical Physics*, 51(12):122201, 2010.

[62] Persi Diaconis and Daniel Stroock. Geometric bounds for eigenvalues of markov chains. *The Annals of Applied Probability*, pages 36–61, 1991.

[63] James Allen Fill. Eigenvalue bounds on convergence to stationarity for nonreversible markov chains, with an application to the exclusion process. *The annals of applied probability*, pages 62–87, 1991.

[64] O Viyuela, A Rivas, and MA Martin-Delgado. Generalized toric codes coupled to thermal baths. *New Journal of Physics*, 14(3):033044, 2012.

[65] Erik G Boman and Bruce Hendrickson. Support theory for preconditioning. *SIAM Journal on Matrix Analysis and Applications*, 25(3):694–717, 2003.

[66] Doron Chen and John R Gilbert. Obtaining bounds on the two norm of a matrix from the splitting lemma. *Electronic Transactions on Numerical Analysis*, 21:28–46, 2005.

[67] Alistair Sinclair and Mark Jerrum. Approximate counting, uniform generation and rapidly mixing markov chains. *Information and Computation*, 82(1):93–133, 1989.

[68] H. Bombin. Topological order with a twist: Ising anyons from an abelian model. *Phys. Rev. Lett.*, 105:030403, Jul 2010.

[69] Salman Beigi, Peter W Shor, and Daniel Whalen. The quantum double model with boundary: condensations and symmetries. *Communications in mathematical physics*, 306(3):663–694, 2011.

[70] Charles-Edouard Bardyn and Torsten Karzig. Exponential lifetime improvement in topological quantum memories. *arXiv preprint arXiv:1512.04528*, 2015.

[71] Thomas H Cormen, Charles E Leiserson, and Ronald L Rivest. C. stein introduction to algorithms. *MIT Press*, 5(3):55, 2001.

[72] AD Córcoles, Easwar Magesan, Srikanth J Srinivasan, Andrew W Cross, M Steffen, Jay M Gambetta, and Jerry M Chow. Demonstration of a quantum error detection code using a square lattice of four superconducting qubits. *Nature communications*, 6, 2015.

[73] Vladimir Gershonovich Drinfeld. Quantum groups. *Zapiski Nauchnykh Seminarov POMI*, 155:18–49, 1986.

[74] Hector Bombin and MA Martin-Delgado. Family of non-abelian kitaev models on a lattice: Topological condensation and confinement. *Physical Review B*, 78(11):115421, 2008.

[75] Parsa Hassan Bonderson. *Non-Abelian anyons and interferometry*. PhD thesis, California Institute of Technology, 2007.

[76] Dorit Aharonov and Lior Eldar. On the complexity of commuting local hamiltonians, and tight conditions for topological order in such systems. In *Foundations of Computer Science (FOCS), 2011 IEEE 52nd Annual Symposium on*, pages 334–343. IEEE, 2011.

[77] S. Bravyi and M. Vyalyi. Commutative version of the k-local hamiltonian problem and common eigenspace problem. *Quantum Inf. Comput.*, 5:187, 2005.

[78] Courtney G Brell, Steven T Flammia, Stephen D Bartlett, and Andrew C Doherty. Toric codes and quantum doubles from two-body hamiltonians. *New Journal of Physics*, 13(5):053039, 2011.

[79] Robert Koenig, Greg Kuperberg, and Ben W. Reichardt. Quantum computation with turaev-viro codes. *Annals of Physics*, 325(12):2707 – 2749, 2010.

[80] Jean-Pierre Serre. *Linear representations of finite groups*, volume 42. Springer Science & Business Media, 2012.

[81] Tian Lan, Juven C Wang, and Xiao-Gang Wen. Gapped domain walls, gapped boundaries, and topological degeneracy. *Physical review letters*, 114(7):076402, 2015.

[82] Robert Coquereaux. Character tables (modular data) for Drinfeld doubles of finite groups. *Proceedings of Science, POS (ICMP 2012) 024*, (April):7, 2012.

[83] Carlos Fernández-González, Roger S. K. Mong, Olivier Landon-Cardinal, David Pérez-García, and Norbert Schuch. Constructing topological models by symmetrization: A projected entangled pair states study. *Phys. Rev. B*, 94:155106, Oct 2016.

[84] Cenke Xu and Andreas W. W. Ludwig. Topological quantum liquids with quaternion non-abelian statistics. *Phys. Rev. Lett.*, 108:047202, Jan 2012.

[85] Anna Kómár and Olivier Landon-Cardinal. Anyons are not energy eigenspaces of quantum double hamiltonians. *Physical Review B*, 96(19):195150, 2017.

[86] James R Wootton, Ville Lahtinen, Zhenghan Wang, and Jiannis K Pachos. Non-abelian statistics from an abelian model. *Physical Review B*, 78(16):161102, 2008.

[87] Xiao-Gang Wen and Qian Niu. Ground-state degeneracy of the fractional quantum hall states in the presence of a random potential and on high-genus riemann surfaces. *Physical Review B*, 41(13):9377, 1990.